Patterns and collective behavior in granular media: Theoretical concepts

Igor S. Aranson*

Materials Science Division, Argonne National Laboratory, 9700 S. Cass Avenue, Argonne, Illinois 60439, USA

Lev S. Tsimring†

Institute for Nonlinear Science, University of California, San Diego, 9500 Gilman Drive, La Jolla, California 92093, USA

(Published 2 June 2006)

Granular materials are ubiquitous in our daily lives. While they have been the subject of intensive engineering research for centuries, in the last two decades granular matter has attracted significant attention from physicists. Yet despite major efforts by many groups, the theoretical description of granular systems remains largely a plethora of different, often contradictory concepts and approaches. Various theoretical models have emerged for describing the onset of collective behavior and pattern formation in granular matter. This review surveys a number of situations in which nontrivial patterns emerge in granular systems, elucidates important distinctions between these phenomena and similar ones occurring in continuum fluids, and describes general principles and models of pattern formation in complex systems that have been successfully applied to granular systems.

DOI: 10.1103/RevModPhys.78.641 PACS number(s): 45.70.Qj, 89.75.Kd

CONTENTS

I. PRELIMINARY REMARKS

Granular materials are ubiquitous in our daily lives and basic to many industries. Yet understanding their dynamic behavior remains a major challenge in physics.[1] Granular materials are collections of discrete macroscopic solid grains with sizes large enough that Brown-

*Electronic address: aronson@msd.anl.gov
†Electronic address: ltsimring@ucsd.edu

[1]See, for various reviews Nedderman (1992); Jaeger *et al.* (1996); de Gennes (1999); Duran (1999); Gollub and Langer (1999); Kadanoff (1999); Ottino and Khakhar (2000); Rajchenbach (2000); Ristow (2000).

ian motion is irrelevant (energy of a 1-mm grain moving with a typical velocity of 1 cm/sec exceeds the thermal energy at least by ten orders of magnitude). Despite this seeming simplicity, properties of granular materials are often different from conventional solids, liquids, and gases due to the dissipative nature of forces acting on interacting grains, such as inelastic collisions and friction. Since thermal fluctuations are insufficient to move grains, granular systems exhibit multiple metastable steady states which are far from equilibrium. Consequently, thermodynamic fluctuations do not play a role, and for granular systems to remain active they have to gain energy from either shear or vibration. External volume forces (gravity, electric and magnetic fields) and flows of interstitial fluids such as water or air may also be used to activate the grains. When subjected to a large enough driving force, a granular system may exhibit a transition from a granular solid to a liquid and various ordered patterns of grains may develop. Understanding the fundamentals of granular materials draws upon and gives insights into many fields at the frontier of modern physics: plasticity of solids, fracture, and friction; complex systems from equilibrium such as colloids, foams, suspensions, and biological self-assembled systems. Moreover, particulate flows are central to a large number of industries including the chemical, pharmaceutical, food, metallurgical, agricultural, and construction industries. Beyond these industrial applications, particle-laden flows are widespread in nature, for example, dune migration, erosion/deposition processes, landslides, underwater gravity currents, and coastal geomorphology, etc.

While scientific studies of granular materials began more than two centuries ago and are associated with such illustrious names as Leonard Euler, Michael Faraday, Osborne Reynolds, Charles Coulomb, and many others, for the most part of the last century it has been a domain of applied engineering research. However, in the last two decades this field has experienced a renaissance of sorts. The renewed interest among physicists in granular materials was probably spurred by the seminal idea of self-organized criticality introduced by Bak *et al.* (1987), which was originally associated with the behavior of sandpiles (for a detailed discussion of self-organized criticality, see Sec. VI.B). While it was later realized that real sandpiles do not exhibit self-organized criticality, a new generation of granular experiments using novel techniques ensued. Another reason behind the granular physics renaissance is that many physicists interested in pattern formation in "ordinary" fluids (gases, liquids) turned their attention to the new and exciting domain of granular media. From a theoretical perspective, granular physics represents a fascinating crossroads of fluid dynamics, nonequilibrium statistical mechanics, and the theory of pattern formation.

In recent years, several comprehensive reviews and monographs have appeared on the subject of granular physics; see Jaeger *et al.* (1996), Duran (1999), Ottino and Khakhar (2000), Rajchenbach (2000), Ristow (2000), Aradian *et al.* (2002), Brilliantov and Pöschel (2004), and Kudrolli (2004). Yet in all of them the focus has been either on actual phenomena and experiments or on computer modeling rather than on theoretical concepts and approaches to the problems of granular physics. We believe that the absence of reviews of theoretical developments in granular physics is not coincidental. The difficulty in writing such a review lies in the fact that granular physics is still a mixture of many different concepts, modeling tools, and phenomenological theories. Different experimental results are routinely described by different theories not having a common denominator in the form of a fundamental set of equations, such as Navier-Stokes equations in fluids or Maxwell equations for plasmas. In this review, we attempt to present the variety of sometimes incompatible approaches being developed by many theoretical groups for the description of different (or sometimes the same) experimental problems. While having a unified description of all different types of granular materials may indeed be an unreachable goal, it should be possible to develop such a theory for at least some canonical model systems, e.g., hard frictionless spheres. In fact, a unified description exists for a dilute system of rapid grains with the kinetic theory of dissipative gases. However, for densities approaching close-packing density (and this situation represents the vast majority of experimentally and practically relevant cases), no universal description exists to date. We believe that some combination of fluid dynamics with phase-field modeling based on an order parameter for the state of the granular material can be one possible candidate for the unified theory.

Furthermore, the scope of granular physics has become so broad that we have chosen to limit to reviewing the recent progress in a subfield of granular pattern formation leaving out many interesting and actively developing subjects. In particular, we have left out topics such as granular statics and anisotropic stress propagation in quasistatic granular materials (Goldenberg and Goldhirsch, 2002, 2005; Majmudar and Behringer, 2005), hopper flows (Samadani *et al.*, 1999), acoustic phenomena and flows past obstacles (Rericha *et al.*, 2002), crater formation in granular impacts (Uehara *et al.*, 2003; Walsh *et al.*, 2003; Lohse *et al.*, 2004; Ambroso *et al.*, 2005; Tsimring and Volfson, 2005), diffusion in granular systems (Dufty *et al.*, 2002), etc. We loosely define *pattern formation* as a dynamical process leading to the spontaneous emergence of a nontrivial spatially nonuniform structure which is weakly dependent on initial and boundary conditions. According to our working definition, we include in the scope of this review patterns in thin layers of vibrated grains (Secs. IV and V), patterns in gravity-driven flows (Sec. VI), granular stratification and banding (Sec. VII), as well as a multitude of patterns found in granular assemblies with complex interactions (Sec. VIII). Before delving into the details of theoretical modeling of these pattern-forming systems, we present a brief overview of relevant experimental findings and main theoretical concepts (Secs. II and III).

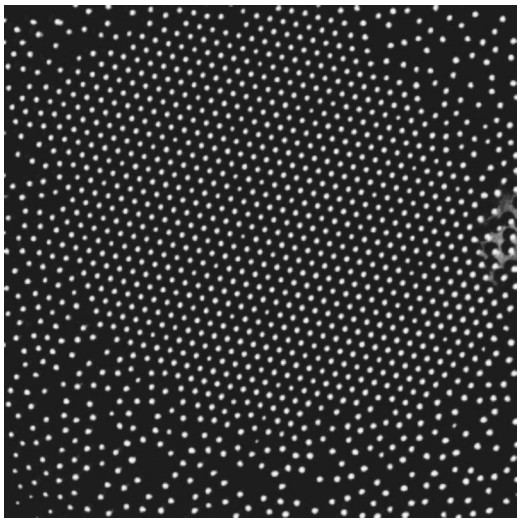

FIG. 1. Top view of a submonolayer of particles on a vibrated plate. Here a dense immobile cluster coexists with a dilute granular gas. From Olafsen and Urbach, 1998.

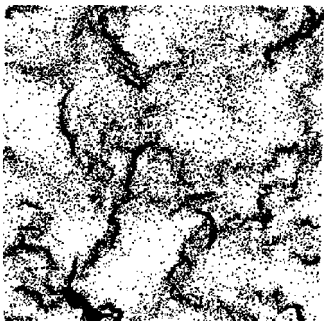

FIG. 2. Numerical simulation of a late phase of a freely cooling inelastic granular gas (restitution coefficient 0.6, number of particles 40 000). A typical clustering configuration is shown. From Goldhirsch and Zanetti, 1993.

II. OVERVIEW OF DYNAMIC BEHAVIOR IN GRANULAR MATTER

In this section we give a brief overview of the main experiments illustrating the dynamical behavior of granular media and the phenomena to be discussed in greater depth in the following sections. We classify experiments according to the way energy is injected into the system: vibration, gravity, or shear.

A. Pattern formation in vibrated layers

Quasi-two-dimensional submonolayers[2] of grains subjected to vertical vibration exhibit a bimodal regime characterized by a dense cluster of closely packed almost immobile grains surrounded by a gas of agitated particles (Olafsen and Urbach, 1998); see Fig. 1. This clustering transition occurs when the magnitude of vibration is reduced (the system is "cooled down"), which is reminiscent of the clustering instability observed in a nondriven (freely cooling) gas of inelastic particles discovered by Goldhirsch and Zanetti (1993); see Fig. 2. A detailed consideration of clustering phenomena in submonolayer systems is given in Sec. IV.

Multilayers of granular materials subject to vertical vibration exhibit spectacular pattern formation. In a typical experimental realization a layer of granular material about 10–30 particle diameters thick is energized by a precise vertical vibration produced by an electromagnetic shaker. Depending on experimental conditions, a plethora of patterns can be observed, from stripes and squares to hexagons and interfaces; see Fig. 3. While the first observations of patterns in vibrated layers were made more than two centuries ago by Chladni (1787) and Faraday (1831), current interest in these problems was initiated by Douady *et al.* (1989), Fauve *et al.* (1989), and culminated by Umbanhowar *et al.* (1996) with the discovery of a remarkable localized object, an *oscillon*; Fig. 4. A detailed consideration of these observations and modeling efforts is given in Sec. V.

In another set of experiments, pattern formation was studied in a horizontally vibrated system; see, for example, Liffman *et al.* (1997), Ristow *et al.* (1997), and Tennakoon *et al.* (1998). While there are certain common features, such as subharmonic regimes and instabilities, horizontally vibrated systems do not show the richness of behavior typical of vertically vibrated systems, and nontrivial flow regimes are typically localized near the walls. When the granular matter is polydisperse, vertical or horizontal shaking often leads to segregation. The most well-known manifestation of this segregation is the "Brazil nut" effect when large particles rise to the surface of a granular layer under vertical shaking (Rosato *et al.*, 1987; Shinbrot, 2004). Horizontal shaking is also known to produce interesting segregation band patterns oriented orthogonally to the direction of shaking (Mullin. 2000, 2002); see Fig. 5.

B. Gravity-driven granular flows

Gravity-driven systems such as chute flows and sandpiles often exhibit nontrivial patterns and spatiotemporal structures. Possibly the most spectacular are avalanches observed in the layers of granular matter if the inclination exceeds a certain critical angle (which is sometimes called the static angle of repose). Avalanches were a subject of continued research for many decades, however, only recently was it established that the avalanche shape depends sensitively on the thickness of the layer and the inclination angle: triangular downhill avalanches in thin layers and balloon-shaped avalanches in thicker layers, which expand both uphill and downhill; see Fig. 6, Daerr (2001a, 2001b), Daerr and Douady (1999). Gravity-driven granular flows are prone to a variety of nontrivial secondary instabilities in granular chute flow: fingering (Pouliquen *et al.*, 1997), see Fig. 7,

[2]Submonolayer implies less than 100% coverage by particles of the bottom plate.

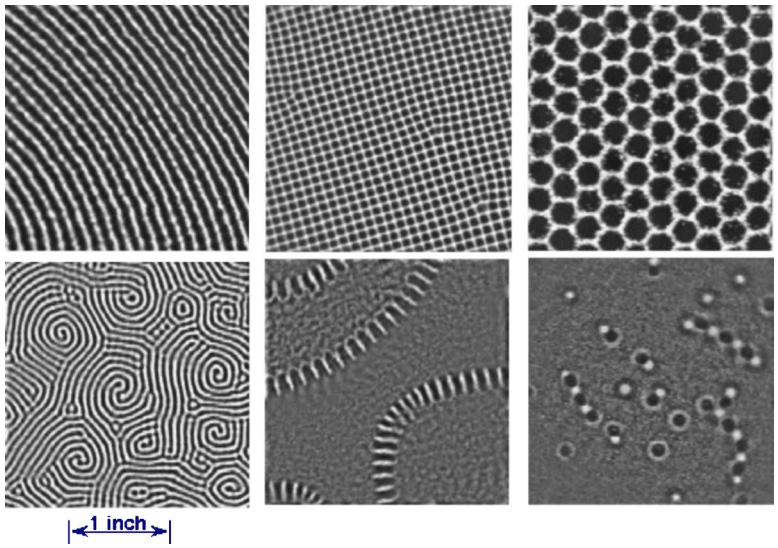

FIG. 3. (Color online) Representative patterns in vertically vibrated granular layers for various values of frequency and amplitude of the vibration: stripes, squares, hexagons, spiral, interfaces, and localized oscillons. Snapshots of the layer surface under low-angle oblique lighting. Courtesy of Paul Umbanhowar.

longitudinal vortices in rapid chute flows (Forterre and Pouliquen, 2001), see Fig. 8, long modulation waves (Forterre and Pouliquen, 2003), and others.

A rich variety of patterns and instabilities has also been found in underwater flows of granular matter: transverse instability of avalanche fronts, fingering, pattern formation in the sediment behind the avalanche, etc. [see Daerr *et al.* (2003) and Malloggi *et al.* (2005)]. Whereas certain pattern-forming mechanisms are specific to the water-granulate interaction, one also finds striking similarities with the behavior of *dry* granular matter.

C. Flows in rotating cylinders

Energy is often supplied to a granular system through the shear which is driven by the moving walls of the container. One of the most commonly used geometries for this class of systems is a horizontal cylinder rotated around its axis, or rotating drum. Rotating drums partly filled with granular matter are often used in chemical engineering for mixing and separation of particles. Flows in rotating drums have recently become a subject of active research in the physics community. For not-too-high rotating rates the flow regime in the drum is separated into an almost solid-body rotation in the bulk of the drum and a localized fluidized layer near the free surface (Fig. 9). Slowly rotating drums exhibit oscillations related to the gradual increase of the free-surface angle to the static angle of repose and subsequent fast

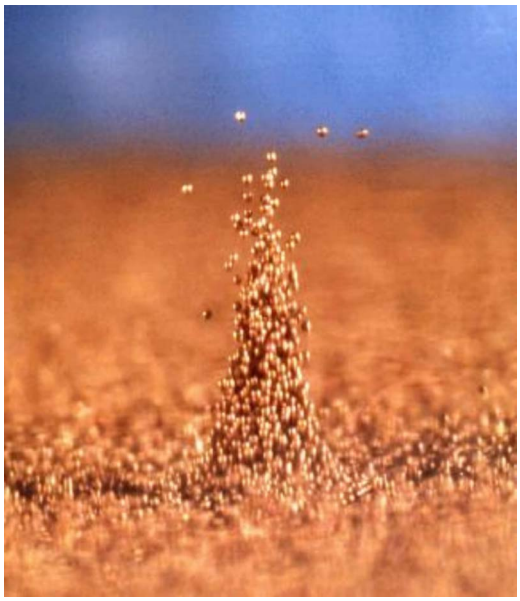

FIG. 4. (Color online) Localized oscillon in a vertically vibrated granular layer. Courtesy of Paul Umbanhowar.

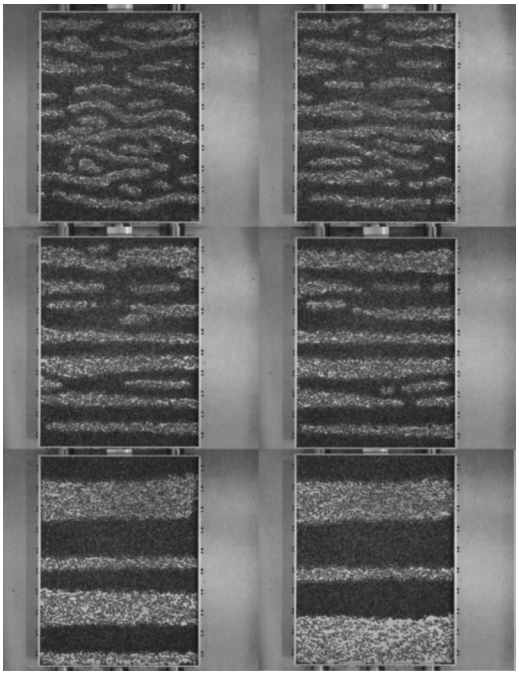

FIG. 5. Snapshots demonstrating segregation in a layer of copper balls–poppy seeds mixture in a horizontally shaken cavity (frequency 12.5 Hz, amplitude 2 mm) at 5 min, 10 min, 15 min, 30 min, 1 h, and 6 h. From Mullin, 2000.

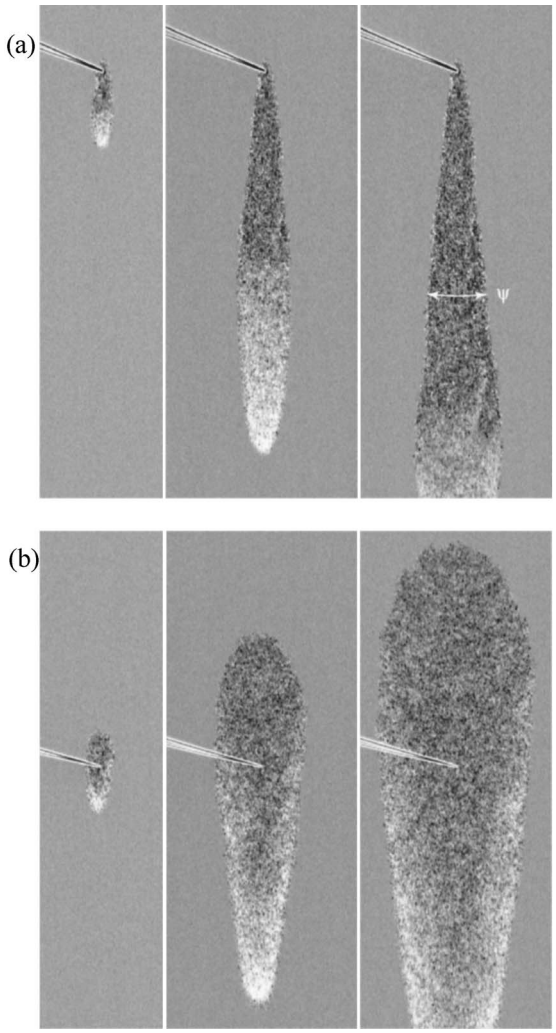

FIG. 6. Evolution of avalanches in thin layers on an incline for two different layer thicknesses. Three images on left: development of a triangular avalanche in a thin layer, point **b** in Fig. 24. Three right images: evolution of an uphill avalanche in a thicker layer, point **c** in Fig. 24. The images were formed by subtracting the photo of the unperturbed layer from photos of the layer with developing avalanches. From Daerr and Douady, 1999.

relaxation to a lower dynamic angle of repose via avalanche. Transition to steady flow is observed for the higher rotation rate (Rajchenbach, 1990). The scaling of various flow parameters with the rotation speed (e.g., the width of the fluidized layer, etc.) and the development of correlations in "dry" and "wet" granular matter were recently studied by Tegzes *et al.* (2002, 2003).

Rotating drums are typically used to study size segregation in binary mixtures of granular materials. Two types of segregation are distinguished: radial and axial. Radial segregation is a relatively fast process and occurs after a few revolutions of the drum. As a result of radial segregation, larger particles are expelled to the periphery and a core of smaller particles is formed in the bulk (Metcalfe *et al.*, 1995; Khakhar *et al.*, 1997; Metcalfe and Shattuck, 1998; Ottino and Khakhar, 2000); see Fig. 10.

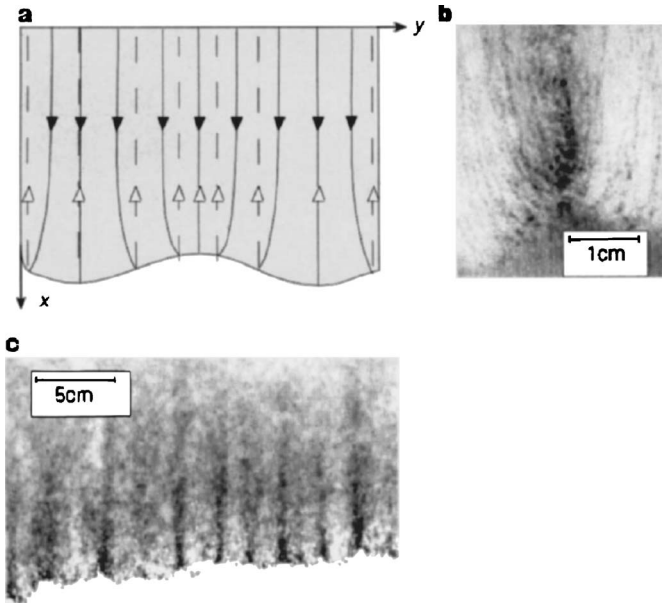

FIG. 7. Fingering instability in a chute flow. (a) Schematics of the instability mechanism; the arrows represent trajectories of coarse particles on the surface of the flowing layer. Images taken from the (b) front and (c) bottom of the layer illustrate accumulation of coarse particles between advancing fingers. From Pouliquen *et al.*, 1997.

Axial segregation, occurring in the long drums, happens on a much longer time scale (hundreds of revolutions). As a result of axial segregation, bands of segregated materials are formed along the drum axis (Hill and Kakalios, 1994, 1995; Zik *et al.*, 1994); see Fig. 11. Segregated bands exhibit slow coarsening behavior. Even more surprisingly, under certain conditions axial segregation patterns show oscillatory behavior and traveling waves (Choo *et al.*, 1997; Fiedor and Ottino, 2003; Arndt *et al.*, 2005; Charles *et al.*, 2005). Possible mechanisms leading to axial segregation are discussed in Sec. VII.

D. Grains with complex interactions

Novel collective behaviors emerge when interactions between grains have additional features caused by shape

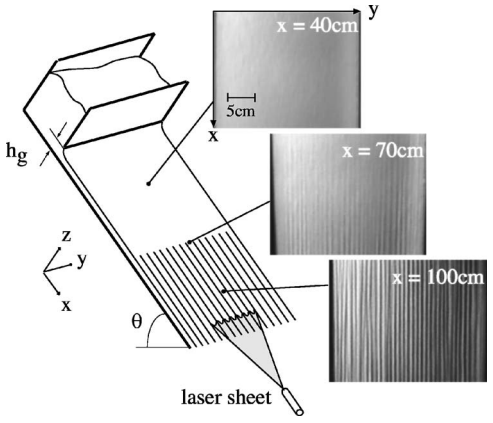

FIG. 8. Development of longitudinal vortices in the rapid granular flow down a rough incline. Three photographs were taken from above the flowing layer at different distances from the inlet. From Forterre and Pouliquen, 2001.

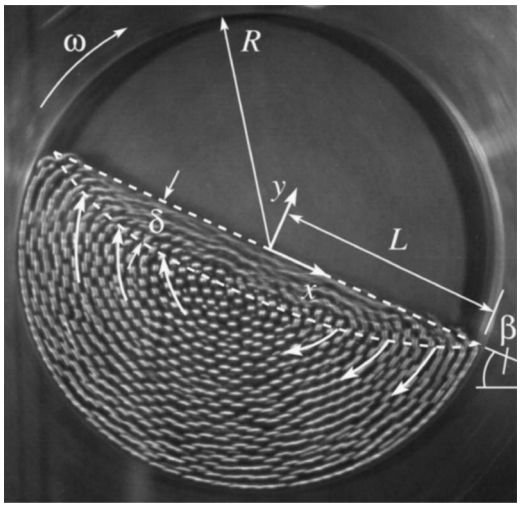

FIG. 9. Streakline photograph illustrating flow structure in the cross section of a rotating drum. The flow regime is separated into an almost solid-body rotation in the bulk of the drum and a localized fluidized layer near the free surface. From Ottino and Khakhar, 2002.

anisotropy, interstitial fluid, magnetization or electrical charge, etc. In this situation short-range collisions, the hallmark of "traditional" granular systems, can be augmented by long-range forces.

Remarkable patterns, including multiple rotating vortices of nearly vertical rods, have been observed by Blair *et al.* (2003) in a system of vibrated rods; see Fig. 12. The rods jump on their ends, slightly tilted, and drift in the direction of the tilt.

Mechanically (Blair and Kudrolli, 2003) or electrostatically (Snezhko *et al.*, 2005) driven magnetic grains exhibit the formation of chains, rings, or interconnecting networks; see Fig. 13. In this situation a magnetic dipole-dipole interaction augments hard-core collisions.

Ordered clusters and nontrivial dynamic states have been observed by Thomas and Gollub (2004) and Voth *et al.* (2002) in a small system of particles vibrated in a liquid (Fig. 14). They have shown that the fluid-mediated interaction between particles in a vibrating cavity leads to both long-range attraction and short-range repulsion. A plethora of nontrivial patterns, including rotating vortices, pulsating rings, chains, hexagons, etc., has been observed by Sapozhnikov, Tolmachev, *et al.* (2003) in a system of conducting particles in a dc electric field immersed in a poor electrolyte (Fig. 15). The nontrivial competition between electrostatic forces and self-induced electro-hydrodynamic flows determines the structure of the emerging pattern.

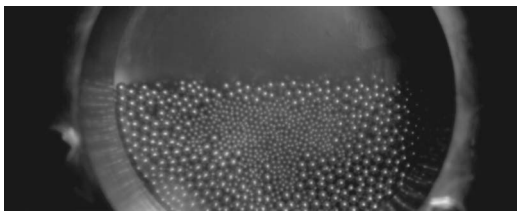

FIG. 10. Radial size segregation in a rotating drum. The core of smaller particles is formed in the bulk of the drum, while larger particles are expelled to the periphery. Courtesy of Wolfgang Losert.

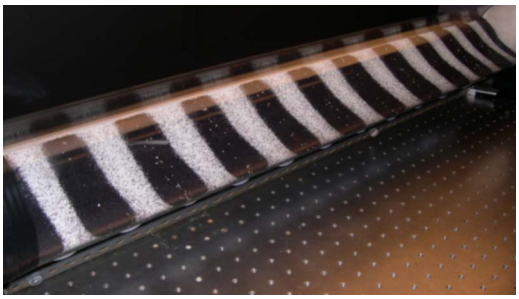

FIG. 11. (Color online) Long rotating drum partially filled with a mixture of large black glass spheres and small transparent glass spheres showing axial size segregation after many revolutions. Courtesy of Christopher Charles, Zeina Khan, and Stephen Morris.

Granular systems with complex interactions serve as a natural bridge to seemingly different systems such as foams, dense colloids, dusty plasmas, and ferrofluids.

III. MAIN THEORETICAL CONCEPTS

The physics of granular media is a diverse and eclectic field incorporating many different concepts and ideas, from hydrodynamics to the theory of glasses. Consequently, many different theoretical approaches have been proposed to address observed phenomena. They can be roughly divided into three classes: (i) microscopic models and molecular-dynamics simulations, (ii) statistical mechanics and kinetic theories, and (iii) continuum and phenomenological models.

A. Microscopic models and molecular-dynamics simulations

Probably the most fundamental microscopic property of granular materials is irreversible energy dissipation in the course of interaction (collision) between particles.

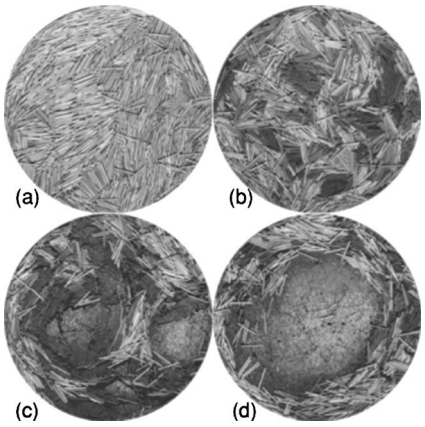

FIG. 12. Select patterns observed in a system of vertically vibrated rods with an increase of vibration amplitude (snapshots taken from above): (a) nematiclike gas phase, (b) moving domains of nearly vertical rods, (c) multiple rotating vortices, and (d) single vortex. From Blair *et al.*, 2003.

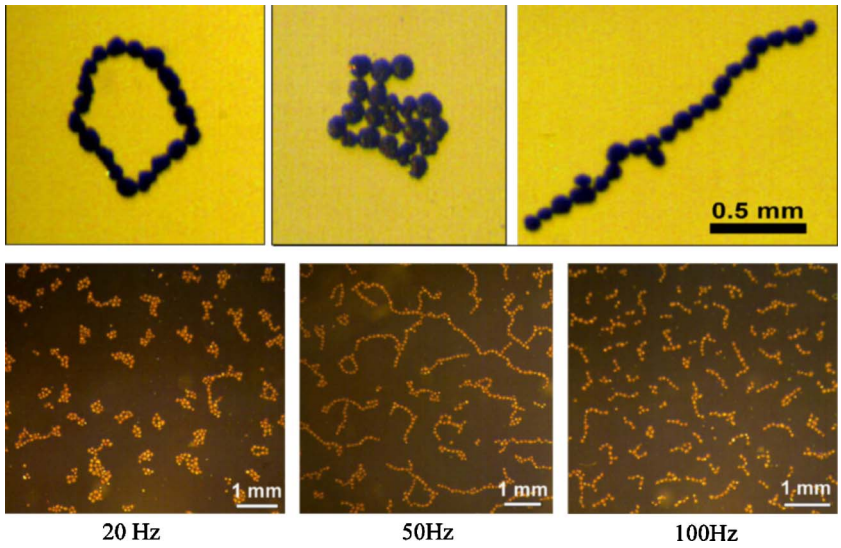

FIG. 13. (Color online) Structures formed in the submonolayer of magnetic microparticles subjected to an alternating magnetic field. Select structures such as rings, compact clusters, and chains are shown in the top panel. Changes in the pattern morphology with an increase of magnetic-field frequency are illustrated in the three bottom images. From Snezhko *et al.*, 2005.

For the case of *dry* granular materials, i.e., when the interaction with an interstitial fluid such as air or water is negligible, the encounter between grains results in dissipation of energy while total mechanical momentum is conserved. In contrast to the interaction of particles in molecular gases, collisions of macroscopic grains are generally inelastic.

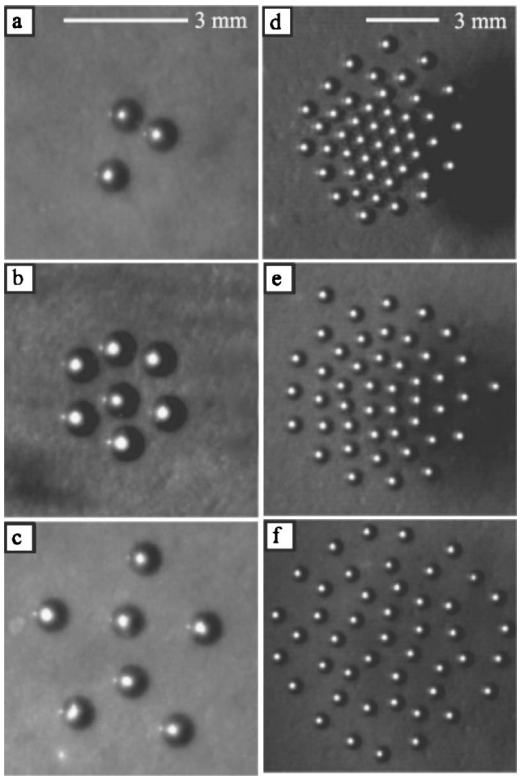

FIG. 14. Arrangements of particles near the bottom of a vibrated water-filled container when both attraction and repulsion are important. All images are taken at the frequency 20 Hz and for different values of dimensionless acceleration or for different initial conditions: (a), (b) $\Gamma=3$; (c), (d) $\Gamma=3.7$; (e) $\Gamma=3.9$; and (f) $\Gamma=3.5$. From Voth *et al.*, 2002.

There are several well-accepted models addressing the specifics of energy dissipation in the course of a collision; see, for details, Brilliantov and Pöschel (2004). The simplest case corresponds to indeformable (hard) frictionless particles with fixed restitution coefficient $0<e<1$ characterizing the fraction of a energy lost in the course of a collision. The relation between velocities after the collision ($\mathbf{v}'_{1,2}$) and before the collision ($\mathbf{v}_{1,2}$) for two identical spherical particles is given by

$$\mathbf{v}'_{1,2}=\mathbf{v}_{1,2}\mp\frac{1+e}{2}[\mathbf{n}_{12}(\mathbf{v}_1-\mathbf{v}_2)]\mathbf{n}_{12}. \tag{1}$$

Here $\mathbf{n}_{12}$ is the unit vector pointed from the center of particle 1 to the center of particle 2 at the moment of collision. The case $e=1$ corresponds to elastic collisions

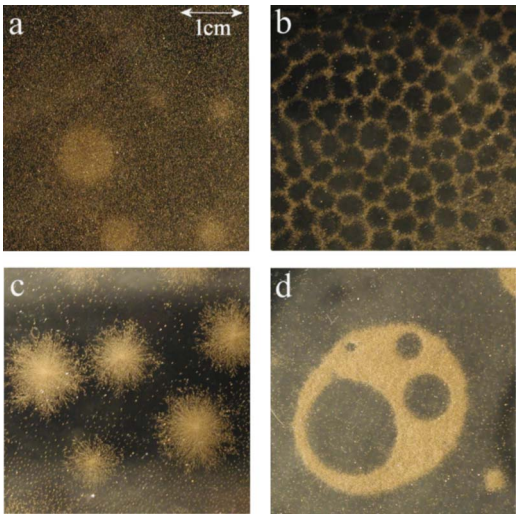

FIG. 15. (Color online) Structures of electrostatically driven granular media in a weakly conducting nonpolar fluid (toluene-ethanol mixture). Representative patterns were obtained for different values of applied field and concentration of ethanol: (a) static clusters, (b) honeycombs, (c) dynamic vortices, and (d) pulsating rings. From Sapozhnikov, Tolmachev, *et al.*, 2003.

(particles exchange their velocities) and $e=0$ characterizes fully inelastic collisions. For $0<e<1$, the total energy loss is of the form

$$\Delta E = -\frac{1-e^2}{4}|\mathbf{n}_{12}(\mathbf{v}_1-\mathbf{v}_2)|^2.$$

Modeling collisions between particles by a fixed restitution coefficient is very simple and intuitive, however, this approximation can be questionable in certain cases. For example, the approximation of granular media by a gas of hard particles with fixed e often yields nonphysical behavior such as inelastic collapse (McNamara and Young, 1996): divergence of the number of collisions in a finite time; see Sec. IV.A. In fact, the restitution coefficient is known to depend on the relative velocities of colliding particles and approaches unity as $|\mathbf{v}_1-\mathbf{v}_2|\to 0$. This dependence is captured by the viscoelastic modeling of particle collisions [see, for example, Ramirez *et al.* (1999)]. For nonspherical grains the restitution coefficient may also depend on the point of contact (Goldsmith, 1964).

Tangential friction forces play an important role in the dynamics of granular matter, especially in dense systems. Friction forces are hysteretic and history dependent (the contact between two grains can be either stuck due to dry friction or sliding depending on the history of interaction). This strongly nonlinear behavior makes the analysis of frictional granular materials extremely difficult. In the majority of theoretical studies, the simplest Coulomb law is adopted: friction is independent of sliding velocity as long as the tangential force exceeds a certain threshold (Walton, 1993). However, the main problem is the calculation of static friction forces. It is well known that frictional contact forces among solid particles exhibit indeterminacy in the case of multiple contacts per particle because there are less force balance constraints than stress components [see, for example, McNamara *et al.* (2005) and Unger *et al.* (2005)]. To resolve this indeterminacy in simulations, various approximate algorithms have been proposed (see Sec. III.A).

Viscous drag forces due to interactions with an interstitial fluid often affect the dynamics of granular materials. Gas-driven particulate flow is an active research area in the engineering community; see Jackson (2000). Fluid-particle interactions are also involved in many geophysical processes, e.g., dune formation (Bagnold, 1954). Whereas interactions of small individual particles with a fluid is well understood in terms of Stokes law, collective interactions and mechanical momentum transfer from particles to fluid remains an open problem. Various phenomenological constitutive equations are used in the engineering community to model fluid-particulate flows; see Duru *et al.* (2002).

Finally, small particles can acquire electric charge or magnetic moment. In this situation fascinating collective behavior emerges due to competition between short-range collisions and long-range electromagnetic forces; see Aranson *et al.* (2000), Blair *et al.* (2003), and Sapozhnikov, Tolmachev, *et al.* (2003). The effects of complex interparticle interactions on pattern formation in granular systems are discussed are Sec. VIII.

A detailed knowledge of the collisional properties of particles is essential for realistic discrete-element (or molecular-dynamics) simulations of granular matter. Due to a relatively small number of particles in granular flows as compared to atomic and molecular systems, such simulations have been very successful in capturing many phenomena occurring in granular systems.

There exist three fundamentally different approaches to molecular-dynamics simulations: the soft-particles simulation method, the event-driven algorithm, and the contact-dynamics method for rigid particles. For a review on various molecular-dynamics simulation methods we recommend Luding (2004), Rapaport (2004), and Pöeschel and Schwager (2005).

In the soft-particle algorithm, all forces acting on a particle from either walls or other particles or external forces are calculated based on the positions of the particles. Once the forces are found, time is advanced by the explicit integration of the corresponding Newton equations of motion. Various models are used for calculating normal and tangential contact forces. In the majority of implementations, the normal contact forces are determined from the particle overlap Δ_n which is defined as the difference of the distance between the centers of mass of two particles and the sum of their radii. The normal force $\mathbf{F}_n$ is either proportional to Δ_n (linear Hookian contact) or proportional to $\Delta^{3/2}$ (Hertzian contact). In the spring-dashpot model, an additional dissipative force proportional to the normal component of the relative velocity is added to model the inelasticity of grains. A variety of approaches are used to model tangential forces, the most widely accepted of them being the Cundall-Strack algorithm (Cundall and Strack, 1979; Schäffer *et al.*, 1996) in which the tangential contact is modeled by a dissipative linear spring, whose force $\mathbf{F}_t=-k_t\boldsymbol{\Delta}_t-m/2\,\gamma_t\mathbf{v}_t$ (here $\boldsymbol{\Delta}_t$ is the relative tangential displacement, $\mathbf{v}_t$ is the relative tangential velocity, and k_t, γ_t are model constants). It is truncated when its ratio to the normal force $|\mathbf{F}_t|/|\mathbf{F}_n|$ reaches the friction coefficient μ according to the Coulomb law. Soft-particle methods are relatively slow and used mostly for the analysis of dense flows when generally faster event-driven algorithms are not applicable; see, for example, Silbert, Ertas, *et al.* (2002a, 2002b); Silbert, Grest, *et al.* (2002), Landry *et al.* (2003), and Volfson *et al.* (2003a, 2003b).

In the event-driven algorithm, particles are considered infinitely rigid and move freely (or are driven by macroscopic external fields) in the intervals between (instantaneous) collisions. The algorithm updates the velocities and positions of two particles involved in a binary collision [in the simplest frictionless case, according to Eq. (1)]. It then finds the time of the next collision and the velocities and positions of all particles at that time according to Newton's law. Thus time is advanced directly from one collision to the next, and so the variable time step is dictated by the interval between collisions. While event-driven methods are typically faster for dilute rapid granular flows, they become impractical for dense flows

in which collisions are very frequent and, furthermore, particles develop persistent contacts. As a related numerical problem, event-driven methods are known to suffer from "inelastic collapse" when the number of collisions between particles diverges in finite time (McNamara and Young, 1996). Introducing a velocity-dependent restitution coefficient which approaches 1 as the collision velocity approaches zero makes it possible to avoid the inelastic collapse conundrum [see Bizon, Shattuck, Swift, *et al.* (1998)], but the computational cost still becomes prohibitively high for dense systems, so event-driven methods are mostly applied to rapid granular flows; see McNamara and Young (1996), Nie *et al.* (2002), Ferguson *et al.* (2004), and Khain and Meerson (2004).

Contact dynamics is a discrete-element method like soft-particle and event-driven ones, with the equations of motion integrated for each particle. Similar to the event-driven algorithm and unlike the soft-particle method, particle deformations are suppressed by considering particles as infinitely rigid. The contact-dynamics method considers contacts occurring within a certain short time interval as simultaneous and computes contact forces by satisfying simultaneously kinematic constraints imposed by the impenetrability of the particles and the Coulomb friction law. Imposing kinematic constraints requires contact forces (constraint forces) which cannot be calculated from the positions and velocities of particles alone. The constraint forces are determined in such a way that constraint-violating accelerations are compensated (Moreau, 1994). For a comprehensive review of contact dynamics, see Brendel *et al.* (2004).

Sometimes different molecular-dynamics methods are applied to the same problem. Radjai *et al.* (1998), Staron *et al.* (2002), and Lois *et al.* (2005) applied contact-dynamics methods and Silbert *et al.* (2002a, 2002b) and Volfson *et al.* (2003a, 2003b) used the soft-particle technique for the analysis of instabilities and constitutive relations in dense granular systems. Patterns in vibrated layers were studied with event-driven simulations by Bizon, Shattuck, Swift, *et al.* (1998) and Moon *et al.* (2003) and with soft-particle simulations by Nie *et al.* (2000) and Prevost *et al.* (2004).

B. Kinetic theory and hydrodynamics

Kinetic theory deals with the probability distribution functions describing the state of a granular gas. The corresponding equations, similar to Boltzmann equations for rarefied gases, can be rigorously derived for the dilute gas of inelastically colliding particles with fixed restitution coefficient, although certain generalizations are known (Goldstein and Shapiro, 1995; Jenkins and Zhang, 2002). Kinetic theory is formulated in terms of the Boltzmann-Enskog equation for the probability distribution function $f(\mathbf{v},\mathbf{r},t)$ to find particles with velocity $\mathbf{v}$ at point $\mathbf{r}$ at time t. In the simplest case of identical frictionless spherical particles of radius d with fixed restitution coefficient e, it assumes the following form:

$$[\partial_t + (\mathbf{v}_1 \cdot \nabla)] f(\mathbf{v}_1,\mathbf{r}_1,t) = I[f], \tag{2}$$

with the binary collision integral $I[f]$ in the form

$$I = d^2 \int d\mathbf{v}_2 \int d\mathbf{n}_{12} \Theta(-\mathbf{v}_{12}\cdot\mathbf{n}_{12}) |\mathbf{v}_{12}\cdot\mathbf{n}_{12}| \times [\chi f(\mathbf{v}_1'',\mathbf{r}_1,t) f(\mathbf{v}_2'',\mathbf{r}_1 - d\mathbf{n}_1 2,t) - f(\mathbf{v}_1,\mathbf{r}_1,t) f(\mathbf{v}_2,\mathbf{r}_1 + d\mathbf{n}_{12},t)], \tag{3}$$

where $\chi = 1/e^2$, Θ is the theta function, and precollision velocities $v_{1,2}$ and "inverse collision" velocities $v_{1,2}''$ are related as follows:

$$\mathbf{v}_{1,2}'' = \mathbf{v}_{1,2} \mp \frac{1+e}{2e} [\mathbf{n}_{12}(\mathbf{v}_1 - \mathbf{v}_2)] \mathbf{n}_{12} \tag{4}$$

[cf. Eq. (1)]. Equation (2) is derived with the usual "molecular-chaos" approximation, which implies that correlations between colliding particles are neglected. One should keep in mind, however, that in dense granular systems this approximation can be rather poor due to the excluded-volume effects and the inelasticity of collisions introducing velocity correlations among particles [see, for example, Brilliantov and Pöschel (2004)].

Hydrodynamic equations were obtained by Jenkins and Richman (1985) truncating the hierarchy of moment equations obtained from the Boltzmann equation (2) via an appropriately modified Chapman-Enskog procedure and in a more general form by Brey *et al.* (1998), Sela and Goldhirsch (1998), and Garzó and Dufty (1999). As a result, a set of continuity equations for mass, momentum, and fluctuation kinetic energy (or "granular temperature") is obtained. However, in contrast to conventional hydrodynamics, the applicability of granular hydrodynamics is often questionable because typically there is no separation of scale between microscopic and macroscopic motions;[3] see Tan and Goldhirsch (1998).

The mass, momentum, and energy conservation equations in granular hydrodynamics have the form

$$\frac{D\nu}{Dt} = -\nu \nabla \cdot \mathbf{u}, \tag{5}$$

$$\nu \frac{D\mathbf{u}}{Dt} = -\nabla \cdot \boldsymbol{\sigma} + \nu \mathbf{g}, \tag{6}$$

$$\nu \frac{DT}{Dt} = -\boldsymbol{\sigma} : \dot{\boldsymbol{\gamma}} - \nabla \cdot \mathbf{q} - \varepsilon, \tag{7}$$

where ν is the filling fraction (the density of granular material normalized by the density of grains), $\mathbf{u}$ is the velocity field, $T = (\langle \mathbf{u}\mathbf{u} \rangle - \langle \mathbf{u} \rangle^2)/2$ is the granular temperature, $D/Dt = \partial_t + (\mathbf{u}\cdot\nabla)$ is the material derivative, $\mathbf{g}$ is the gravity acceleration, $\sigma_{\alpha\beta}$ is the stress tensor, $\mathbf{q}$ is the energy-flux vector, $\dot{\gamma}_{\alpha\beta} = \partial_\alpha u_\beta + \partial_\beta u_\alpha$ is the strain-rate tensor, and ε is the energy dissipation rate. Equations (5)–(7) are structurally similar to the Navier-Stokes

[3] An exception is the case of almost elastic particles with the restitution coefficient $e \to 1$.

equations for conventional fluids except for the last term ε in Eq. (7) for granular temperature which accounts for the energy loss due to inelastic collisions.

Equations (5)–(7) have to be supplemented by the constitutive relations for the stress tensor $\boldsymbol{\sigma}$, energy flux $\mathbf{q}$, and energy dissipation rate ε. For dilute systems, a linear relation between stress $\boldsymbol{\sigma}$ and strain rate $\dot{\boldsymbol{\gamma}}$ is obtained (Jenkins and Richman, 1985),[4]

$$\sigma_{\alpha\beta} = [p + (\mu - \lambda)\mathrm{Tr}\dot{\boldsymbol{\gamma}}]\delta_{\alpha\beta} - \mu\dot{\boldsymbol{\gamma}}_{\alpha\beta}, \tag{8}$$

$$\mathbf{q} = -\kappa \boldsymbol{\nabla} T. \tag{9}$$

In the kinetic theory of a two-dimensional gas of slightly inelastic hard disks (Jenkins and Richman, 1985), Eqs. (5)–(7) are closed with the following equation of state:

$$p = \frac{4\nu T}{\pi d^2}[1 + (1+e)G(\nu)], \tag{10}$$

and the expressions for shear and bulk viscosities

$$\mu = \frac{\nu T^{1/2}}{2\pi^{1/2} d G(\nu)}\left[1 + 2G(\nu) + \left(1 + \frac{8}{\pi}\right)G(\nu)^2\right], \tag{11}$$

$$\lambda = \frac{8\nu G(\nu) T^{1/2}}{\pi^{3/2} d}, \tag{12}$$

thermal conductivity

$$\kappa = \frac{2\nu T^{1/2}}{\pi^{1/2} d G(\nu)}\left[1 + 3G(\nu) + \left(\frac{9}{4} + \frac{4}{\pi}\right)G(\nu)^2\right], \tag{13}$$

and energy dissipation rate

$$\varepsilon = \frac{16\nu G(\nu) T^{3/2}}{\pi^{3/2} d^3}(1 - e^2). \tag{14}$$

The radial pair distribution function $G(\nu)$ for a dilute 2D gas of elastic hard disks can be approximated by (Song *et al.*, 1989)

$$G_{\mathrm{CS}}(\nu) = \frac{\nu(1 - 7\nu/16)}{(1-\nu)^2}. \tag{15}$$

This is a two-dimensional analog of the Carnahan-Starling (1969) formula for elastic spheres. Equation (15) is expected to work for densities roughly below 0.7. For high-density granular gases, Eq. (15) has been calculated by Buehler *et al.* (1951) using free volume theory,

$$G_{\mathrm{FV}} = \frac{1}{(1+e)[(\nu_c/\nu)^{1/2} - 1]}, \tag{16}$$

where $\nu_c \approx 0.82$ is the density of the random close-packing limit. Luding (2001) proposed a global fit

$$G_L = G_{\mathrm{CS}} + \{1 + \exp[-(\nu - \nu_0)/m_0)]^{-1}\}(G_{\mathrm{FV}} - G_{\mathrm{CS}}),$$

with empirically fitted parameters $\nu_0 \approx 0.7$ and $m_0 \approx 10^{-2}$. However, even with this extension, the continuum theory comprised of Eqs. (5)–(14) cannot describe the force chains which transmit stress via persistent contacts remaining in the dense granular flows as well as the hysteretic transition from solid to static regimes and coexisting solid and fluid phases.

Granular hydrodynamics is probably the most universal (however, not always the most appropriate) tool for modeling large-scale collective behavior in driven granular matter. The granular hydrodynamics equations (5)–(7) and their modifications are widely used in the engineering community to describe a variety of large-scale granular flows, especially for the design of gas-fluidized bed reactors (Gidaspow, 1994). In the physics community granular hydrodynamics is used to understand various instabilities in relatively small-scale flows, such as flow past obstacles (Rericha *et al.*, 2002), convection (Livne *et al.*, 2002a, 2002b), floating clusters (Meerson *et al.*, 2003), longitudinal rolls (Forterre and Pouliquen, 2002, 2003), patterns in vibrated layers (Bougie *et al.*, 2005), and others. However, Eqs. (5)–(7) are often used far beyond their applicability limits, viz., dilute flows. Consequently, certain parameters and constitutive relations need to be adjusted heuristically in order to accommodate the observed behavior. For example, Bougie *et al.* (2002) had to introduce artificial nonzero viscosity in Eq. (6) for $\nu \to 0$ in order to avoid artificial blowup of the solution. Similarly, Losert *et al.* (2000) introduced a viscosity diverging as the density approached the close-packed limit as $(\nu - \nu_c)^\beta$, with $\beta \approx 1.75$ the fitting parameter used in order to describe the structure of dense shear granular flows.

In a recent paper Pouliquen *et al.* (2005) have suggested a constitutive relation for dense granular flow. Based on a compilation of experimental data obtained for granular flows in different geometries (G.D.R. MiDi, 2004), they have proposed that the ratio of shear to normal stress τ/P is a function of the universal dimensionless parameter $I = \dot{\gamma} d/\sqrt{P/\nu}$, which is the ratio of the time scale of microscopic grain rearrangements $d/\sqrt{P/\nu}$ to the characteristic time scale associated with the flow $\dot{\gamma}^{-1}$. Pouliquen *et al.* (2005) have postulated a simple expression for the friction coefficient,

$$\mu(I) \equiv \tau/P = \mu_s + \frac{\mu_2 - \mu_s}{I_0/I + 1}, \tag{17}$$

for which typical values of the parameters of glass beads are $\mu_s = \tan 21°$, $\mu_2 = \tan 33°$, and $I_0 = 0.3$. According to Eq. (17), the friction coefficient increases during the transition from the quasistatic regime ($I \to 0$) to the kinetic regime $I \gg I_0$. This simple constitutive law augmented by another constitutive relation for the volume fraction $\phi = \phi_{\max} - (\phi_{\max} - \phi_{\min})I$ allowed Pouliquen *et al.* (2005) to quantitatively describe several types of granular flow including plane shear, Couette flow, quasistationary chute flow, and flow on a pile in a narrow chan-

[4]The more general approach by Brey *et al.* (1988) and Sela and Goldhirsch (1998) resulted in additional non-Fourier contributions to the heat flux (9).

nel. However, this description fails near the quasistatic limit as it cannot describe shear bands or the hysteretic properties of many granular systems leading to avalanching and stick-slip friction.

C. Phenomenological models

A generic approach to the description of dense granular flows was suggested by Aranson and Tsimring (2001, 2002) who proposed treating the shear-stress-mediated fluidization of granular matter as a phase transition. An order parameter characterizing the local state of granular matter and the corresponding phase-field model were introduced. According to the model, the order parameter has its own relaxation dynamics and defines the static and dynamic contributions to the shear stress tensor. This approach is discussed in more detail in Sec. VI.A.1.

Another popular approach is based on the two-phase description of granular flow, one phase corresponding to rolling grains and the other phase to static ones. This approach, the Bouchaud-Cates-Ravi Prakash-Edwards (BCRE) model, was suggested by Bouchaud *et al.* (1994, 1995) for a description of surface gravity-driven flows. The BCRE model has a direct relation to depth-averaged hydrodynamic equations (the Saint-Venant model). Note that the BCRE and Saint-Venant models can be derived in a certain limit from the more general order-parameter model mentioned above; for details see Sec. VI.A.2.

Many pattern-forming systems are often described by generic models, such as the Ginzburg-Landau or Swift-Hohenberg equations (Cross and Hohenberg, 1993; Aranson and Kramer, 2002). This approach allows one to explain many generic features of patterns, however, in any particular system there are peculiarities which need to be taken into account. This often requires modifications to the generic models. This approach was taken by Tsimring and Aranson (1997), Aranson and Tsimring (1998), Venkataramani and Ott (1998), Aranson, Tsimring, *et al.* (1999a), and Crawford and Riecke (1999), in order to describe patterns in a vibrated granular layer. Details of these approaches can be found in Sec. V.D.

In addition, a variety of statistical physics tools have been applied to diverse phenomena occurring in granular systems. For example, the Lifshitz and Slyozov (1958) theory developed for coarsening phenomena in equilibrium systems was applied to coarsening of clusters in granular systems (Aranson, Meerson, *et al.*, 2002); see Sec. VIII.C.

IV. PATTERNS IN SUBMONOLAYERS: CLUSTERING, COARSENING, AND PHASE TRANSITIONS

A. Clustering in freely cooling gases

The properties of granular gases are dramatically different from the properties of molecular gases due to the inelasticity of collisions between grains. This leads to the emergence of a correlation between colliding particles and violation of the molecular-chaos approximation. This in turn gives rise to various pattern-forming instabilities. Perhaps the simplest system exhibiting nontrivial pattern formation in the context of granular matter is that of a freely cooling granular gas: an isolated system of inelastically colliding particles. The interest in freely cooling granular gases was triggered by Goldhirsch and Zanetti's (1993): discovery of clustering spontaneously forming dense clusters emerge as a result of the instability of the initially homogeneous cooling state; see Fig. 2. This generic instability, which can be traced in many other particle systems, has a very simple physical interpretation: the local increase of the density of a granular gas results in an increase in the number of collisions, and therefore further dissipation of energy and decrease in the granular temperature. Due to the proportionality of pressure to temperature, the decrease of temperature will consequently decrease local pressure, which in turn will create a flux of particles towards this pressure depression and further increase the density. This clustering instability has interesting counterparts in astrophysics: the clustering of self-gravitating gas (Shandarin and Zeldovich, 1989) and "radiative instability" in optically thin plasmas (Meerson, 1996) resulting in interstellar dust condensation.

According to Goldhirsch and Zanetti (1993), the initial stage of clustering can be understood in terms of the instability of a homogeneously cooled state described by the density ν and granular temperature T. This state is characterized by the zero hydrodynamic velocity v, and the temperature evolution follows from Eq. (7):

$$\partial_t T \sim -T^{3/2}, \tag{18}$$

which results in Haff's (1983) cooling law $T \sim t^{-2}$. However, the uniform cooling state becomes unstable in large enough systems masking Haff's law. A discussion of linear instability conditions can be found, e.g., in the works of Babic (1993) and Brilliantov and Pöschel (2004). For the case of particles with fixed restitution coefficient e, an analysis in the framework of linearized hydrodynamics equations (5)–(7) yields the critical wave number k^* for the clustering instability

$$k^* \sim \sqrt{1-e^2}. \tag{19}$$

As one can see, the length scale of the clustering instability diverges in the limit of elastic particles $e \to 1$.

The clustering instability in a system of grains with a constant restitution coefficient results in the inelastic collapse discussed in Sec. III.A. Whereas the onset of clustering can be well understood in the framework of granular hydrodynamics [see, for example, Babic (1993), Goldhirsch (2003), Hill and Mazenko (2003), and Brilliantov and Pöschel (2004)] certain subtle features (e.g., scaling exponents for temperature) are only accessed within a molecular-dynamics simulation because the hydrodynamic description often breaks down in dense cold clusters. A recent theoretical approach to the description of late stage clustering instability consists of intro-

ducing additional regularization into the hydrodynamic description due to the finite size of particles (Nie *et al.*, 2002; Efrati *et al.*, 2005).

Nie *et al.* (2002) argued that cluster formation and coalescence in freely cooling granular gases can be heuristically described by the Burgers equation for hydrodynamic velocity v with random initial conditions:

$$\partial_t v + v \nabla v = \mu_0 \nabla^2 v, \tag{20}$$

where μ_0 is the effective viscosity (which is different from the shear viscosity in hydrodynamic equations). In this context clustering is associated with the formation of shocks in the Burgers equation. Perhaps not surprising, a very similar approach was applied to a gas of "sticky" particles for describing the large-scale matter formation in the universe (Gurbatov *et al.*, 1985; Shandarin and Zeldovich, 1989).

Meerson and Puglisi (2005) have conducted molecular-dynamics simulations of the clustering instability of a freely cooling dilute inelastic gas in a quasi-one-dimensional setting. This problem was also examined by Efrati *et al.* (2005) in the framework of granular hydrodynamics. It has been observed that as the gas cools, stresses become negligibly small, and the gas flows only by inertia. A hydrodynamic description reveals a finite-time singularity, as the velocity gradient and the gas density diverge at some location. Molecular-dynamics studies show that finite-time singularities, intrinsic in such flows, are arrested only when close-packed clusters are formed. It was confirmed that the late-time dynamics and coarsening behavior are describable by the Burgers equation (20) with vanishing viscosity μ_0. Correspondingly, the average cluster mass grows as $t^{2/3}$ and the average velocity decreases as $t^{-1/3}$. Due to clustering, the long-term temperature evolution is $T \sim t^{-2/3}$, which is different from Haff's law $T \sim t^{-2}$ derived for spatially homogeneous cooling. Efrati *et al.* (2005) have argued that flow by inertia represents a generic intermediate asymptotic of the unstable free cooling of dilute granular gases consistent with the Burgers equation (20) description of a one-dimensional gas of "sticky particles" suggested by Nie *et al.* (2002).

While there is a qualitative similarity between Burgers shocks and clusters in granular materials at least in one dimension, the applicability of the Burgers equation for the description of granular media is still an open question, especially in two and three dimensions. The main problem is that the Burgers equation can be derived from hydrodynamics only in the one-dimensional situation; in two and three dimensions the Burgers equation assumes zero vorticity, which possibly oversimplifies the problem and may miss important physics. In fact, molecular-dynamics simulations illustrate the development of large-scale vortex flows in the course of clustering instability (van Noije and Ernst, 2000; Cattuto and Marconi, 2004).

Das and Puri (2003) have proposed a phenomenological description of the long-term cluster evolution in granular gases. Using the analogy between clustering in granular gases and phase-ordering dynamics in two-component mixtures, Das and Puri (2003) have postulated generalized Cahn-Hilliard equations for the evolution of density ν and complex velocity $\psi = v_x + i v_y$ [see Bray (1994)]:

$$\partial_t \nu = (-\nabla^2)^m [\nu - \nu^3 + \nabla^2 \nu], \tag{21}$$

$$\partial_t \psi = (-\nabla^2)^m [\psi - |\psi|^2 \psi + \nabla^2 \psi], \tag{22}$$

with $m \to 0+$, which characterize the globally conserved dynamics of ν and ψ similar to that considered in Sec. VIII.C.1. Das and Puri (2003) have argued that this choice is most appropriate due to the nondiffusive character of the particle's motion and is consistent with the observed morphology of clusters. While it might be very challenging to derive Eqs. (21) and (22) from first principles or to deduce them from hydrodynamic equations, the connection to phase-ordering dynamics certainly deserves further investigation.

FIG. 16. Sample image showing dense cold cluster formed opposite the driving wall (at the bottom of image); total number of particles 1860. From Kudrolli *et al.*, 1997.

B. Patterns in driven granular gases

Discovery of clustering instability stimulated a large number of experimental and theoretical studies, even experiments in low-gravity conditions (Falcon *et al.*, 1999). Since "freely cooling granular gas" is difficult to implement in the laboratory, most experiments were performed by injecting energy into the granular system in one or another way. Kudrolli *et al.* (1997) studied two-dimensional granular assemblies interacting with a horizontally vibrating (or "hot") wall. In agreement with granular hydrodynamics, the maximum gas density occurs opposite to the vibrating wall; see Fig. 16. The experimental density distributions were consistent with the modified hydrodynamic approach proposed by Grossman *et al.* (1997). Khain and Meerson (2002a, 2002b), Livne *et al.* (2002a, 2002b), and Khain *et al.* (2004) have studied the dynamics of granular gases interacting with a hot wall using the granular hydrodynamic theory of Jen-

kins and Richman (1985) for rigid disks and have predicted a phase-separation or van der Waals–type instability of the one-dimensional density distribution. This instability, reproduced later by molecular-dynamics simulations (Argentina *et al.*, 2002), is different from the usual convection instability as it occurs without gravity and is driven by the coarsening mechanism. Simulations indicated the profound role of fluctuations. One may expect that noise amplification near the instability thresholds in granular systems will be important due to the nonmacroscopic number of grains. In the context of phase-separation instability, Meerson *et al.* (2004) have raised the nontrivial question of the origin of giant fluctuations and the breakdown of the hydrodynamic description in granular systems near the threshold of instability [see also Goldman *et al.* (2004) and Bougie *et al.* (2005) on the effect of fluctuations in multilayers]. Remarkably, for the granular gas confined between two oscillating walls, Khain and Meerson (2004) have predicted, on the basis of event-driven simulations, a novel oscillatory instability for the position of the dense cluster. These predictions, however, have not yet been confirmed experimentally, most likely due to the relatively small aspect ratio of available experimental cells.

Olafsen and Urbach (1998) pioneered experiments with submonolayers of particles subject to vertical vibration. Their studies revealed a surprising phenomenon: formation of a dense close-packed cluster coexisting with a dilute granular gas; see Fig. 1. The phenomenon bears a strong resemblance to the first-order solid-liquid phase transition in equilibrium systems. Similar experiments by Losert *et al.* (1999) uncovered propagating fronts between gaslike and solidlike phases in vertically vibrated submonolayers. Such fronts are expected in extended systems in the vicinity of the first-order phase transition, e.g., solidification fronts in supercooled liquids. Prevost *et al.* (2004) have performed experiments with a vibrated granular gas confined between two plates. A qualitatively similar phase coexistence has been found. Cluster formation in vibrofluidized submonolayers shares many common features with processes in freely cooling granular gases because it is also caused by the energy dissipation due to the inelasticity of collisions. However, there is a significant difference: the instability described in Sec. IV.A is insufficient to explain the phase separation. An important additional factor is bistability and the coexistence of states due to the nontrivial density dependence of the transfer rate of a particle's vertical to horizontal momentum. Particles in a dense close-packed cluster tend to obtain less horizontal momentum than in a moderately dilute gas because in the former particle vibrations are constrained to the vertical plane by interaction with neighbors. In turn, in a very dilute gas the vertical to horizontal momentum transfer is also inhibited due to the lack of particle collisions. Another factor is that the vibration is not fully equivalent to the interaction with a heat bath. It is well known that even a single particle interacting with a periodically vibrating plate exhibits coexistence of dynamic and static states (Losert *et al.*, 1999).

There have been several simulation studies of clustering and phase coexistence in vibrated granular submonolayers. Nie *et al.* (2000) and Prevost *et al.* (2004) have reproduced certain features of cluster formation and two-phase coexistence by means of large-scale three-dimensional molecular-dynamics simulations. Since realistic three-dimensional simulations are still expensive and extremely time consuming, simplified modeling of a vibrating wall by a certain multiplicative random forcing on individual particles was employed by Cafiero *et al.* (2000). While the multiplicative random forcing is an interesting theoretical idea, it has to be used with caution as it is not guaranteed to reproduce the subtle details of particle dynamics, especially the sensitive dependence of the vertical to horizontal momentum transfer as a function of density.

C. Coarsening of clusters

One of the most intriguing questions in the context of phase coexistence in vibrofluidized granular submonolayers is the possibility of Ostwald-type ripening and coarsening of clusters similar to that observed in equilibrium systems (Lifshitz and Slyozov, 1958, 1961). In particular, the scaling law for the number of macroscopic clusters is of special interest because it gives a deep insight into the similarity between equilibrium thermodynamic systems and nonequilibrium granular systems. The experiments (Olafsen and Urbach, 1998; Losert *et al.*, 1999; Sapozhnikov *et al.*, 2003; Prevost *et al.*, 2004) demonstrated the emergence and growth of multiple clusters but did not have sufficient aspect ratios to address the problem of coarsening in a quantitative way.

Nevertheless, as suggested by Aranson *et al.* (2000), statistical information on out-of-equilibrium Ostwald ripening can be obtained in a different granular system: electrostatically driven granular media. This system permits operating with extremely small particles and obtains a large number of macroscopic clusters. In this system the number of clusters N decays with time as $N \sim 1/t$. This law is consistent with interface-controlled Ostwald ripening in two dimensions; see Wagner (1961). Whereas the mechanisms of energy injection are different, both vibrofluidized and electrostatically driven systems show similar behavior: macroscopic phase separation, coarsening, transition from two- to three-dimensional cluster growth, etc. (Sapozhnikov, Aranson, and Olafsen (2003). Aranson, Meerson, *et al.* (2002) developed a theoretical description of granular coarsening in application to electrostatically driven grains, however, we postpone the description of this theory to Sec. VIII.C. We anticipate that a theory similar to that formulated by Aranson, Meerson, *et al.* (2002) can be applied to mechanically fluidized granular materials as well. The main difference there is the physical mechanism of energy injection, which will possibly affect the specific form of the conversion rate function ϕ in Eq. (71) in Sec. VIII.C.

V. SURFACE WAVES AND PATTERNS IN VIBRATED MULTILAYERS OF GRANULAR MATERIALS

A. Chladni patterns and heaping

Driven granular systems often manifest collective fluidlike behavior: shear flows, convection, surface waves, and pattern formation [see Jaeger *et al.* (1996)]. Surprisingly, even very thin (less than ten) layers of sand under excitation exhibit pattern formation which is quite similar (however, with some important differences) to corresponding patterns in fluids. One of the most fascinating examples of these collective dynamics is the appearance of long-range coherent patterns and localized excitations in vertically vibrated thin granular layers.

Experimental studies of vibrated layers of sand have a long and illustrious history, beginning from the seminal works of Chladni (1787) and Faraday (1831) in which they used a violin bow and a membrane to excite vertical vibrations in a thin layer of grains. The main effect observed in those early papers was *heaping* of granular matter, or formation of mounds near the nodal lines of membrane oscillations. In fact, this phenomenon was used to visualize and study vibrational modes of membranes of different geometrical shapes at different frequencies. The behavior of powder on a vibrated plate was immediately (and correctly) attributed to the nonlinear detection of the nonuniform excitation of grains by membrane modes. One puzzling result of Chladni's work was that a very thin powder would collect at antinodal regions where the amplitude of vibrations is maximal. As Faraday demonstrated by evacuating the container, this phenomenon is caused by air permeating the grains in motion. A vibrating membrane generates convective flows in the air above it due to "acoustic streaming," and these flows transport sand towards antinodal regions. Evidently, the interstitial gas becomes important as the terminal velocity of a free fall $v_t = \nu g d^2/18\mu$ becomes of the order of the plate velocity, and this condition is fulfilled for 10–20-μm particles on a plate vibrating with frequency 50 Hz and acceleration amplitude g.

In subsequent years the focus of attention was diverted from dynamical properties of thin layers of vibrated sand, and only in the last third of the 20th century have physicists returned to this old problem equipped with new experimental capabilities. The dawn of the new era was marked by the studies of heaping by Jenny (1964). In subsequent papers (Walker, 1982; Dinkelacker *et al.*, 1987; Douady *et al.*, 1989; Evesque and Rajchenbach, 1989; Laroche *et al.*, 1989), more research on heaping was undertaken with and without interstitial gas, with somewhat controversial conclusions on the necessity of ambient gas for heaping [see, for example, Evesque (1990)]. Eventually, after more careful analysis, Pak *et al.* (1995) concluded that heaping indeed disappears as the pressure of the ambient gas tends to zero or the particle size increases. This agreed with numerical molecular-dynamics simulations (Gallas and Sokolowski, 1992; Gallas *et al.*, 1992a, 1992b, 1992c; Taguchi, 1992; Luding *et al.*, 1994), which showed no heaping without interstitial gas effects. Recent studies of deep layers ($50 < N < 200$) of small particles ($10 < d < 200$ μm) by Duran (2000, 2001), and Falcon, Wunenburger, *et al.* (1999) showed a number of interesting patterns and novel instabilities caused by interstitial air, e.g., Duran (2001) observed the formation of isolated droplets of grains after periodic tapping similar to the Rayleigh-Taylor instability in ordinary fluids.

Jia *et al.* (1999) proposed a simple model for heap formation which was motivated by these experiments. In a discrete lattice version of the model, the decrease in local density due to vibrations was modeled by the random creation of empty sites in the bulk. The bulk flow was simulated by the dynamics of empty sites, while the surface flow was modeled by rules similar to the sandpile model (see Sec. VI.B). This model reproduced both convection inside the powder and heap formation for a sufficiently large probability of empty-site formation (which mimics the magnitude of vibration). Jia *et al.* (1999) also proposed the continuum model, which has the simple form of a nonlinear reaction-diffusion equation, for the local height of the sandpile,

$$\partial_t h = D\nabla^2 h + \Omega h - \beta h^2. \tag{23}$$

However, this model is perhaps too generic and lacks the specific physics of the heaping process.

B. Standing-wave patterns

While heaping may or may not appear depending on the gas pressure and particle properties at small vertical acceleration, at higher vertical acceleration patterns of standing waves emerge in thin layers. They were first reported by Douady *et al.* (1989) and Fauve *et al.* (1989) in a quasi-two-dimensional geometry. These waves oscillated at half of the driving frequency, which indicated the subharmonic resonance characteristic for parametric instability. This first observation spurred a number of experimental studies of standing waves in thin granular layers in two- and three-dimensional geometries (Melo *et al.*, 1994, 1995; Clément *et al.*, 1996; Umbanhowar *et al.*, 1996; Mujica and Melo, 1998; Aranson, Blair, *et al.*, 1999). Importantly, these studies were performed in evacuated containers, which allowed them to obtain reproducible results not contaminated by heaping. Figure 3 shows a variety of regular patterns observed in vibrated granular layers under vibration (Melo *et al.*, 1994). As a result of these studies, the emerging picture of pattern formation appears as follows.

The particular pattern is determined by the interplay between driving frequency f and acceleration of the container $\Gamma = 4\pi^2 \mathcal{A} f^2/g$ ($\mathcal{A}$ is the amplitude of oscillations, g is the gravity acceleration) (Melo *et al.*, 1994, 1995). For $\Gamma < 1$ the layer lies on the plate, and particles do not lose contact with the plate surface. Furthermore, the layer remains flat for $\Gamma < 2.4$ more or less independent of driving frequency, even though it leaves the plate for a part of the vibration cycle. At higher Γ patterns of standing waves emerge which correspond to spatiotemporal

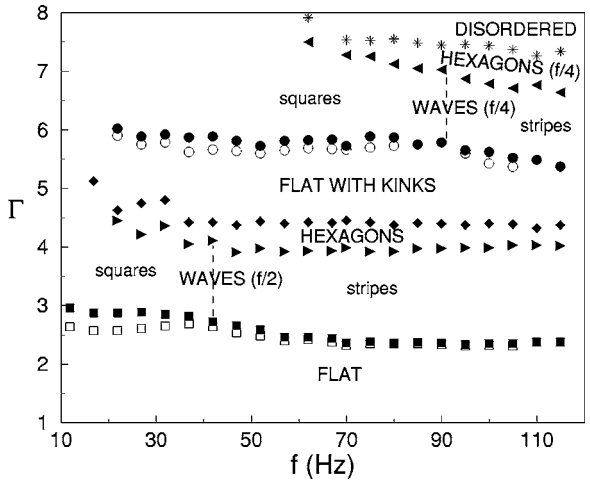

FIG. 17. Phase diagram of various regimes in vibrated granular layers. From Melo *et al.*, 1995.

variations of layer thickness and height. These variations are subharmonic: crests are replaced by troughs at successive periods of plate vibrations. At small frequencies $f<f^*$ [for the experimental conditions of Melo *et al.* (1995), $f^*\approx 45$ Hz], the transition is subcritical leading to the formation of square wave patterns; see Fig. 3(b). For higher frequencies $f>f^*$, the selected pattern is quasi-one-dimensional stripes [Fig. 3(a)], and the transition becomes supercritical. In the intermediate region $f\sim f^*$, various localized excitations were observed within the hysteretic region of the parameter plane. The simplest radially symmetrical localized structure, the *oscillon*, is shown in Fig. 4. This particlelike structure also oscillates at half of the driving frequency, so at one oscillation cycle it has a mound shape, and at the next cycle it forms a crater. These oscillons weakly interact with each other and form various bound states [Fig. 3(f)]. Both squares and stripes, as well as oscillons, oscillate at half of the driving frequency, which indicates the parametric mechanism of their excitation. The wavelength of cellular patterns near the onset scales linearly with the depth of the layer and diminishes with the frequency of vibration (Umbanhowar and Swinney, 2000). The frequency corresponding to the stripe square transition was shown to depend on the particle diameter d as $d^{-1/2}$. This scaling suggests that the transition is controlled by the relative magnitude of the energy influx from the vibrating plate $\propto f^2$ and the gravitational dilation energy $\propto gd$. At higher acceleration ($\Gamma>4$), stripes and squares become unstable, and hexagons appear instead [Fig. 3(c)]. Further increase of acceleration at $\Gamma\approx 4.5$ converts hexagons into a domainlike structure of flat layers oscillating with frequency $f/2$ with opposite phases. Depending on the parameters, interfaces separating flat domains are either smooth or "decorated" by periodic undulations [Fig. 3(e)]. For $\Gamma>5.7$ various quarter-harmonic patterns emerge. The complete phase diagram of different regimes observed in a three-dimensional container is shown in Fig. 17. For even higher acceleration ($\Gamma>7$), experiments reveal surprising phase bubbles and spatiotemporal chaos oscillating approximately at one-fourth the driving frequency (Moon *et al.*, 2002).

Subsequent investigations revealed that periodic patterns share many features with convective rolls in Rayleigh-Bénard convection, for example, skew-varicose and cross-roll instabilities (de Bruyn *et al.*, 1998).

C. Simulations of vibrated granular layers

A general understanding of standing-wave patterns in thin granular layers can be gained by an analogy with ordinary fluids. The Faraday instability in fluids and the corresponding pattern-selection problems have been studied theoretically and numerically in great detail [see Zhang and Viñals (1997)]. The primary mechanism of instability is the parametric resonance between the spatially uniform periodic driving at frequency f and two counterpropagating gravity waves at frequency $f/2$. However, this instability in ordinary fluids leads to a supercritical bifurcation and square wave patterns near onset, and as a whole the phase diagram lacks the richness of the granular system. Of course, this can be explained by the fact that there are many qualitative differences between granular matter and fluids, such as the presence of strong dissipation, friction, and the absence of surface tension in the former. Interestingly, localized oscillon-type objects were subsequently observed in vertically vibrated layers of a non-Newtonian fluid (Lioubashevski *et al.*, 1999), and stripe patterns were observed in a highly viscous fluid (Kiyashko *et al.*, 1996). A theoretical understanding of pattern formation in a vibrated granular system presents a challenge, since unlike fluid dynamics there is no universal theoretical description of dense granular flows analogous to the Navier-Stokes equations. In the absence of this common base, theoretical and computational efforts in describing these patterns followed several different directions. Aoki *et al.* (1996) were the first to perform molecular-dynamics simulations of patterns in the vibrated granular layer. They concluded that grain-grain friction is necessary for pattern formation in this system. However, as noted by Bizon *et al.* (1997), this conclusion is a direct consequence of the fact that the algorithm used by Aoki *et al.* (1996), which is based on the Lennard-Jones interaction potential and velocity-dependent dissipation, leads to the restitution coefficient of particles approaching unity for large collision speeds rather than decreasing according to experiments.

Bizon, Shattuck, Swift, *et al.* (1998) and Bizon, Shattuck, de Bruyn, *et al.* (1998) performed event-driven simulations of colliding grains on a vibrated plate assuming constant restitution [see also Luding *et al.* (1996) for earlier two-dimensional event-driven simulations]. It was demonstrated that even without friction patterns do form in the system, however, only supercritical bifurcation to stripes is observed. It turned out that friction is necessary to produce other patterns observed in experiments, such as squares and $f/4$ hexagons. Simulations with frictional particles reproduced the majority of pat-

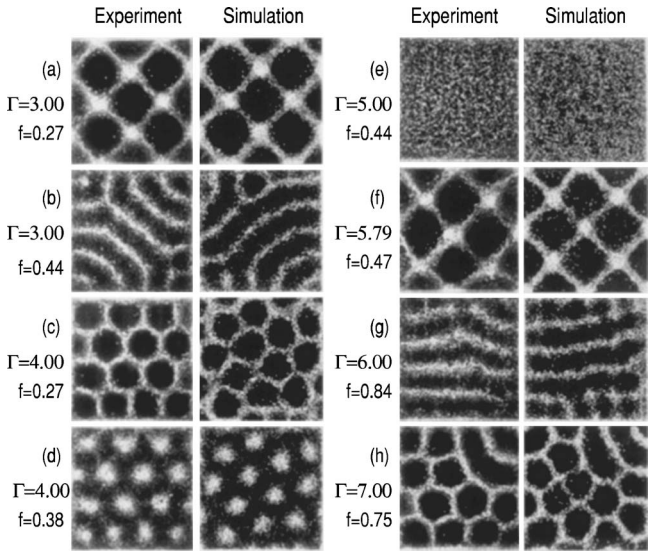

FIG. 18. Comparison between subharmonic patterns in experiment (left) and three-dimensional molecular-dynamics simulations (right) of 30 000 particles in a square vibrated container for different frequencies and amplitudes of vibration. From Bizon, Shattuck, Swift, *et al.*, 1998.

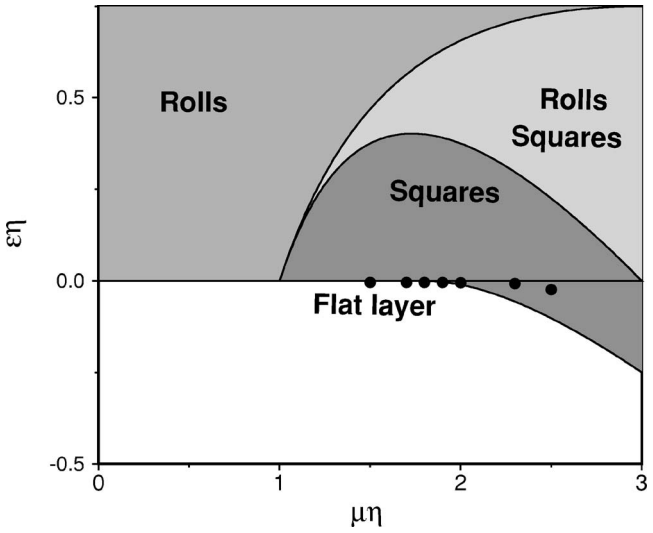

FIG. 19. Phase diagram showing primary stable patterns derived from Eqs. (24) and (25). Points indicate stable oscillons obtained by the numerical solution of Eqs. (24) and (25); $\eta = \alpha/\beta$, $\mu = \langle \nu \rangle$ is the average density, and $\epsilon \sim \gamma - \gamma_c$ is the supercriticality parameter. From Tsimring and Aranson, 1997.

terns observed in experiments and many features of the phase diagram (with the important exception of the oscillons). Bizon, Shattuck, Swift, *et al.* (1998) set out to match an experimental cell and a numerical system, maintaining exactly the same size container and same size and number of particles. After fitting only two parameters of the numerical model, Bizon, Shattuck, Swift, *et al.* (1998) were able to find close quantitative agreement between various patterns in the experimental cell and patterns in simulations throughout the parameter space of the experiment (frequency of driving, amplitude of acceleration, thickness of the layer); see Fig. 18.

Shinbrot (1997) proposed a model which combined ideas from molecular-dynamics and continuum modeling. Specifically, the model ignored the vertical component of particle motion and assumed that impact with the plate adds certain randomizing horizontal velocity to the individual particles. The magnitude of the random component being added at each impact served as a measure of impact strength. After the impact particles were allowed to travel freely in the horizontal plane for a certain fraction of a period after which they inelastically collide with each other (a particle acquires momentum averaged over all particles in its neighborhood). This model reproduced a variety of patterns seen in experiments (stripes, squares, and hexagons) for various values of control parameters (frequency of driving and impact strength), however, it did not describe some of the experimental phenomenology (localized objects as well as interfaces); besides, it also produced a number of intricate patterns not seen in experiments.

D. Continuum theories

The first continuum models of pattern formation in vibrating sand were purely phenomenological. In the spirit of weakly nonlinear perturbation theories Tsimring and Aranson (1997) introduced the complex amplitude $\psi(x,y,t)$ of subharmonic oscillations of the layer surface, $h = \psi \exp(i\pi ft) + \text{c.c.}$ The equation for this function on symmetry grounds in lowest order was written as

$$\partial_t \psi = \gamma \psi^* - (1 - i\omega)\psi + (1 + ib)\nabla^2 \psi - |\psi|^2 \psi - \nu\psi. \quad (24)$$

Here γ is the normalized amplitude of forcing at the driving frequency f. The linear terms in Eq. (24) can be obtained from the complex growth rate for infinitesimal periodic layer perturbations $h \sim \exp[\Lambda(k)t + ikx]$. Expanding $\Lambda(k)$ for small k, and keeping only two leading terms in the expansion $\Lambda(k) = -\Lambda_0 - \Lambda_1 k^2$, gives rise to the linear terms in Eq. (24), where $b = \text{Im}\,\Lambda_1 / \text{Re}\,\Lambda_1$ characterizes the ratio of dispersion to diffusion and the parameter $\omega = -(\text{Im}\,\Lambda_0 + \pi f)/\text{Re}\,\Lambda_0$ characterizes the frequency of the driving.

The only difference between this equation and the Ginzburg-Landau equation for the parametric instability (Coullet *et al.*, 1990) is the coupling of the complex amplitude ψ to the "slow mode" ν, which characterizes local dissipation in the granular layer (ν can be interpreted as the coarse-grained layer's number density). This slow mode obeys its own dynamical equation

$$\partial_t \nu = \alpha \boldsymbol{\nabla} \cdot (\nu \boldsymbol{\nabla} |\psi|^2) + \beta \nabla^2 \nu. \quad (25)$$

Equation (25) describes the redistribution of the averaged thickness due to the diffusive flux $\propto -\nabla\nu$, and an additional flux $\propto -\nu\nabla|\psi|^2$ is caused by spatially nonuniform vibrations of the granular material. This coupled model was used by Aranson and Tsimring (1997) and Tsimring and Aranson (1998) to describe the pattern selection near the threshold of the primary bifurcation. The phase diagram of various patterns found in this model is shown in Fig. 19. At small $\alpha\langle\nu\rangle\beta^{-1}$ (which cor-

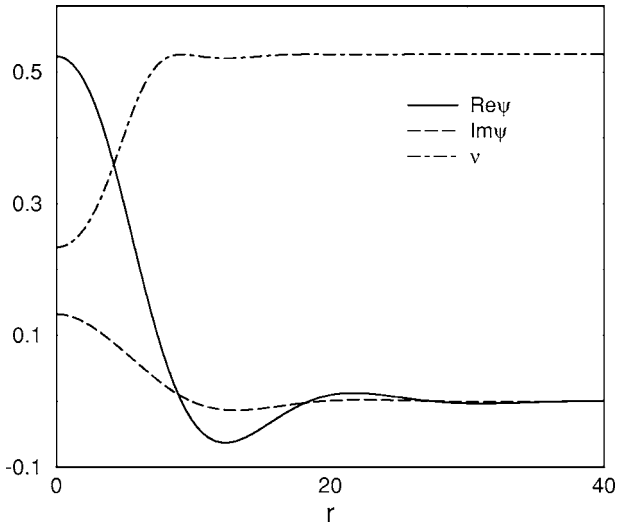

FIG. 20. Radially symmetric oscillon solution of Eqs. (24) and (25) for $\gamma=1.8$, $\mu=0.567$, $b=2$, $\omega=\alpha=1$, and $\eta=5/\gamma$. From Tsimring and Aranson, 1997.

responds to low frequencies and thick layers), the primary bifurcation is subcritical and leads to the emergence of square patterns. For higher frequencies and/or thinner layers, the transition is supercritical and leads to roll patterns. At intermediate frequencies, stable localized solutions of Eqs. (24) and (25) corresponding to isolated oscillons and a variety of bound states were found in agreement with experiment. The mechanism of oscillon stabilization is related to the oscillatory asymptotic behavior of the tails of the oscillon (see Fig. 20), since this underlying periodic structure provides pinning for the circular front forming the oscillon. Without such pinning, the oscillon solution could only exist at a certain unique value of a control parameter (e.g., γ) and would either collapse or expand otherwise.

We note that stable localized solutions somewhat resembling oscillons have recently been found in the nonlinear Schrödinger equation with additional linear dissipation and parametric driving (Barashenkov *et al.*, 2002).

The phenomenological model (24) and (25) also provides a good description of patterns away from the primary bifurcation—hexagons and interfaces (Aranson, Tsimring, *et al.*, 1999a). In the high-frequency limit the slow-mode dynamics can be neglected (ν becomes enslaved by ψ), and the dynamics can be described by a single parametric Ginzburg-Landau equation (24).

It is convenient to shift the phase of the complex order parameter via $\tilde{\psi}=\psi\exp(i\phi)$ with $\sin 2\phi=\omega/\gamma$. The equations for the real and imaginary parts of $\tilde{\psi}=A+iB$ are

$$\partial_t A = (s-1)A - 2\omega B - (A^2+B^2)A + \nabla^2(A-bB),$$

$$\partial_t B = -(s+1)B - (A^2+B^2)B + \nabla^2(B+bA), \qquad (26)$$

where $s^2=\gamma^2-\omega^2$. At $s<1$, Eqs. (26) have only one trivial uniform state $A=0$, $B=0$. At $s>1$, two new uniform states appear, $A=\pm A_0$, $B=0$, $A_0=\sqrt{s-1}$. The onset of these states corresponds to the period doubling of the layer flight sequence observed in experiments (Melo *et al.*, 1994, 1995) and predicted by the simple inelastic ball model (Mehta and Luck, 1990; Melo *et al.*, 1994, 1995). The $\pm$ signs reflect two relative phases of the layer flights with respect to container vibrations.

A weakly nonlinear analysis reveals that the uniform states $\pm A_0$ lose their stability with respect to finite wavenumber perturbations at $s<s_c$, and the nonlinear interaction of growing modes leads to hexagonal patterns. The reason for this is that the nonzero base state $A=\pm A_0$ lacks the up-down symmetry $\psi\rightarrow-\psi$ and the corresponding amplitude equations contain quadratic terms which are known to favor hexagons close to onset [see Cross and Hohenberg (1993)]. In the regime when the uniform states $A=\pm A_0$, $B=0$ are stable, there is an interface solution connecting these two asymptotic states. This interface may exhibit transversal instability, which leads to decorated interfaces [see Fig. 3(e)]. Due to symmetry, the interfaces are immobile, however breaking the symmetry of driving can lead to interface motion. This symmetry breaking can be achieved by additional subharmonic driving at frequency $f/2$. The interface will move depending on the relative phases of the f and $f/2$ harmonics of driving. This interface drift was predicted by Aranson, Tsimring, *et al.* (1999a) and observed in subsequent work (Aranson, Blair, *et al.*, 1999). As was noted by Aranson, Blair, *et al.* (1999) [see also later work by Moon *et al.* (2003)], moving interfaces can be used to separate granular material of different sizes. The stability and transition between flat and decorated interfaces was studied theoretically and experimentally by Blair *et al.* (2000). It was shown that nonlocal effects are responsible for the saturation of transverse instability of interfaces. Moreover, new localized solutions ("superoscillons") were found for large accelerations. In contrast with conventional oscillons existing on the flat background oscillating with driving frequency f, i.e., in our notation $\psi=0$, the superoscillons exist on the background of the flat period-doubled solution $\psi\neq 0$.

Another description of the primary pattern-forming bifurcation was by Crawford and Riecke (1999) in the framework of the generalized Swift-Hohenberg equation

$$\partial_t\psi = R\psi - (\partial_x^2+1)^2\psi + b\psi^3 - c\psi^5 + \varepsilon\,\boldsymbol{\nabla}\cdot[(\boldsymbol{\nabla}\psi)^3] - \beta_1\psi(\boldsymbol{\nabla}\psi)^2 - \beta_2\psi^2\nabla^2\psi. \qquad (27)$$

Here the (real) function ψ characterizes the amplitude of the oscillating solution, so implicitly it is assumed that the whole pattern always oscillates in phase. Terms proportional to ε have been added to the standard Swift-Hohenberg equation, first introduced for the description of convective rolls [see Cross and Hohenberg (1993)], since they are known to favor square patterns, and extended fifth-order local nonlinearity allowed the simulation of the subcritical bifurcation for $R<0$. Equation (27) also describes both square and stripe patterns depending on the magnitude of ε and for negative R has a stable oscillon-type solution.

An even more generic approach was taken by Venkataramani and Ott (1998, 2001), who argued that the spatiotemporal dynamics of patterns generated by parametric forcing can be understood in the framework of a discrete-time, continuous-space system, which locally exhibits a sequence of period-doubling bifurcations and whose spatial coupling operator selects a certain spatial scale. In particular, they studied the discrete-time system

$$\xi_{n+1}(\mathbf{x}) = \mathcal{L}[M(\xi_n(\mathbf{x}))], \tag{28}$$

where local mapping $M(\xi)$ is modeled by a Gaussian map

$$M(\xi) = \tilde{r}\exp[-(\xi-1)^2/2]$$

and the linear spatial operator $\mathcal{L}$ has an azimuthaly symmetric Fourier transform

$$f(k) = \mathrm{sgn}[k_c^2 - k^2]\exp\{\, k^2(1 - k^2/2k_0^2)/2k_0^2\}.$$

Here k is the wave number, k_c, k_0 are two inverse length scales characterizing the spatial coupling, and $\tilde{r}$ describes the amplitude of forcing. With an appropriate choice of the control parameters, this model leads to a phase diagram on the plane $(k_c/k_0, r)$, which is similar to the experimental one.

Several authors (Cerda *et al.*, 1997; Eggers and Riecke, 1999; Park and Moon, 2002) attempted to develop a quasi-two-dimensional fluid-dynamics-like continuum description of vibrated sand patterns. These models dealt with mass and momentum conservation equations, which were augmented by specific constitutive relations for the mass flux and pressure. Cerda *et al.* (1997) assumed that during impact particles acquired horizontal velocities proportional to the gradient of the local thickness, then during flight they moved freely with these velocities and redistributed the mass, and during the remainder of the cycle the layer diffusively relaxed on the plate. The authors found that a flat layer is unstable with respect to square pattern formation, however, the transition was supercritical. In order to account for the subcritical character of the primary bifurcation to square patterns, they postulated the existence of a certain critical slope (related to the angle of repose) below which the free flight initiated by the impact did not occur. They also observed the existence of localized excitations (oscillons and bound states), however, they appeared only as transients in the model. Park and Moon (2002) generalized this model by explicitly writing the momentum conservation equation and introducing the equation of state for the hydrodynamic pressure which is proportional to the square of the velocity divergence. This effect provides saturation of the free-flight focusing instability and leads to a squares-to-stripes transition at higher frequencies, which was missing in the original model (Cerda *et al.*, 1997). By introducing multiple free-flight times and contact times, Park and Moon (2002) were also able to reproduce hexagonal patterns and superlattices.

Full three-dimensional continuum studies of granular hydrodynamics, Eqs. (5)–(7), has been performed by Bougie *et al.* (2005). Quantitative agreement has been found between this description and the event-driven molecular-dynamics simulations and experiments in terms of the wavelength dependence on the vibration frequency (Fig. 21), although the authors had to introduce a certain regularization procedure in the hydrodynamic equations in order to avoid artificial numerical instabilities for $\nu \to 0$. Since standard granular hydrodynamics does not take into account friction among particles, the simulations have only yielded the stripe pattern, in agreement with earlier molecular-dynamics simulations. Furthermore, the authors have found a small but systematic difference ($\sim 10\%$) between the critical value of the plate acceleration in fluid-dynamical and molecular-dynamics simulations, which could be attributed to the role of fluctuations near the onset. A proper account of interparticle friction and fluctuations within the full hydrodynamics description still remains an open problem (see Sec. VI).

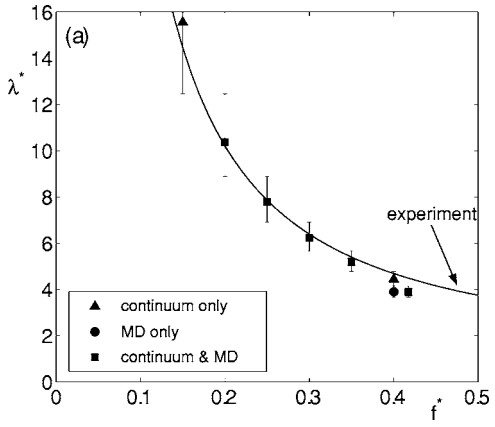

FIG. 21. Dispersion relation for stripes near the onset according to continuum granular hydrodynamics equations and molecular-dynamics simulations compared with experimental data. From Bougie *et al.*, 2005.

Fluctuations are expected to play a greater role in granular hydrodynamics than in usual fluids, because the total number of particles involved in the dynamics per characteristic spatial scale of the problem is many orders of magnitude smaller than the Avogadro number. The apparatus of fluctuating hydrodynamics, which was developed in particular for a description of the transition to rolls in Rayleigh-Bénard convection (Swift and Hohenberg, 1977), has been recently applied to granular patterns (Goldman *et al.*, 2004; Bougie *et al.*, 2005). The Swift-Hohenberg theory is based on the equation for the order parameter ψ,

$$\partial_t \psi = [\epsilon - (\nabla^2 + k_0^2)^2]\psi - \psi^3 + \eta(\mathbf{x},t), \tag{29}$$

where ϵ is the bifurcation parameter, k_0 is the wave number corresponding to unstable perturbations, and η is the Gaussian δ-correlated noise term with intensity F. The Swift-Hohenberg theory predicts that noise offsets the bifurcation value of the control parameter from the mean-field value $\epsilon_{\mathrm{MF}}=0$ to the critical value $\epsilon_c \propto F^{2/3}$. Furthermore, the Swift-Hohenberg theory describes the

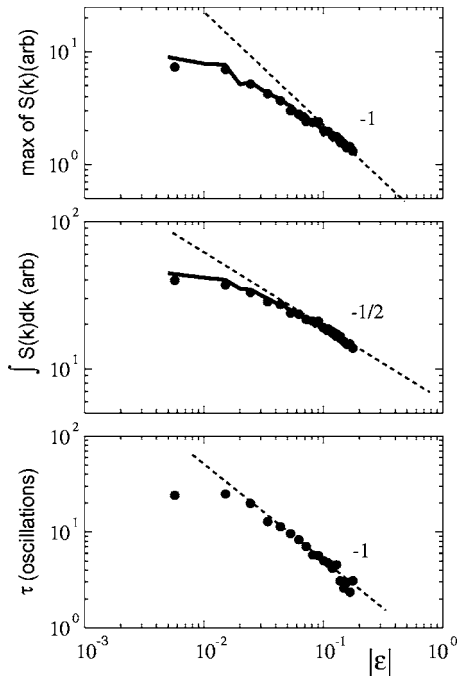

FIG. 22. Comparison between the Swift-Hohenberg theory and experiment for (a) noise peak intensity, (b) total noise power, and (c) the correlation time. ●, experiment; solid lines, Swift-Hohenberg theory; dashed lines, linear theory for small noise magnitude. From Goldman *et al.*, 2004.

transition to the linear regime, which is expected to work far away from the bifurcation point for small noise intensity when the magnitude of noise-excited modes scales as $|\epsilon-\epsilon_c|^{-1/2}$, while the time coherence of fluctuations and amplitude of spectral peaks decays as $|\epsilon-\epsilon_c|^{-1}$. Fitting the Swift-Hohenberg equation (29) to match the transition in the vibrated granular layer, Goldman *et al.* (2004) and Bougie *et al.* (2005) have found a good agreement with molecular-dynamics simulations and experiments (see Fig. 22). Interestingly, the magnitude of the fitted noise term in Eq. (29), $F\approx 3.5\times 10^{-3}$, turned out to be an order of magnitude greater than for convective instability in a fluid near a critical point (Oh and Ahlers, 2003). This difference with fluid dynamics probably stems from the fact that the granular system is not thermal, and fluctuations have a much higher effective temperature than that predicted by thermodynamics. An additional difference with fluids is that the classical Swift-Hohenberg theory developed for ordinary fluids is formally valid for second-order phase transitions (at least in the mean-field approximation), whereas in the vibrated granular layer with the parameters used by Goldman *et al.* (2004) and Bougie *et al.* (2005) the transition is known to be weakly first order and leads to square patterns rather than rolls. Consequently, nonlinear terms can be important close to the transition point and may distort the scaling of the fluctuation power.

There have been attempts to connect patterns in vibrated layers with the phenomenon of granular "thermoconvection." Since high-frequency vibration in many aspects is similar to a hot wall, it was argued that one should expect granular temperature gradients, density inversion, and, consequently, convection instability similar to that observed in heated from below liquid layers. The theoretical analysis based on granular hydrodynamics, Eqs. (5)–(7), supports the existence of a convective instability in a certain range of parameters (He *et al.*, 2002; Khain and Meerson, 2004). Multiple convection roles were observed in molecular-dynamics simulations (Sunthar and Kumaran, 2001; Paolotti *et al.*, 2004; Risso *et al.*, 2005). However, experiments are not conclusive enough (Wilman *et al.*, 2001). In particular, it appears hard to discriminate experimentally between convection induced by vibration and convective flows induced by walls; see, for example, Pak and Behringer (1993) and Garcimartín *et al.* (2002). However, inverse density profiles of vibrated two-dimensional granular material were indeed observed experimentally [granular Leidenfrost effect (Eshuis *et al.*, 2005)]. Talbot and Viot (2002) have presented a molecular-dynamics simulation study of a model motivated by the Wildman *et al.* (2001) work on the vibrofluidized system of glass spheres. The results have demonstrated the key role played by inelastic sphere-wall collisions in lowering the onset threshold for the convection roll. When elastic sphere-wall collisions were imposed, the convection roll was almost totally suppressed. More recently, Wildman *et al.* (2005) have conducted experimental and simulations studies of convection in vibrated annual granular beds. It has been shown that one can control the direction of rotation of the convection role by adjusting the restitution coefficient between particles and inner/outer walls.

A vibrated bottom plate is not the only way to induce parametric patterns in thin granular layers. Li *et al.* (2003) have demonstrated that periodically modulated airflow through a shallow fluidized bed also produces interesting patterns in the granular layer, which oscillate at half the driving frequency (Fig. 23). While the physical mechanism of interaction between the airflow and grains is quite different from the collisional energy transfer in vibrated containers, phenomenological models based on the principal symmetry of the problem should be able to describe the gas-driven granular layer as well. In case of the parametric Ginzburg-Landau model (24), the order parameter corresponds to the amplitude of the subharmonic component of the surface deformation, and the driving term is related to the amplitude of the flow modulation. Moreover, variations of the mean flow rate act similarly to variations of the gravitational acceleration in the mechanical system, which may give an additional means to control the state of the system.

VI. PATTERNS IN GRAVITY-DRIVEN DENSE GRANULAR FLOWS

In this section we give an overview of the theoretical models for various pattern-forming instabilities in dense gravity-driven granular flows.

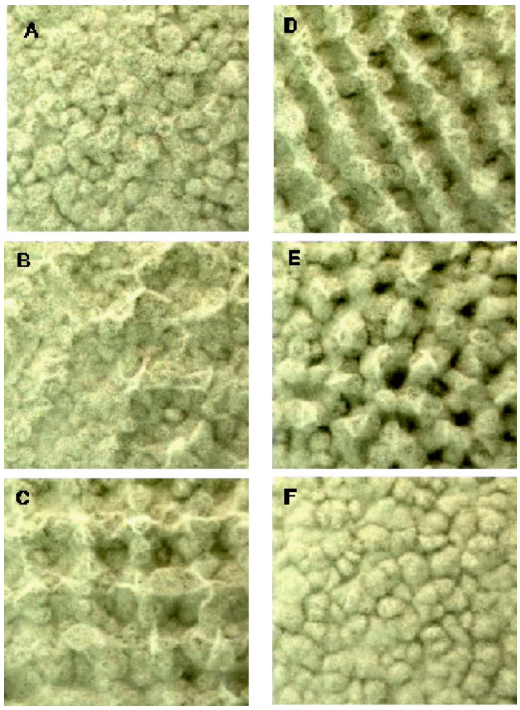

FIG. 23. (Color online) Selected patterns in a shallow fluidized bed with periodically modulated air flow. Snapshots of the granular layer surface are shown for different flow parameters. From Li *et al.*, 2003.

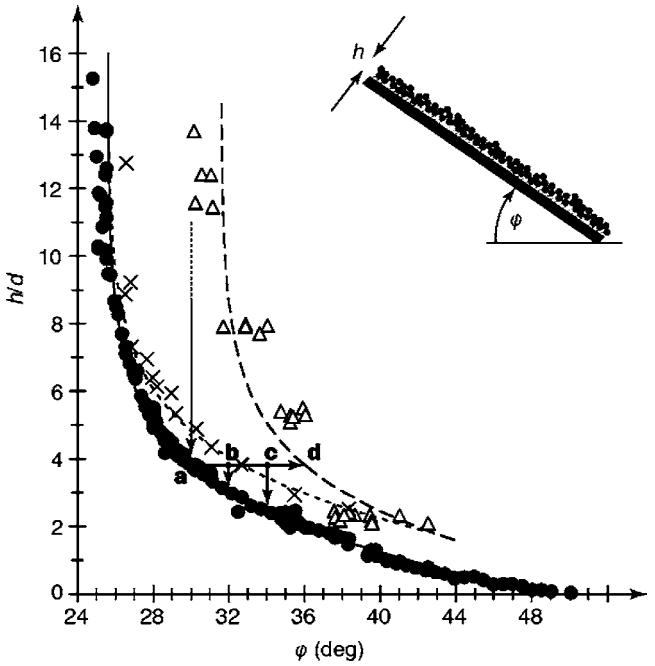

FIG. 24. Stability diagram for avalanches in thin layers; h is the layer thickness, d is the average grain size, and φ is the inclination angle (see also Fig. 6). From Daerr and Douady, 1999.

A. Avalanches in thin granular layers

Gravity-driven particulate flows are a common occurrence in nature (dune migration, erosion/deposition processes, landslides, underwater gravity currents, and coastal geomorphology) and in various industrial applications having to do with handling granular materials, including their storage, transport, and processing. One of the most spectacular (and often very dangerous) manifestations of gravity-driven granular flows is the avalanche. Avalanches occur spontaneously when the slope of the granular material exceeds a certain angle (static angle of repose) or they can be initiated at a somewhat smaller angle by applying a finite perturbation. Laboratory studies of avalanches are often carried out in rotating drums (see below) or in a chute geometry when a layer of sand is tilted at a certain fixed angle φ. Daerr and Douady (1999) have conducted experiments with a thin layer of granular matter on a sticky (velvet) inclined plane; see Fig. 24. In thin layers, the avalanche develops downstream from the point of initial perturbations and has a triangular shape with an opening angle which depends on the system parameters. In thicker and/or steeper layers, the region of flowing sand expands both downstream and upstream from the initial perturbation, however, the sand of course only flows downstream. The avalanche region in this case has a characteristic balloon shape; see Fig. 6. According to Rajchenbach (2002a, 2003), the rear front of the balloon-like avalanche propagates uphill with a velocity roughly one-half of the downhill velocity of the head front, and the velocity of the head is two times larger than the depth-averaged flow velocity. The stability diagram is outlined in Fig. 24: a granular layer is stable below the solid line [the h_{stop} limit according to Pouliquen (1999)], spontaneous avalanching was observed above the dashed line. Between the dashed and solid lines the layer exhibits bistable behavior: a finite perturbation can trigger an avalanche, otherwise the layer remains stable. The dotted line with cross symbols indicates the transition between triangular and balloon avalanches.

1. Partially fluidized flows

The avalanche dynamics described above is an example of a wide class of *partially fluidized* granular flows. In such flows some grains flow past each other while other grains maintain static contacts with their neighbors. The description of such flows still represents a major challenge for the theory: one is faced with the problem of constructing the constitutive relation for the stress tensor $\boldsymbol{\sigma}$. In dense flows a significant part of stresses is transmitted through quasistatic contacts between particles as compared with short collisions in dilute flows.

Stimulated by the nontrivial avalanche dynamics in experiments by Daerr (2001a, 2001b) and Daerr and Douady (1999), Aranson and Tsimring (2001, 2002) suggested a generic continuum description of partially fluidized granular flows. According to their theory, the ratio of the static part $\boldsymbol{\sigma}^s$ to the fluid part $\boldsymbol{\sigma}^f$ of the full stress tensor is controlled by the order parameter ρ. The order parameter is scaled in such a way that in a granular solid $\rho=1$ and in a well-developed flow (granular liq-

uid) $\rho \to 0$. On the "microscopic level," the order parameter is defined as a fraction of the number of static (or persistent) contacts of the particles Z_s to the total number of the contacts Z, $\rho = \langle Z_s/Z \rangle$ within a mesoscopic volume, which is large with respect to the particle size but small compared with the characteristic size of the flow.

Due to a strong dissipation in dense granular flows, the order parameter ρ is assumed to obey purely relaxational dynamics controlled by the Ginzburg-Landau-type equation for the generic first-order phase transition,

$$\frac{\partial \rho}{\partial t} + \mathbf{v} \nabla \rho = D \nabla^2 \rho - \frac{\partial F(\rho, \delta)}{\partial \rho}. \tag{30}$$

Here D is the diffusion coefficient. $F(\rho, \delta)$ is a free-energy density, which is postulated to have two local minima at $\rho = 1$ (solid phase) and $\rho = 0$ (fluid phase) to account for the bistability near the solid-fluid transition.

The relative stability of the two phases is controlled by the parameter δ, which in turn is determined by the stress tensor. The simplest assumption consistent with the Mohr-Coloumb yield criterion (Nedderman, 1992) is to take it as a function of $\phi = \max|\sigma_{mn}/\sigma_{nn}|$, where the maximum is sought over all possible orthogonal directions m and n (we consider only a two-dimensional formulation of the model). Furthermore, there are two angles which characterize the fluidization transition in the bulk of granular material, an internal friction angle $\tan^{-1}\phi_1$ such that if $\phi > \phi_1$ the static equilibrium is unstable, and the "dynamic angle of repose" $\tan^{-1}\phi_0$ such that at $\phi < \phi_0$ the "dynamic" phase $\rho = 0$ is unstable. Values of ϕ_0 and ϕ_1 depend on microscopic properties of the granular material, and in general they do not coincide. Aranson and Tsimring (2001, 2002) adopted the simple algebraic form of the control parameter δ,

$$\delta = (\phi^2 - \phi_0^2)/(\phi_1^2 - \phi_0^2). \tag{31}$$

Equation (30) has to be augmented by boundary conditions. While this is a complicated issue, in general, a simple but meaningful choice is to take no-flux boundary conditions at free surfaces and smooth walls and the solid-phase condition $\rho = 1$ near sticky or rough walls.

For the flow of thin granular layers on inclined planes, Eqs. (6) and (30) can be simplified. Using the no-slip boundary condition at the bottom and the no-flux condition at the top of the layer and fixing the lowest-mode structure of the order parameter in the direction perpendicular to the bottom of the chute ($z = 0$), $\rho = 1 - A(x,y)\sin(\pi z/h)$, h is the local layer thickness and $A(x,y)$ is a slowly varying function, one obtains equations governing the evolution of the thin layer (Aranson and Tsimring, 2001, 2002):

$$\partial_t h = -\alpha \partial_x (h^3 A) + \frac{\alpha}{\phi} \nabla (h^3 A \nabla h), \tag{32}$$

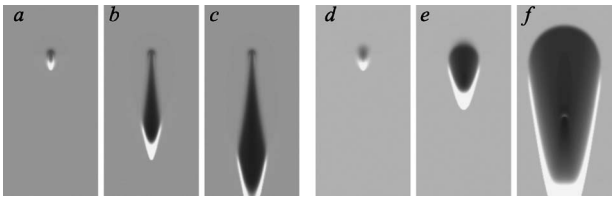

FIG. 25. Sequence of images demonstrating the evolution of (a)–(c) a triangular avalanche and (d)–(f) an uphill avalanche obtained from a numerical solution of Eqs. (33) and (32). From Aranson and Tsimring, 2001, 2002.

$$\partial_t A = \lambda A + \nabla_\perp^2 A + \frac{8(2-\delta)}{3\pi} A^2 - \frac{3}{4} A^3, \tag{33}$$

where $\nabla_\perp^2 = \partial_x^2 + \partial_y^2$, $\lambda = \delta - 1 - \pi^2/4h^2$, $\alpha \approx 0.12 \mu^{-1} g \sin\bar{\varphi}$, μ is the shear viscosity, $\bar{\varphi}$ is the chute inclination, and $\phi = \tan\bar{\varphi}$. The control parameter δ includes a correction due to the change in the local slope $\delta = \delta_0 + \beta h_x$, $\beta \approx 1/(\phi_1 - \phi_0) \approx 1.5$–$3$ depending on the value of ϕ. The last term in Eq. (32) is also due to the change of the local slope angle φ and is obtained from the expansion $\varphi \approx \bar{\varphi} + h_x$. This term is responsible for the saturation of the avalanche front slope (without it the front would be arbitrarily steep). While it was not included in the original publications (Aranson and Tsimring, 2001, 2002), this term is important for the large wave-number cutoff of long-wave instability observed by Forterre and Pouliquen (2003); see Sec. VI.C. Solutions of Eqs. (32) and (33) exhibit a strong resemblance to experiment: triangular avalanches in thin layers and balloonlike avalanches in thicker layers; see Fig. 25. The corresponding phase diagram agrees quantitatively with an experimental one having only one fitting parameter (viscosity μ), Fig. 26.

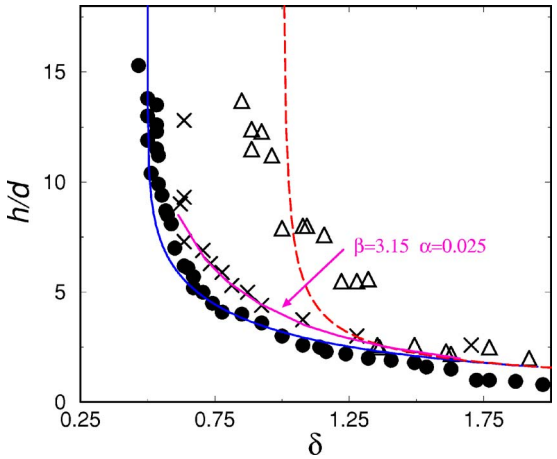

FIG. 26. (Color online) Comparison of theoretical and experimental phase diagrams. Lines obtained from theory; symbols depict experimental data from Daerr and Douady, 1999. Solid line and circles limit the range of existence of avalanches; line and triangles correspond to the linear stability boundary of the static chute, and the line and crosses denote the boundary between triangular and balloon avalanches. From Aranson and Tsimring, 2001, 2002.

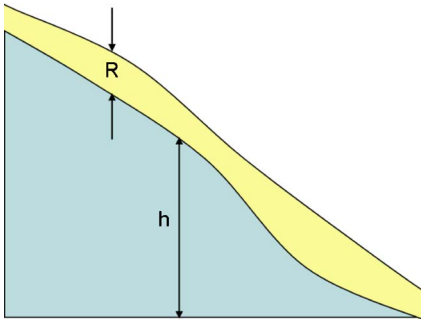

FIG. 27. (Color online) Schematic diagram of the Bouchaud-Cates-Ravi Prakash-Edwards (BCRE) model.

In subsequent work (Aranson and Tsimring, 2002), this theory was generalized to other dense shear granular flows including flows in rotating drums, two- and three-dimensional shear cells, etc. The model was also tested in soft-particle molecular-dynamics simulations (Volfson, Tsimring, and Aranson, 2003a, 2003b, 2004). Orpe and Khakhar (2006) have used the partial fluidization model of Aranson and Tsimring (2001, 2002) and Volfson, Aranson, and Tsimring (2003a) for a description of velocity profiles of three-dimensional shear flows in a rotating drum. The comparison between experimental data and theory shows that the partial fluidization model describes reasonably well the entire velocity profile and the flow rheology, however, experimental methods for independently estimating the order-parameter model are needed. Gao *et al.* (2005) have recently developed an objective (coordinate-system independent) formulation of the partial fluidization theory, which allows for a straightforward generalization to three-dimensional systems.

2. Two-phase flow approach of granular avalanches

Another approach treating near-surface granular flows as two-phase systems was developed by a number of authors; see Bouchaud *et al.* (1994, 1995), Mehta (1994), Boutreux *et al.* (1998), Douady *et al.* (1999), and Khakhar *et al.* (2001). For a review on recent models of surface flows, see Aradian *et al.* (2002). All these models distinguish rolling and static phases of granular flow described by the set of coupled equations for the evolution of thicknesses of both phases R and h, respectively (see Fig. 27). The phenomenological theory of Bouchaud *et al.* (1994, 1995) and Mehta (1994) (often called the BCRE theory) provides an intuitive description of the flow. In shallow granular layers, even simpler depth-averaged granular hydrodynamic equations (Saint-Venant models) often provide quite an accurate description; see Savage and Hutter (1989), Douady *et al.* (1999), Khakhar *et al.* (2001), and Lajeunesse *et al.* (2004).

The most general and compact form of the BCRE theory is represented by two equations for the evolution of R and h,

$$\partial_t h = \Gamma(h,R), \tag{34}$$

$$\partial_t R = v_d \partial_x R - \Gamma(h,R), \tag{35}$$

where $\Gamma(h,R)$ is the *exchange term*, or a conversion rate between rolling and static grains, and v_d is the downhill grain velocity. The physical meaning of the BCRE model is very simple: Eq. (34) expresses the increase in height due to the deposition of rolling grains, and Eq. (35) describes advection of the rolling fraction by flow with velocity v_d and depletion due to conversion to a static fraction. The limitations and generalizations of the BCRE model have been discussed by Boutreux *et al.* (1998) and Aradian *et al.* (2002).

Douady *et al.* (2002) applied the following two-phase model to describe avalanches in thin granular layers:

$$\partial_t h + 2U\partial_x h = \frac{g}{\bar{\Gamma}}[\tan\varphi - \mu(h)], \tag{36}$$

$$\partial_t \zeta + 2U\partial_x h = 0, \tag{37}$$

where $\zeta = R + h$ is the position of the free surface and U is the depth-averaged velocity of the flow. In addition to the BCRE model, Eqs. (36) and (37) include two phenomenological functions: $\bar{\Gamma}$ characterizes the mean velocity gradient of a single bead on incline and $\mu(h)$ describes the depth-dependent friction with the bottom. According to Douady *et al.* (2002), a three-dimensional version of Eqs. (36) and (37) describes the transition from triangular to uphill avalanches, however, details of the transition depend sensitively on the choice of the functions $\bar{\Gamma}$ and $\mu(h)$.

A depth-averaged description in the form of Eqs. (36) and (37) has been used by Börzsönyi *et al.* (2005) to address the difference between shapes of avalanches for sand and glass particles in a chute flow. The authors have reduced Eqs. (36) and (37) to the modified Burgers equation

$$\partial_t h + a(h)\partial_x h = \mu(h)\partial_x^2 h, \tag{38}$$

where $a(h) \sim h^{3/2}$ and the effective viscosity $\mu \sim \sqrt{h}$. This description connects avalanches with the Burgers shocks. Equation (38) implies that all avalanches will eventually decay, in contrast to experiments indicating that only small avalanches decay, whereas large avalanches grow and/or form stationary waves (Daerr and Douady, 1999; Daerr, 2001a). This discrepancy is likely due to the fact that reduction of the full model (36) and (37) to the single equation (38) does not take into account the bistable nature of granular flows.

While a two-phase description of granular flow is simple and rather intuitive, it can be problematic when a clear-cut separation between rolling and static phases is absent, especially near the onset of motion. The order-parameter approach can be more appropriate in this situation. Furthermore, the two-phase equations can be derived from the partial fluidization model described in Sec. VI.A.1 as a sharp-interface limit of the continuum order-parameter model (Aranson and Tsimring, 2002).

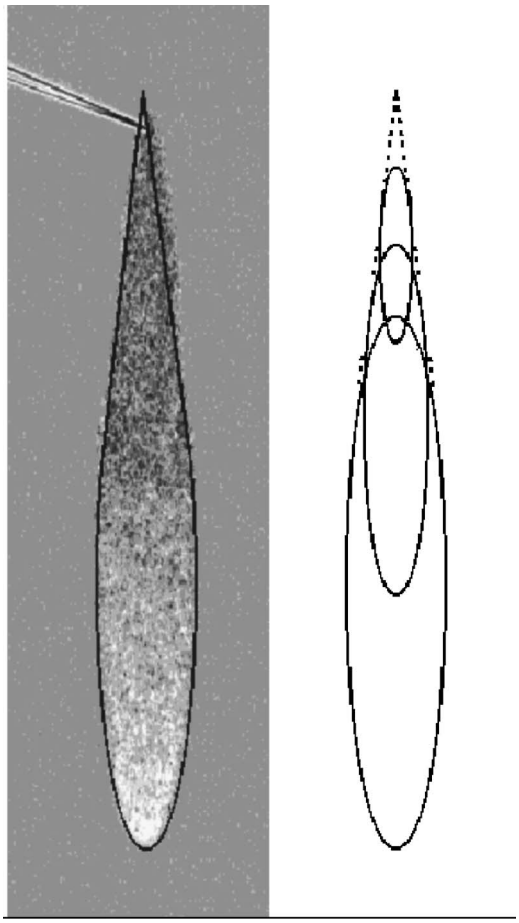

FIG. 28. Shape of triangular avalanche. Left, solid line, total area overrun by the avalanche compared with the experimental image. From Daerr and Douady, 1999. Right, superimposition of avalanche boundaries given by Eq. (40) for three different moments of time. From Rajchenbach, 2002b.

3. Avalanche shape

On the basis of simple kinematic considerations, Rajchenbach (2002b) had suggested an expression for the shape of triangular and balloonlike avalanches. For balloonlike avalanches, the shape is given by the envelope of expanding circles with the center drifting downhill:

$$x^2 + (y - 2\bar{v}t + \tfrac{5}{2}\bar{v}\tau)^2 = (\tfrac{1}{2}\bar{v}\tau)^2, \quad 0 < \tau < t, \tag{39}$$

where $\bar{v}$ is the velocity of the rear front. For triangular avalanches, the shape is given by the envelope of dilating ellipses,

$$\left(\frac{\bar{v}x}{2v_\perp}\right)^2 + \left(y - \frac{3}{2}\bar{v}t\right)^2 = \left(\frac{1}{2}\bar{v}t\right)^2. \tag{40}$$

Here $v_\perp$ is the perpendicular velocity. While these heuristic relations are consistent with experimental observation (see Fig. 28), their connection to continuum dynamical models of granular flows remains to be understood.

B. Statistics of avalanches and the sandpile model

It is well known that in real sandpiles avalanches can vary widely in size. The wide distribution of scales in real avalanches stimulated Bak *et al.* (1987) to introduce a "sandpile cellular automaton" as a paradigm model for the *self-organized criticality*, the phenomenon which occurs in slowly driven nonequilibrium spatially extended systems when they asymptotically reach a critical state characterized by a power-law distribution of event sizes. The set of rules which constitute the sandpile model is very simple. Unit size "grains" are dropped one by one on a one-dimensional lattice in random places and form vertical stacks. If a local slope (the difference between heights of two neighboring stacks) exceeds a certain threshold value, a grain hops from the higher to the lower stack. This may trigger an "avalanche" of subsequent hops until the sandpile returns to the stable state. After that another grain is dropped and the relaxation process repeats. The size of an avalanche is determined by the number of grains set into motion by adding a single grain to a sandpile. This model asymptotically reaches a critical state in which the mean angle is equal to the critical slope, and avalanches have a universal power-law distribution of sizes $P(s) \propto s^{-\alpha}$ with $\alpha \approx 1.5$.

The relevance of this model and its generalizations to real avalanches are still a matter of debate. The sandpile model developed by Bak *et al.* (1987) was defined via a single angle of repose and so its asymptotic behavior had the properties of the critical state for a second-order phase transition. Real sandpiles are characterized by two angles of repose and thus exhibit features of the first-order phase transition. Moreover, the concept of self-organized criticality is related to a power-law distribution of avalanche sizes, thus reliable experimental verification of self-organized criticality requires the accumulation of very large statistics of avalanche events and a large-scale experimental setup. Finite-size effects should strongly affect the power-law behavior.

Experiments with avalanches in slowly rotating drums (Jaeger *et al.*, 1989; Rajchenbach, 2000) and chute flows (Lemieux and Durian, 2000) did not confirm the scale-invariant distribution of avalanches. In other experiments with large monodisperse glass beads dropped on a conical sandpile, Costello *et al.* (2003) have claimed the existence of self-organized criticality with $\alpha \approx 1.5$. Characteristics of the size distribution depended on the geometry of the sandpile, the physical and geometrical properties of the grains, and the way the grains were dropped on the pile, contrary to the universal concept of self-organized critical behavior. Self-organized criticality was also claimed in the avalanche statistics in three-dimensional piles of anisotropic grains (long rice), however, a smaller scaling exponent, $\alpha \approx 1.2$, was measured for the avalanche size distribution (Aegerter *et al.*, 2003). Interestingly, rice piles were found to demonstrate roughening dynamics of their surface as the distribution of active sites in the self-organized critical state showed a self-affine structure with the fractal exponent $d_B = 1.85$ (Aegerter *et al.*, 2003, 2004). This is consistent with

the theoretically predicted mapping between self-organized criticality and roughening observed, for example, in the Kardar-Parizi-Zhang model (Paczuski and Boettcher, 1996).

One can argue that real sandpiles should not exhibit self-organized criticality in a strict sense due to hysteresis and the existence of two angles of repose. However, since the difference between the angles is relatively small, one cannot exclude power-law-type behavior in the finite range of avalanche sizes. This circumstance possibly explains the significant scatter in experimental results and scaling exponents for an avalanche size distribution and the dependence on grain shape and material properties.

C. Instabilities in granular chute flows

Granular chute flows exhibit a variety of pattern-forming instabilities, including fingering (Pouliquen *et al.*, 1997; Malloggi *et al.*, 2005a), longitudinal vortices (Forterre and Pouliquen, 2001, 2002), long surface waves (Forterre and Pouliquen, 2003), segregation and stratification (Gray and Hutter, 1997; Makse, Havlin, *et al.*, 1997), etc.

Pouliquen *et al.* (1997) have experimentally studied a granular chute flow on a rough inclined plane. Experiments performed with polydisperse sand particles demonstrated fingering instability of the front propagating down the slope, similar to that observed in fluid films flowing down an inclined plane (Troian *et al.*, 1989; Zhou *et al.*, 2005). However, similar experiments with smooth monodisperse glass beads exhibited no instability. The authors argued that the instability was due to a flow-induced size segregation in a polydisperse granular matter. The segregation was found near the avalanche front. However, similar experiments (Malloggi *et al.*, 2005a,) have shown a fingering front instability without a significant size segregation. Thus the question of the mechanism of fingering instability is still open.

Experiments by Forterre and Pouliquen (2001, 2002), showed the development of longitudinal vortices in rapid chute flows; see Fig. 8. The vortices developed for large inclination angles and large flow rates in the regime of accelerating flow when the flow thickness decreased and the mean flow velocity increased along the chute. Forterre and Pouliquen (2001) proposed an explanation of this phenomenon in terms of granular *thermoconvection*. Namely, rapid granular flow has a high shear near the rough bottom which leads to the local increase of granular temperature and consequently creates a density inversion. In turn, the density inversion triggers a convection instability similar to that in ordinary fluids. The instability wavelength λ_c is determined by the depth of the layer h (in experiment $\lambda_c \approx 3h$).

In a subsequent work, Forterre and Pouliquen (2002) have studied the formation of longitudinal vortices and stability of granular chute flows in the framework of granular hydrodynamics Eqs. (5)–(7). The inverse density profile appears when a heuristic boundary condition at the bottom relating slip velocity and heat flux is introduced. A steady-state solution of Eqs. (5)–(7) indeed yields an inverse density profile (Fig. 29), which turns out to be unstable with respect to short-wavelength perturbations for large flow velocities; see Fig. 30. While the linear stability analysis captured many important features of the phenomenon, there are still open questions. The stability analysis was performed for the steady flow, whereas the instability occurs in the regime of accelerating flow. Possibly due to this assumption, the linear stability analysis yielded oscillatory instability near the onset of vortices, whereas for the most part the vortices appear to be steady. Another factor which is ignored in the theory is air drag. The high flow velocity in the experiment (about 1–2 m/sec) is of the order of the terminal velocity of an individual grain in air, and therefore air drag may affect the granular flow.

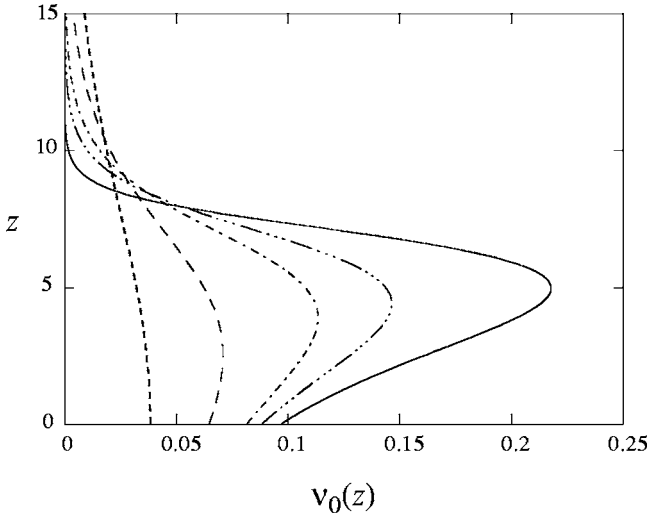

FIG. 29. Density profiles $\nu(z)$ as a function of distance from the chute bottom z for different values of mean flow velocity. From Forterre and Pouliquen, 2002.

Forterre and Pouliquen (2003) have presented an experimental study of the long surface wave instability developing in granular flows on a rough inclined plane (see Fig. 31). This instability was known from previous studies (Savage, 1979; Davies, 1990), however, no precise characterization of the instability had been performed. Forterre and Pouliquen (2003) have measured the threshold and dispersion relation of the instability by imposing a controlled perturbation at the inlet of flow and measuring its evolution down the slope; see Fig. 32. The results are compared with the linear stability analysis conducted with depth-averaged Saint-Venant-type equations similar to those described in Sec. VI.A.2:

$$\partial_t h + \partial_x(uh) = 0,$$

$$\partial_t(uh) + \alpha\partial_x(u^2 h) = [\tan\varphi - \mu(u,h) - \partial_x h]gh\cos(\varphi), \tag{41}$$

where h is the local thickness, φ is the inclination angle, u is the depth-averaged flow velocity, $\mu(h,u)$ is a function describing effective depth and velocity-dependent bottom friction, and $\alpha \sim O(1)$ is a constant determined

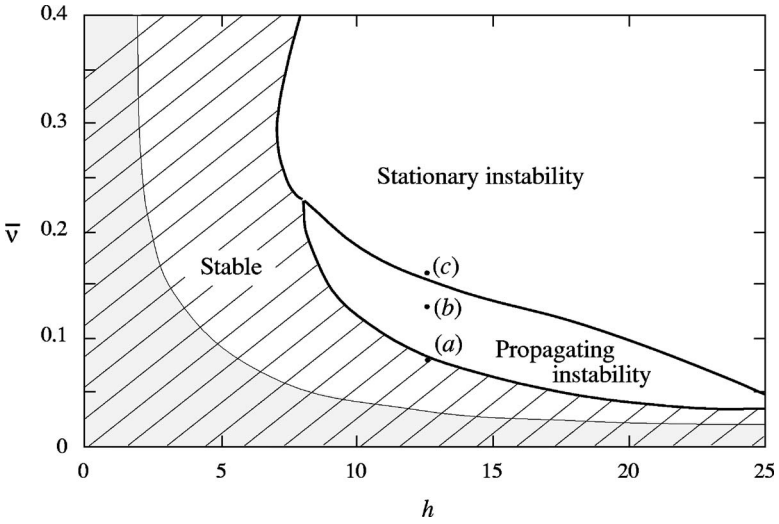

FIG. 30. Phase diagram in mean density ($\bar{\nu}$) and flow thickness (h) plane delineating various flow instabilities. Smaller $\bar{\nu}$ corresponds to faster flow. From Forterre and Pouliquen, 2002.

by the velocity profile within the layer. According to Forterre and Pouliquen (2003), the instability is similar to the long-wave instability observed in classical fluids but with characteristics that can dramatically differ due to the specificity of the granular rheology. The theory is able to predict quantitatively the stability threshold and phase velocity of the waves but fails to describe the observed cutoff of the instability at high wave numbers. Most likely, one needs to include higher-order terms such as $\partial_x^2 h$ in the first Eq. (41) in order to account for the cutoff.

The order-parameter theory based on Eqs. (32) and (33) also reproduces the long surface-wave instability.

FIG. 31. (Color online) Long surface-wave instability observed in the flow of sand down a rough incline. From Forterre and Pouliquen, 2003.

Furthermore, by linearizing Eqs. (32) and (33) near the steady flowing solution, $A=A_0+\tilde{a}\exp[\sigma t+ikx]$, $h=h_0+\tilde{h}\exp[\sigma t+ikx]$, one obtains, after simple algebra, that the growth rate of linear perturbations σ is positive only in a band restricted by some critical wave number and only in the vicinity of h_{stop} (see Fig. 33). With the increase of h, i.e., the granular flux, the instability disappears, in agreement with experiments. The nonlinear saturation of the instability results in the development of a sequence of avalanches, which is generally nonperiodic (see Fig. 34). The structure shows slow coarsening due to merging of avalanches. This instability is a possible candidate mechanism for the formation of the inhomogeneous deposit structure behind the front of an avalanche.

Conway *et al.* (2003) have studied free-surface waves in granular chute flows near a frictional boundary. The experiments have shown that the sub-boundary circulation driven by the velocity gradient plays an important role in the pattern formation, suggesting a similarity between wave generation in granular and fluid flows.

A Kelvin-Helmholtz-like shear instability in chute flows was observed by Goldfarbs *et al.* (2002) when two streams of sand flowing on an inclined plane with different velocities were in side-by-side contact with each other. For sufficiently high chute angles and shear rates the interface remains flat. The instability of the interface develops when the chute angle and/or shear rate is reduced. This instability has been reproduced in soft-particle molecular-dynamics simulations by Ciamarra *et al.* (2005), who also observed that in a polydisperse medium this instability leads to grain segregation (see below Sec. VII).

D. Pattern-forming instabilities in rotating cylinders

Granular media in rotating horizontal cylinders (drums) often show behavior similar to chute flows. For very small rotation rates (as defined by a small Froude number $\text{Fr}=\omega^2 R/g$, where ω is the angular velocity of drum rotation and R its radius) well separated in time,

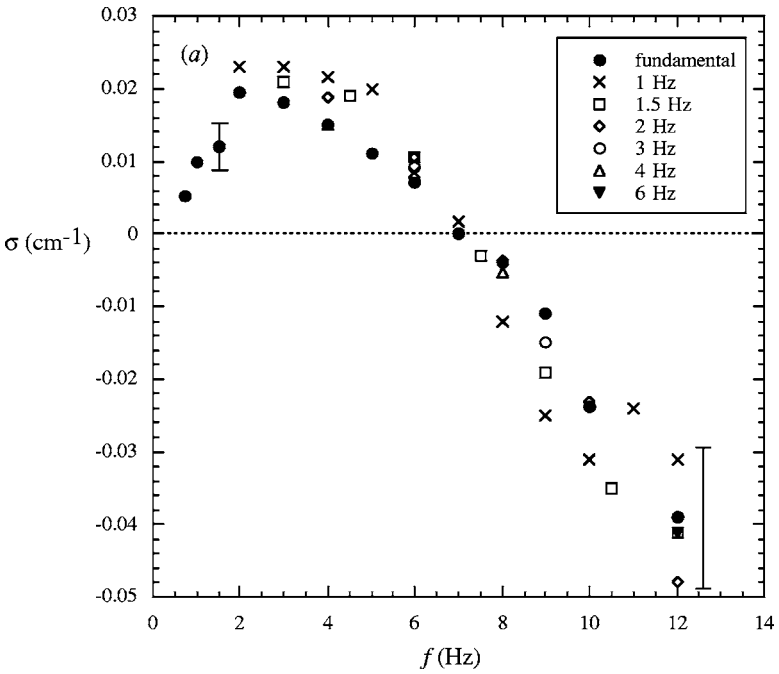

FIG. 32. Spatial growth rate σ of long surface-wave instability as a function of the frequency of the forcing wave f. From Forterre and Pouliquen, 2003.

avalanches occur when the slope of the free surface exceeds a certain critical angle φ_c thereby diminishing this angle to a smaller static angle of repose φ_s (Jaeger *et al.*, 1989; Rajchenbach, 1990; Tegzes *et al.*, 2002, 2003). The difference between φ_c and φ_s is usually a few degrees. At an intermediate rotation speed, a continuous flow of sand emerges instead of discrete avalanches through a hysteretic transition, similar to the transition in chute flows at large rates of grain deposition (Lemieux and Durian, 2000). In the bulk, the granular material rotates almost as a solid body with some internal slipping. As moving grains reach the free surface, they slide down within a thin near-surface layer (Zik *et al.*, 1994) (see sketch in Fig. 9). The surface has a nearly flat shape; the arctangent of its average slope defines the so-called dynamic angle of repose φ_d.

There are various models addressing the nature of the transition from discrete avalanches to continuum flow. Linz and Hänggi (1995) proposed a phenomenological model based on a system of equations for the angle of repose φ and mean flow velocity v,

$$\dot{v} = g[\sin\varphi - k(v)\cos\varphi]\chi(\varphi, v),$$

$$\dot{\varphi} = \bar{\omega} - av, \tag{42}$$

where $\bar{\omega}$ is the rotation frequency of the drum, $k(v) = b_0 + b_2 v^2$ is the velocity-dependent friction coefficient, $\chi(\varphi, v)$ is some cutoff function, and a, b_0, b_2 are the parameters of the model. Despite the simplicity, the model yields a qualitatively correct transition from discrete avalanches to continuous flow with the increase of rotation rate $\bar{\omega}$ and also predicts logarithmic relaxation of the free-surface angle in the presence of vibration.

The transition from avalanches to flow naturally arises in the framework of the partial fluidization theory

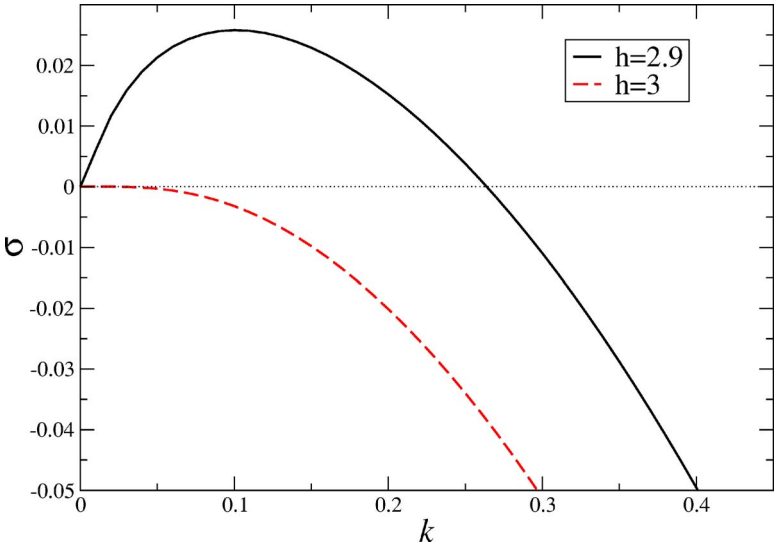

FIG. 33. (Color online) The growth rate of small perturbations σ vs wavelength k derived from Eqs. (32) and (33) for $\beta=2$, $\alpha=0.025$, and $\delta=1.1$. Instability occurs near the h_{stop} curve in Figs. 24 and 26 ($h=2.9$) and disappears with a further increase of h.

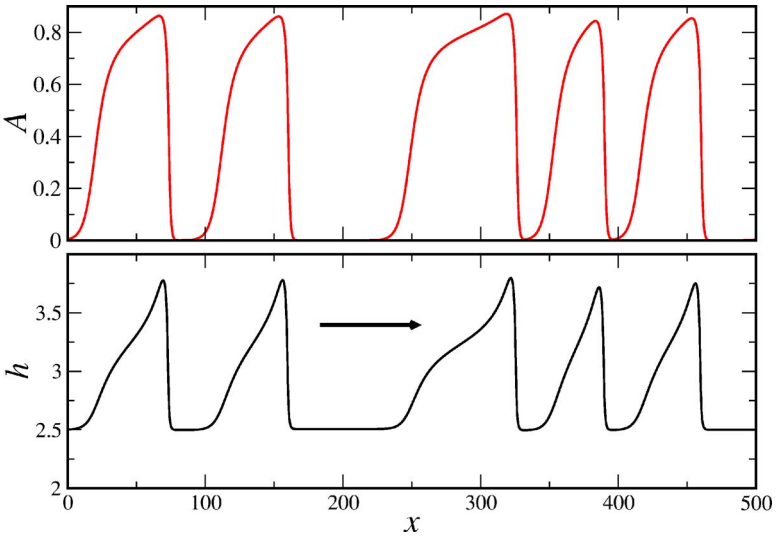

FIG. 34. (Color online) Typical profiles of height h and order parameter A in the regime of long surface-wave instability for $\beta=2$, $\alpha=0.025$, and $\delta=1.1$. Starting from generic initial conditions $h=h_0$, $A=$const plus small noise, a sequence of avalanches develops.

(Aranson and Tsimring, 2002). In this case, one can derive a system of coupled equations for the parameter δ [which is related to the surface local angle φ; see Eq. (31)] and the width of the fluidized layer z_0,

$$\partial_t z_0 = \partial_s^2 z_0 + F(z_0,\delta) - \bar{v}\partial_s z_0,$$

$$\partial_t \delta = \bar{\omega} + \partial_s^2 J, \tag{43}$$

where s is the coordinate along the slope of the granular surface inside the drum, $J=f(z_0)$ is the downhill flux of grains, $\bar{v}$ is the averaged velocity in the flowing layer, and the functions F, f, and v_0 are derived from Eq. (30). This model bears a resemblance to the BCRE-type models of surface granular flows, which were applied to rotating drums by Khakhar *et al.* (1997) and Makse (1999).

Equations (43) exhibit stick-slip-type oscillations of the surface angle for slow rotation rates and a hysteretic transition to a steady flow for larger rates, and they yield the following scaling for the width of the flowing layer z_0 in the middle of the drum versus rotation frequency: $z_0 \sim \bar{\omega}^{2/3}$, which is consistent with experiment (Tegzes *et al.*, 2002, 2003). After integration over s, Eqs. (43) can be reduced to a system of two coupled equations for averaged drum angle $\langle\delta\rangle$ and averaged flow thickness $\langle z_0\rangle$, somewhat similar to the model of Linz and Hänggi (1995).

Granular flows in long rotating drums under certain conditions also exhibit fingering instability (Fried *et al.*, 1998; Shen, 2002). Similarity between fingering in rotating drums and chute flows (Forterre and Pouliquen, 2002) suggests that mechanisms described in Sec. VI.C can be responsible for this effect; see also Sec. VII.

VII. MODELS OF GRANULAR SEGREGATION

One of the most fascinating features of heterogeneous (i.e., consisting of different distinct components) granular materials is their tendency to segregate under external agitation rather than to mix, as one would expect from the naive entropy consideration. This property is ubiquitous in nature [see Iverson (1997)] and has important technological implications (Cooke *et al.*, 1976). In fact, some aspects of the segregation of small and large particles can be understood on equilibrium thermodynamics grounds (Asakura and Oosawa, 1958). Since the excluded volume for small particles around large ones becomes smaller when large grains clump together, a separated state possesses lower entropy. However, granular systems are driven and strongly dissipative, and this simple equilibrium argument can only be applied qualitatively. Granular segregation is more widespread than would be dictated by thermodynamics. In fact, any variation in the mechanical properties of particles (size, shape, density, surface roughness, etc.) may lead to their segregation. At least for bidisperse rapid dilute flows, granular segregation can be rigorously treated in the framework of the kinetic theory of dissipative gases; see Sec. III.B. Jenkins and Yoon (2002) have employed the kinetic theory for a binary mixture of spheres or disks in gravity and derived a simple segregation criterion based on the difference of the partial pressures for each type of particle due to the difference in size and/or mass.

Segregation has been observed in most flows of granular mixtures, including granular convection (Knight *et al.*, 1993), hopper flows (Gray and Hutter, 1997; Makse, Havlin, *et al.*, 1997; Samadani *et al.*, 1999; Samadani and Kudrolli, 2001), flows in rotating drums (Zik *et al.*, 1994; Choo *et al.*, 1997; Hill, 1997), and even in freely cooling binary granular gases (Cattuto and Marconi, 2004). Segregation among large and small particles due to shaking has been termed the Brazil nut effect (Rosato *et al.*, 1987). The phenomenon of granular segregation was discovered a long time ago, and several "microscopic" mechanisms have been proposed to explain its nature, including interparticle collisions (Brown, 1939), percolation (Williams, 1976), and others. In certain cases, separation of grains produces interesting patterns. For example, if a binary mixture of particles which differ both in size and in shape is poured down a plane, a heap which consists of thin alternating layers of separated

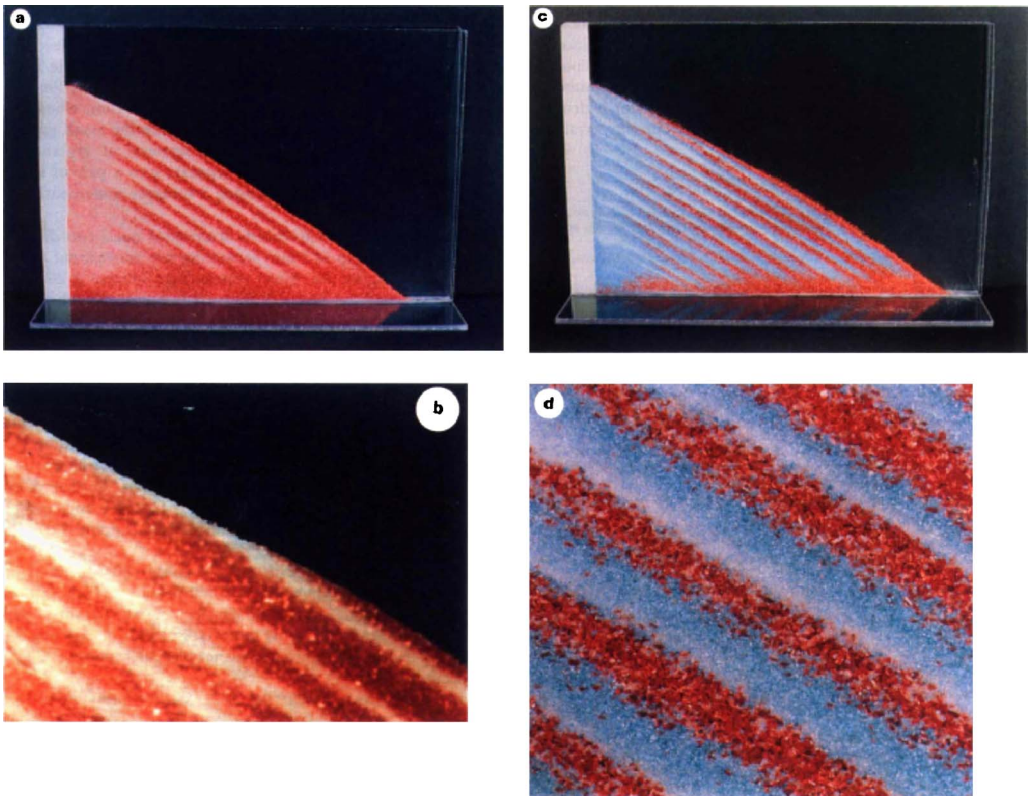

FIG. 35. (Color online) Granular stratification in a flow down a two-dimensional sandpile between two glass walls. A side view of the stratified sandpile is shown for different parameters and magnifications. From Makse, Havlin, *et al.*, 1997.

particles is formed (Gray and Hutter, 1997; Makse, Havlin, *et al.*, 1997); see Fig. 35. The rotating of mixtures of grains with different sizes in long drums produces well-separated bands of pure monodisperse particles (Zik *et al.*, 1994; Chicarro *et al.*, 1997; Choo *et al.*, 1997; Hill, 1997), see Fig. 11. In this section we only address models of pattern formation due to segregation (stratification and banding), without discussing other manifestations of granular segregation.

A. Granular stratification

Granular stratification occurs when a binary mixture of particles with different physical properties is slowly poured on a plate (Gray and Hutter, 1997; Makse, Havlin, *et al.*, 1997; Koeppe *et al.*, 1998). More specifically, it occurs when larger grains have, additionally, larger roughness, resulting in a larger angle of repose and the flux of falling particles is small enough to cause intermittent avalanches down the slopes of the heap. The basic mechanism of stratification is related to the avalanches acting as *kinetic sieves* (Savage, 1988, 1993; Gray and Thornton, 2005). During an avalanche, voids are continuously being created within a flowing near-surface layer, and small particles are more likely to fall into them. This creates a downward flux of smaller particles, which is compensated by the upward flux of larger particles in order to maintain a zero total particle flux across the flowing layer. Other models of granular segregation in a thin flowing layer (Khakhar *et al.*, 1997, 1999; Dolgunin *et al.*, 1998) lead to a similar result. Each avalanche leads to the formation of a new pair of layers in which the grains of different sorts are separated (see Fig. 35). This pair of layers grows from the bottom of the pile by upward propagation of a kink at which small particles are stopped underneath large ones. However, when larger particles were smooth and small particles were rough, instead of stratification only large-scale segregation with small particles near the top and large particles near the bottom was observed.

Makse, Cizeau, *et al.* (1997) and Makse, Havlin, *et al.* (1997) have proposed a cellular automata model, which generalized the classical sandpile model (Bak *et al.*, 1987); see Sec. VI.B. In this model, a sandpile is built on a lattice, and the rectangular grains have identical horizontal size but different heights [see Fig. 36(a)]. Grains are released at the top of the heap sequentially, and they are allowed to roll down the slope. A particle would become rolling if the local slope (defined as the height difference between neighboring columns) exceeds the angle of repose. To account for the difference in grain properties, four different angles of repose $\varphi_{\alpha\beta}$ were introduced for grains of type α rolling on a substrate of type β ($\alpha,\beta\in\{1,2\}$, where 1 and 2 stand for small and large grains, respectively). Normally, $\varphi_{21}<\varphi_{12}$ because of the geometry (small grains tend to get trapped by large grains), and one-component angles of repose usually lie within this range, $\varphi_{21}<\varphi_{11},\varphi_{22}<\varphi_{12}$. However, the ratio of $\varphi_{11},\varphi_{22}$ depends on the relative roughness of grains. For $\varphi_{21}<\varphi_{11}<\varphi_{22}<\varphi_{12}$ (large grains are more rough),

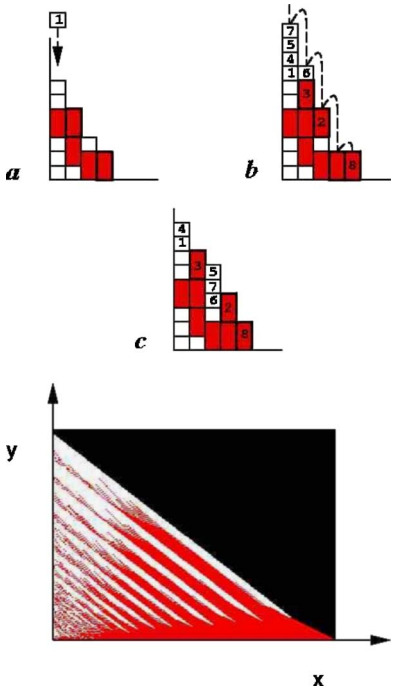

FIG. 36. (Color online) Cellular automata model of granular stratification. (a)–(c) Relaxation rules. Bottom image shows representative stratification patterns obtained in numerical simulations. From Makse, Havlin, *et al.*, 1997.

the model yields stratification in agreement with experiment [see Fig. 36(b)]. If, on the other hand, $\varphi_{22}<\varphi_{11}$ (which corresponds to smaller grains being more rough), the model yields only large-scale segregation: large particles collect at the bottom of the sandpile.

This physical model can also be recast in the form of continuum equations (Boutreux and de Gennes, 1996; Makse, Cizeau, *et al.*, 1997), which generalize the single-species BCRE model of surface granular flows (Bouchaud *et al.*, 1994) (see Sec. VI):

$$\partial_t R_\alpha = -v_\alpha \partial_x R_\alpha + \Gamma_\alpha, \tag{44}$$

$$\partial_t h = -\sum_\alpha \Gamma_\alpha, \tag{45}$$

where $R_\alpha(x,t), v_\alpha$ are the thickness and velocity of rolling grains of type α, $h(x,t)$ is the instantaneous profile of the sandpile, and Γ_α characterizes the interaction between the rolling grains and substrate of static grains. In the same spirit as in the discrete model, the interaction function Γ_α is chosen in the form

$$\Gamma_\alpha = \begin{cases} \gamma_\alpha[\varphi_l - \varphi_\alpha(\phi_\beta)]R_\alpha, \\ \gamma_\alpha \phi_\alpha[\varphi_l - \varphi_\alpha(\phi_\beta)]R_\alpha. \end{cases} \tag{46}$$

Here $\phi_\alpha(x,t)$ is the volume fraction of grains of type α and $\varphi_l = -\partial_x h$ is the local slope of the sandpile. This form of the interaction terms implies that grains of type α become rolling if the local slope exceeds the angle of repose $\varphi_\alpha(\phi_\beta)$ on a surface with composition $\phi_\beta(x,t)$. Assuming that the generalized angles of repose $\varphi_\alpha(\phi_\beta)$ are linear functions of the concentration,

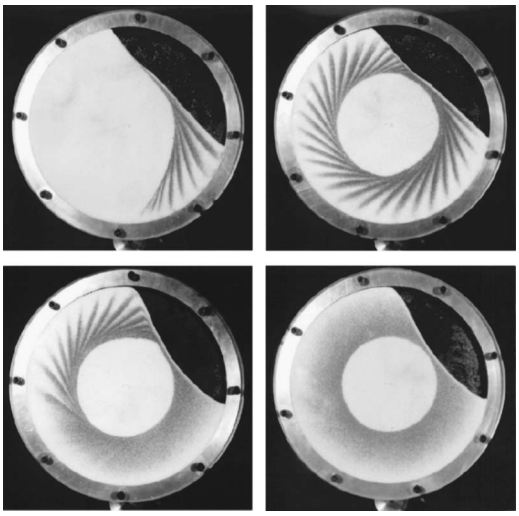

FIG. 37. Granular avalanche-induced stratification in a rotating drum observed for low rotation rates. Side view of the drum is shown at different times after the beginning of the revolutions; dark and light regions correspond to high concentrations of two different species comprising the mixture. From Gray and Hutter, 1997.

$$\varphi_1(\phi_2) = (\varphi_{12} - \varphi_{11})\phi_2 + \varphi_{11}, \tag{47}$$

$$\varphi_2(\phi_2) = (\varphi_{12} - \varphi_{11})\phi_2 + \varphi_{21}. \tag{48}$$

Equations (44)–(46) possess a stationary solution in which the heap is separated into two regions, where $\varphi_2(\phi_2)<\varphi<\varphi_1(\phi_2)$ and $\varphi<\varphi_2(\phi_2)<\varphi_1(\phi_2)$. This solution corresponds to small grains localized near the top and small grains near the bottom with a continuous transition between the two regions. Makse, Havlin, *et al.* (1997) have shown that this stationary solution is unstable if $\delta=\varphi_{22}-\varphi_{11}>0$ and gives rise to the stratification pattern.

A similar effect of stratification patterns was observed experimentally in a thin slowly rotating drum which was more than half filled with a similar binary mixture (Gray and Hutter, 1997); see Fig. 37. Periodic avalanches, occurring in the drum, led to the formation of strata by the same mechanism described above.

Recently Gray and Thornton (2005) have proposed a continuum theory of particle-size segregation in shallow granular free-surface flows. The theory, based on the assumption of kinetic sieving of large and small grains in a shear avalanche-type flow, is formulated in terms of granular hydrodynamics equations (5) and (6) for each phase [small (s) and large (l) particles]. The interaction between phases is introduced through the additional interaction drag terms $\beta_{s,l}$ in Eq. (6):

$$\beta^i = p\,\nabla f^i - \nu^i c(\mathbf{u}^i - \mathbf{u}), \quad i = l,s, \tag{49}$$

where the factors $f^{s,l}$ determine the proportion of hydrostatic load carried by small and large particles, p is the pressure, $u^{s,l}$ and $\nu^{s,l}$ are partial velocities and densities of each phase, and $c=$const is the coefficient of interparticle drag. Assuming some functional dependence of the

factors $f^{l,s}$ on the corresponding filling fractions $\phi^{s,l}$, the model reproduces certain experimental features, e.g., formation of segregation shocks. An open question is, however, the applicability of this approach to dense granular flows in which the validity of hydrodynamics is rather limited (see Sec. III.B).

B. Axial segregation in rotating drums

The most common system in which granular segregation is studied is a rotating drum or a partially filled cylinder rotating around its horizontal axis (see Sec. VI.D). When a polydisperse mixture of grains is rotated in a drum, strong *radial segregation* usually occurs within just a few revolutions. Small and rough particles aggregate to the center (*core*) of the drum, large and smooth particles rotate around the core (see Figs. 9 and 10). Since there is almost no shear flow in the bulk, the segregation occurs predominantly within a thin fluidized near-surface layer. For long narrow drums, with length exceeding the radius, radial segregation is often followed by *axial segregation* occurring at later stages (after several hundred revolutions) when the angle of repose of small particles exceeds that of large particles. As a result of axial segregation, a pattern of well-segregated bands is formed (Zik *et al.*, 1994; Hill, 1997) (see Fig. 11), which slowly merge and coarsen. Depending on the rotation speed, coarsening can either saturate at a certain finite bandwidth at low rotation speeds when discrete avalanches provide granular transport (Frette and Stavans, 1997), or at higher rotation rates in a continuous-flow regime it can lead to a final state in which all sand is separated in two bands (Zik *et al.*, 1994; Fiedor and Ottino, 2003; Arndt *et al.*, 2005).

Axial segregation has been well known in the engineering community; it was first observed by Oyama (1939). The different frictional properties of grains lead to different dynamic angles of repose. These are defined as the angle of the slope in the drum corresponding to the continuous-flow regime, however, in real drums the free surface often has a more complicated S shape (Zik *et al.*, 1994; Elperin and Vikhansky, 1998; Makse, 1999; Orpe and Khakhar, 2001). It is appealing to suggest that variations in dynamic angles of repose provide the driving mechanism for axial segregation. This approach was adopted by early models. According to Zik *et al.* (1994) [see also Levine (1999)] if there is a local increase in the concentration of particles with higher dynamic angles of repose, the local slope there will be higher, and that will lead to a local bump near the top of the free surface and a dip near the bottom. As particles tend to slide along the steepest descent path, more particles with higher angles of repose will accumulate in this location, and instability will develop. Zik *et al.* (1994) have proposed a quantitative continuum model of axial segregation based on the conservation law for the relative concentration of the two components ("glass" and "sand"), $c(z,t)=(\nu_A-\nu_B)/(\nu_A+\nu_B)$,

FIG. 38. Image of a shish-kebab-like structure of smaller particles in a rotating drum (illuminated from below). Smaller particles (shown in dark) form bands between bands of larger particles (disconnected rings, shown in white and gray). From Arndt *et al.*, 2005.

$$\partial_t c = -\frac{C}{\nu_T}(\tan\varphi_A - \tan\varphi_B)\partial_z(1-c^2)\left\langle (1+y_x^2)\frac{y_z}{y_x}\right\rangle. \tag{50}$$

Here x and z are Cartesian horizontal coordinates across and along the axis of the drum, $y(x,z,t)$ describes the instantaneous free surface inside the drum, $\nu_T=\nu_A+\nu_B$, and C is a constant related to gravity and the effective viscosity of the granular material in the flowing layer. The term in angular brackets denotes the axial flux of glass beads averaged over the cross section of the drum. The profile of the free surface $y(x,z)$ in turn should depend on $c(z,t)$. If $\langle(1+y_x^2)y_c/y_x\rangle<0$, linearization of Eq. (50) leads to the diffusion equation with a negative diffusion coefficient, which exhibits segregation instability with a growth rate proportional to the square of the wave number. Zik *et al.* (1994) have concluded that the term in angular brackets vanishes for a straight profile $y_x=$const due to the assumption that y_z changes sign exactly in the middle of the drum, and as a result mixing-demixing processes cancel precisely. However, for the experimentally observed S-shaped profile of the free surface, Zik *et al.* (1994) have calculated that the instability condition is satisfied when the drum is more than half full. While experiments show that axial segregation is in fact observed for even less than a 50% filling ratio, the model gives a good intuitive picture for a possible mechanism of instability. Later calculations by Aranson, Tsimring, *et al.* (1999b) showed that segregation generally occurs for straight profiles if the drum filling ratio is different from 50%.

Recent experiments (Choo *et al.*, 1997, 1998; Hill, 1997; Fiedor and Ottino, 2003; Alexander *et al.*, 2004; Arndt *et al.*, 2005; Charles *et al.*, 2005) have revealed interesting new features of axial segregation. Hill (1997) has performed magnetic-resonance imaging studies, which demonstrated that in fact the bands of larger particles usually have a core of smaller particles. More recent experiments by Fiedor and Ottino (2003) and Arndt *et al.* (2005) have shown that small particles form a "shish-kebab-like" (wavy) structure with bands connected by a rodlike core, while large particles form disconnected rings (see Fig. 38). Choo *et al.* (1997, 1998) have found that at early stages small-scale perturbations propagated across the drum in both directions [this was clearly evidenced by experiments on the dynamics of presegregated mixtures (Choo *et al.*, 1997)], while at later times more long-scale static perturbations took over and led to the emergence of quasistationary bands

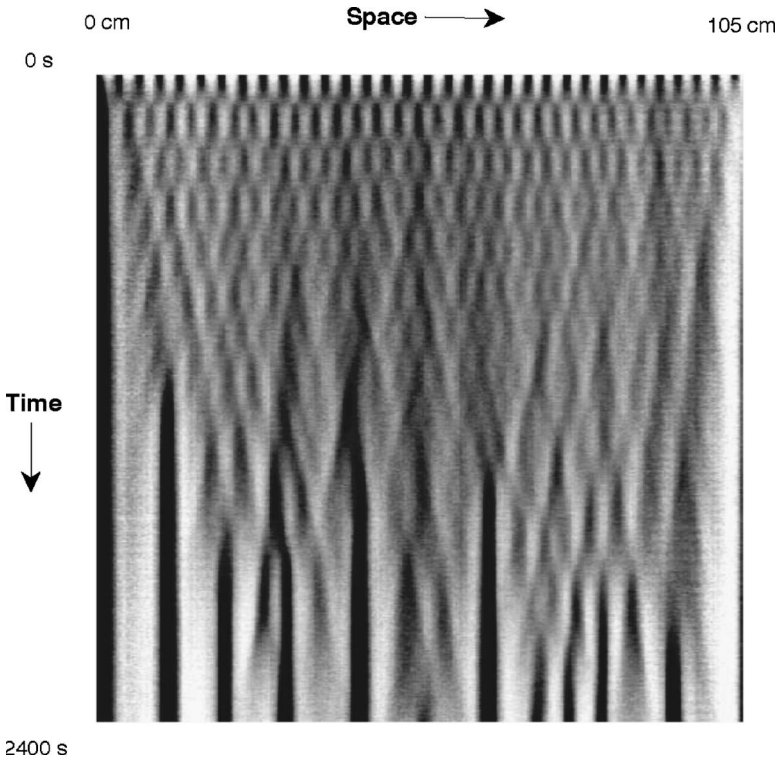

FIG. 39. Space-time diagram of the surface of a long rotating drum demonstrating oscillatory size segregation. The full length of the drum is shown and extends over 2400 sec, or 1850 revolutions. Black bands correspond to 45–250 μm black sand and white bands correspond to 300–850 μm table salt. From Choo *et al.*, 1997.

of separated grains (see Fig. 39). The slow coarsening process can be accelerated in a drum of helical shape (Zik *et al.*, 1994). Alternatively, bands can be locked in an axisymmetric drum with the radius modulated along the axis (Zik *et al.*, 1994). Studies by Alexander *et al.* (2004) and Charles *et al.* (2005) have revealed scaling of the axial band size with drum diameter and grain size. In particular, segregation shuts off (or develops infinitely slowly) if the ratio of the drum diameter to the grain size is too small. The band spacing also scales in a nontrivial way with the drum diameter.

In order to account for the oscillatory behavior of axial segregation at the initial stage, Aranson and Tsimring (1999) and Aranson, Tsimring, *et al.* (1999b) have generalized the model of Zik *et al.* (1994). The key assumption was that besides the concentration difference there is an additional slow variable which is involved in the dynamics. Aranson and Tsimring (1999) and Aranson, Tsimring, *et al.* (1999b) have conjectured that this variable is the instantaneous slope of the granular material (dynamic angle of repose), which unlike Eq. (50) is not slaved to the relative concentration c but obeys its own dynamics. The equations of the model read

$$\partial_t c = -\partial_z[-D\partial_z c + g(c)\partial_z \varphi], \tag{51}$$

$$\partial_t \varphi = \alpha[\Omega - \varphi + f(c)] + D_\varphi \partial_{zz}\varphi + \gamma \partial_{zz} c. \tag{52}$$

The first term on the right-hand side of Eq. (51) describes diffusion flux (mixing), and the second term describes the differential flux of particles due to the gradient of the dynamic angle of repose. This term is equivalent to the right-hand side of Eq. (50), with a particular function $g(c)=G_0(1-c^2)$. For simplicity, the constant G_0 can be eliminated by rescaling the distance $x \to x/\sqrt{G_0}$. The + sign before this term means that particles with the larger static angle of repose are driven towards a greater dynamic angle of repose. This differential flux gives rise to the segregation instability. Since this segregation flux vanishes with $g(c)|c| \to 1$ (which corresponds to pure A or B states), it provides a saturation mechanism for the segregation instability.

The parameter Ω in Eq. (52) is the normalized angular velocity of the drum rotation and $f(c)$ is the static angle of repose, which is an increasing function of the relative concentration (Koeppe *et al.*, 1998) [for simplicity it can be assumed to be linear, $f(c)=F+f_0 c$]. The constant F can be eliminated by the substitution $\varphi \to \varphi - F$. The first term on the right-hand side of Eq. (52) describes the local dynamics of the angle of repose [Ω increases the angle, and $-\varphi+f(c)$ describes the equilibrating effect of the surface flow], and the term $D_\varphi \partial_{xx}\varphi$ describes axial diffusive relaxation. The last term $\gamma \partial_{xx} c$ represents the lowest-order nonlocal contribution from an inhomogeneous distribution of c (the first derivative $\partial_x c$ cannot be present due to reflection symmetry $x \to -x$). This term gives rise to the transient oscillatory dynamics of the binary mixture.

A linear stability analysis of a homogeneous state $c=c_0$, $\varphi_0=\Omega+f_0 c_0$, reveals that for $g_0 f_0 > \alpha D$ long-wave perturbations are unstable, and if $g_0\gamma > (D_\varphi - D)^2/4$, short-wave perturbations oscillate and decay (the two eigenvalues $\lambda_{1,2}$ are complex conjugates with a negative real part for modulation wave numbers $|k| > k^*$); see Fig. 40. This agrees with the general phenomenology observed by Choo *et al.* (1997) both qualitatively and even quantitatively [Fig. 40(b)]. The results of a direct numerical solution of the full model (51) and (52) are illus-

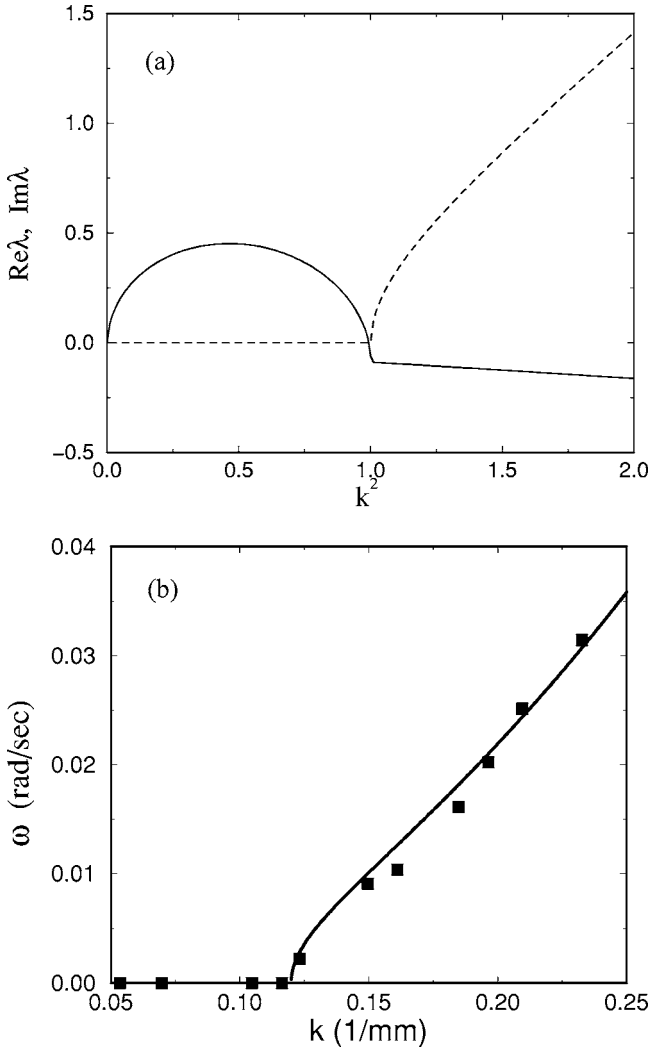

FIG. 40. Segregation instability in Eqs. (51) and (52). (a) Dispersion relation $\lambda(k)$ for the segregation instability; $\mathrm{Re}\,\lambda$ is shown by the solid line, and $\mathrm{Im}\,\lambda$ is shown by the dashed line. $\mathrm{Im}\,\lambda \neq 0$ for $k > k^* \approx 1$. (b) Solid line, comparison of the frequency of band oscillations $\mathrm{Im}(\lambda)$ with ■, experiment. From Aranson and Tsimring, 1999.

trated in Fig. 41. It shows that short-wave initial perturbations decay and give rise to more long-wave nonoscillatory modulations of concentration, which eventually lead to well-separated bands. At long times (Fig. 41, right), the bands exhibit slow coarsening with the number of bands decreasing logarithmically with time [see also Frette and Stavans (1997), Levitan (1998), and Frette and Ottino (2003)]. This scaling follows from the exponentially weak interaction between interfaces separating different bands (Fraerman *et al.*, 1997; Aranson and Tsimring, 1999).

While these continuum models of axial segregation showed a good qualitative agreement with the data, recent experimental observations demonstrate that the theoretical understanding of axial segregation is far from complete (Ottino and Khakhar, 2000). The interpretation of the second slow variable as the local dynamic angle of repose implies that in the unstable mode the slope and concentration modulation should be in phase, whereas in the decaying oscillatory mode these two fields have to be shifted in phase. Further experiments (Khan *et al.*, 2004) have shown that while the in-phase relationship in the asymptotic regime holds true, the quadrature phase shift in the transient oscillatory regime is not observed.[5] That led Khan *et al.* (2004) to hypothesize that some other slow variable other than the angle of repose (possibly related to the core dynamics) may be involved in the transient dynamics. However, so far experiments have failed to identify which second dynamical field is necessary for oscillatory transient dynamics, so it remains an open problem. Another recent experimental observation by Khan and Morris (2005) has suggested that instead of the normal diffusion assumed in Eqs. (51) and (52), a slower subdiffusion of particles in the core takes place, $\langle r \rangle \sim t^{\gamma}$ with the scaling exponent γ close to 0.3. The most plausible explanation is that the apparent subdiffusive behavior is in fact a manifestation of a nonlinear concentration diffusion, which can be described by the equation

$$\partial_t c = \partial_z D(c) \partial_z c. \tag{53}$$

For example, for the generic concentration-dependent diffusion coefficient $D \sim c$, the asymptotic scaling behavior of the concentration $c(z,t)$ is given by the self-similar function $c \sim F(z/t^{\alpha})/t^{\alpha}$ for $t \to \infty$, with the scaling exponent $\alpha = 1/3$, close to 0.3 observed experimentally. The experimentally observed scaling function $F(x/t^{\alpha})$ appears to be consistent with that of Eq. (53) except for the tails of the distribution, where $c \to 0$ and the assumption $D \sim c$ is possibly violated. Normal diffusion behavior corresponding to $D = \mathrm{const}$ and $\alpha = 1/2$ is in disagreement with experiment.

Newey *et al.* (2004) have conducted studies of axial segregation in ternary mixtures of granular materials. It has been found that for certain conditions bands of ternary mixtures oscillate axially, which indicates the supercritical oscillatory instability. Surprisingly, somewhat similar (however, transient) propagating waves were also observed in experiments by Choo *et al.* (1997, 1998) with binary mixtures for initially premixed states. While in binary mixtures oscillations have the form of periodic mixing and demixing of bands, in ternary mixtures oscillations are in the form of periodic band displacements. It is likely that the mechanism of band oscillations in ternary mixtures is very different from that of binary mixtures. One possible explanation could be that the third mixture component provides an additional degree of freedom necessary for oscillations. To demonstrate this we write phenomenological equations for the concentration differences $C_A = c_1 - c_2$ and $C_B = c_2 - c_3$, where $c_{1,2,3}$ are the individual concentrations. By analogy with Eq.

[5]Experiments have reported an in-phase relation between the angle and surface concentration modulations. It does not rule out, however, the quadrature phase shift between the angle and cross-section averaged concentration difference, as was predicted by Aranson, Tsimring, *et al.* (1999b).

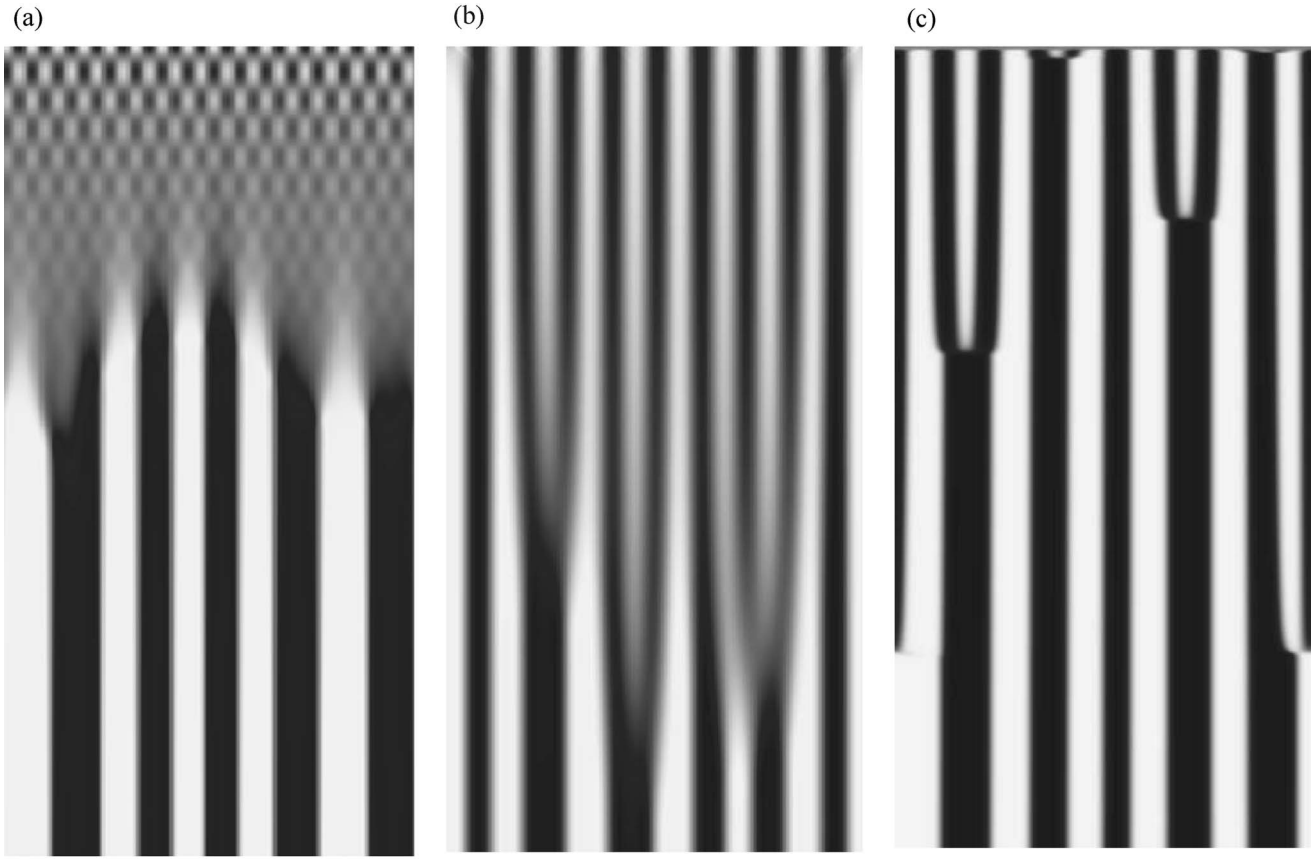

FIG. 41. Space-time diagrams demonstrating initial band oscillations and consequent coarsening. (a) Initial transients, time $0<t<1.25$. Periodic initial conditions with $k>k^*$ excite decaying standing waves. (b) For the same parameters but for $k<k^*$, periodic initial conditions produce no oscillations. (c) Long-term coarsening of bands for $0<t<5000$ at a higher diffusion constant. From Aranson and Tsimring, 1999.

(51), we write the system of coupled equations for the concentration differences $C_{A,B}$ linearized near the fully mixed state:

$$\partial_t C_A = D_A \partial_z^2 C_A + \mu_A \partial_z^2 C_B,$$

$$\partial_t C_B = D_B \partial_z^2 C_B + \mu_B \partial_z^2 C_A. \quad (54)$$

If the cross-diffusion terms have opposite signs, i.e., $\mu_A \mu_B < 0$, the concentrations $C_{A,B}$ will exhibit oscillations in time and in space. Obviously this mechanism is intrinsic to ternary systems and has no counterpart in binary mixtures. However, in experimental situations due to polydispersity effects there often is no clear-cut distinction between binary and ternary mixtures of grains. Thus the mechanism described by Eqs. (54) may also have relevance for binary mixtures with broad size distributions. Experiments by Choo *et al.* (1998) have demonstrated the sensitivity of axial segregation to the details of particle size distribution.

Parallel to the theoretical studies, molecular-dynamics simulations have been performed (Shoichi, 1998; Rapaport, 2002; Taberlet *et al.*, 2004). Simulations have allowed researchers to probe the role of material parameters which would be difficult to access in laboratory experiments. In particular, Rapaport (2002) has addressed the role of particle-particle and wall-particle friction coefficients separately. It was found that the main role is played by friction coefficients between particles and cylinder walls: If the friction coefficient between large particles and the wall is greater than that for smaller particles, axial segregation always occurs irrespective of the ratio of particle-particle friction coefficients. However, if the particle-wall coefficients are equal, segregation may still occur if the friction among large particles is greater than among smaller particles. Taberlet *et al.* (2004) have studied axial segregation in a system of grains made of identical materials differing only by size. The simulations have revealed rapid oscillatory motion of bands, which is not necessarily related to the slow band appearence or disappearence observed in the experiments of Choo *et al.* (1997, 1998), Fiedor and Ottino (2003), and Arndt *et al.* (2005).

A different type of discrete-element modeling of axial segregation was proposed by Yanagita (1999). This model built upon the lattice-based sandpile model and replaced a rotating drum by a three-dimensional square lattice. Drum rotation was modeled by correlated displacement of particles on the lattice: particles in the back were shifted upward by one position, and particles at the bottom were shifted to fill the voids. This displacement steepened the slope of the free surface, and once it reached a critical value particles slid down according to

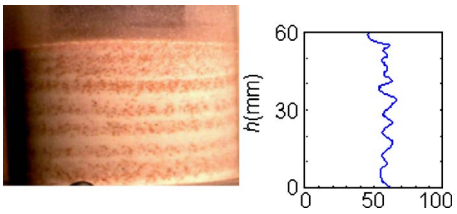

FIG. 42. (Color online) Granular Taylor vortices observed in a vertically rotating air-fluidized cylinder filled with a binary mixture. The left image depicts the entire cylinder height and width, and the right image shows the dependence of concentration of small particles along the bed height. From Conway *et al.*, 2004.

the rules similar to the sandpile model of Bak *et al.* (1987), but taking into account different critical slopes for different particles. This model, despite its simplicity, reproduced both radial and axial segregation patterns and therefore elucidated the critical components needed for an adequate description of the phenomenon.

C. Other examples of granular segregation

As we have seen in the previous section, granular segregation occurs in near-surface shear granular flows, such as silos, hoppers, and rotating drums. However, other types of shear granular flows may also lead to segregation. For example, a Taylor-Couette flow of granular mixtures between two rotating cylinders leads to the formation of Taylor vortices and then in turn to segregation patterns (Conway *et al.*, 2004); see Fig. 42.

Pouliquen *et al.* (1997) have observed granular segregation in a thin granular flow on an inclined plane. In this case, segregation apparently occurred as a result of an instability in which the concentration mode was coupled with the hydrodynamic mode. As a result, segregation occurred simultaneously with a fingering instability of the avalanche front (Fig. 7). As implicit evidence of this relationship between segregation and fingering instability, Pouliquen *et al.* (1997) have found that monodisperse granular material did not exhibit fingering instability. However, other experiments (Shen, 2002) indicated that in other conditions (more rapid flows) fingering instability may occur even in flows of monodisperse granular materials. Thus segregation is likely a consequence rather than the primary cause of the fingering instability.

A recent example of pattern formation caused by granular segregation in a horizontally shaken layer of a binary granular mixture was presented by Mullin (2000, 2002) and Reis and Mullin (2002). After several minutes of horizontal shaking, with frequency 12.5 Hz and displacement amplitude 1 mm (which corresponds to the acceleration amplitude normalized by gravity $\Gamma=0.66$), stripes were formed orthogonal to the direction of shaking. The width of the stripes grew continuously with time as $d \propto t^{0.25}$, thus indicating slow coarsening (Fig. 5). This power law is consistent with the diffusion-mediated mechanism of stripe merging. Reis and Mullin (2002) argued, on the basis of experimental results on patterned segregation in horizontally shaken layers, that segregation bears features of the second-order phase transition. Critical slowdown was observed near the onset of segregation. The order parameter is associated with the combined filling fraction C, or the layer compacity,

$$C = \frac{N_s A_s + N_l A_l}{S}, \tag{55}$$

where $N_{s,l}$ are the numbers of particles in each species, $A_{s,l}$ are projected two-dimensional areas of the respective individual particles, and S is the tray area. Ehrhardt *et al.* (2005) have proposed a simple model to describe the segregation in horizontally vibrated layers. The model is based on a two-dimensional system of hard disks of mass m_α and radius R_α ($\alpha=1,2$ denote the species),

$$m_\alpha \dot{\mathbf{v}}_{\alpha i} = -\gamma_i[\mathbf{v}_{\alpha i} - \mathbf{v}_{\text{tray}}(t)] + \zeta_{\alpha i}(t), \tag{56}$$

where $\mathbf{v}_i$ is the particle velocity, $\mathbf{v}_{\text{tray}}(t)=A_0 \sin(\omega t)$ is the oscillating tray velocity, γ provides linear damping, and $\zeta_{\alpha i}$ is white noise acting independently on each disk. The model reproduced the segregation instability and subsequent coarsening of stripes. More realistic discrete-element simulations were recently performed by Ciamarra *et al.* (2005). In these simulations a binary mixture of round disks of identical sizes, but two different frictions with the bottom plate (in fact, velocity-dependent viscous drag was assumed), segregated in alternating bands perpendicular to the oscillation direction irrespective of initial conditions: both random mixed state and separated along the direction of oscillations state were used. Using particles of the same size eliminated the thermodynamic "excluded-volume" mechanism for segregation, and the authors have argued that the mechanism at work is related to the dynamical shear instability similar to the Kelvin-Helmholtz instability in ordinary fluids. This has been confirmed by a numerical observation of the interfacial instability when two monolayers of grains with different friction constants were placed in contact along a flat interface parallel to the direction of horizontal oscillations. A similar instability is apparently responsible for ripple formation (Scherer *et al.*, 1999; Stegner and Wesfreid, 1999).

Pooley and Yeomans (2004) have proposed a theoretical description of this experiment based on a continuum model for two periodically driven isothermal ideal gases which interact through frictional force. It was shown analytically that segregated stripes form spontaneously above the critical forcing amplitude. While the model reproduces the segregation instability, apparently it does not exhibit the coarsening of stripes observed in experiment. Moreover, applicability of the isothermal ideal-gas model to this experiment, in which particles are almost at rest, is an open question.

A similar coarsening effect in granular segregation in a simple geometry was studied by Aumaître *et al.* (2001). They investigated the dynamics of a monolayer of grains

of two different sizes in a dish involved in a horizontal "swirling" motion. They observed that large particles tend to aggregate near the center of the cavity surrounded by small particles. The qualitative explanation of this effect follows from simple thermodynamic considerations (see above). Indeed, the direct tracing of particle motion showed that the pressure in the area near large particles is smaller than that outside. But small particles do not follow the gradient of pressure and assemble near the center of the cavity because this gradient is counterbalanced by the force from large particles. The inverse of force acting on large particles leads to their aggregation near the center of the cavity. Aumaître *et al.* (2001) proposed a more quantitative model of segregation based on the kinetic-gas theory and found satisfactory agreement with experimental data.

Burtally *et al.* (2002) have studied the spontaneous separation of vertically vibrated mixtures of particles of similar sizes but different densities (bronze and glass spheres). At low frequencies and at sufficient vibrational amplitudes, a sharp boundary between the lower layer of glass beads and the upper layer of heavier bronze spheres was observed. At higher frequencies, the bronze particles emerged as a middle layer separating upper and lower glass-bead layers. The authors argued that the effect of air on the granular motion was a relevant mechanism of particle separation. A somewhat similar conclusion was reached by Möbius *et al.* (2001) in experiments with vertically vibrated column of grains containing a large "intruder" particle.

Fiedor and Ottino (2003) and Arndt *et al.* (2005) have performed detailed experiments on axial segregation in slurries, or bidisperse grain-water mixtures. A mixture of two types of spherical glass beads of two sizes were placed in a water-filled tube at the volume ratio 1:2. The authors have found that both rotation rate and filling fraction play an important role in band formation. Namely, bands are less likely to form at lower fill levels (20–30 %) and slower rotation rates (5–10 rpm). They mostly appear near the ends of the drum. At higher fill levels and rotation rates, bands form faster, and there are more of them throughout the drum. Fiedor and Ottino (2003) and Arndt *et al.* (2005) have also studied the relation between bands visible on the surface and the core of small beads and found that for certain fill levels and rotation speeds the core remains prominent at all times, while in other cases the core disappears completely between bands of small particles. They have also observed an oscillatory instability of interfaces between bands at high rotation speeds. All these phenomena still await theoretical modeling.

VIII. GRANULAR MATERIALS WITH COMPLEX INTERACTIONS

A. Patterns in solid-fluid mixtures

The presence of interstitial fluid significantly complicates the dynamics of granular materials. Hydrodynamic flows lead to viscous drag and anisotropic long-range interactions between particles. Even small amounts of liquid lead to cohesion among particles, which can have a profound effect on the macroscopic properties of granular assemblies, such as the angle of repose, avalanching, ability to segregate, etc. [see, for example, Sec. VII.B and Samadani and Kudrolli (2000, 2001), Tegzes *et al.* (2002), and Li and McCarthy (2005)].

In this section we discuss the case when the volume fraction of a fluid in the two-phase system is large, and grains are completely immersed in fluid. This is relevant for many industrial applications, as well as for geophysical problems such as sedimentation, erosion, dune migration, etc.

One of the most technologically important examples of particle-laden flows is a fluidized bed. Fluidized beds have been widely used since German engineer Fritz Winkler invented the first fluidized bed for coal gasification in 1921. Typically, a vertical column containing granular matter is energized by a flow of gas or liquid. Fluidization occurs when the drag force exerted by the fluid on the granulate exceeds gravity. A uniform fluidization, the most desirable regime for most industrial applications, turns out to be prone to bubbling instability: bubbles of clear fluid are created spontaneously at the bottom, traverse the granular layer, and destroy the uniform state (Jackson, 2000). Instabilities in fluidized beds is an active area of research in the engineering community; see Kunii and Levenspiel (1991), Gidaspow (1994) and Jackson (2000). A shallow fluidized bed shows many similarities to mechanically vibrated layers; see Sec. V. In particular, the modulations of airflow studied by Li *et al.* (2003) resulted in the formation of subharmonic square and stripe patterns (see Fig. 23) similar to those in mechanically vibrated systems (Melo *et al.*, 1994, 1995; Umbanhowar *et al.*, 1996).

Wind- and water-driven granular flows play important roles in geophysical processes. Wind-blown sand forms dunes and beaches. The first systematic study of airborne (or aeolian) sand transport was conducted by R. Bagnold during Wold War II (see Bagnold, 1954), who identified two primary mechanisms of sand transport: saltation and creep. The former denotes the bouncing motion of individual grains on the dune surface driven by wind, and the latter indicates the slow relaxation of sand within the near-surface layer, mostly due to gravity. Bagnold (1954) proposed the first empiric relation for the sand flux q driven by the wind-shear stress τ:

$$q = C_B \frac{\nu_a}{g} \sqrt{\frac{d}{D}} u_*^3, \tag{57}$$

where C_B=const, ν_a is air density, d is the grain diameter, D=0.25 mm is a reference grain size, and $u_* = \sqrt{\tau/\nu_a}$ is the wind friction velocity. Later many refinements of Eq. (57) were proposed; see, for example, Pye and Tsoar (1991).

Nishimori and Ouchi (1993) proposed a simple theory which describes the formation of ripples as well as dunes. The theory was based on a lattice model, which incorporates separately saltation and creep processes.

The model operated with the height of sand at a each lattice side at a discrete time n, $h_n(x,y)$. The full time step includes two substeps. The saltation substep is described as

$$\bar{h}_n(x,y) = h_n(x,y) - q$$

$$\bar{h}_n(x + L(h(x,y)),y) = h_n(x + L(h_n(x,y)),y) + q, \quad (58)$$

where q is the height of grains being transferred from one (coarse-grained) position (x,y) to the other position $(x+L,y)$ on the lee side (the wind is assumed to be blowing in the positive x direction) and L is the flight length in one saltation, which characterizes the wind strength. It is assumed that q is conserved. Since the saltation length L depends on multiple factors, the following simple approximation is accepted:

$$L = L_0 + bh_n(x,y), \quad (59)$$

with L_0 measuring the wind velocity and $b = \text{const}$. The creep substep involves spatial averaging over neighboring sites in order to describe the surface relaxation due to gravity,

$$h_{n+1}(x,y) = \bar{h}_n(x,y) + D\left[\frac{1}{6}\sum_{\mathrm{NN}} \bar{h}(x,y) + \frac{1}{12}\sum_{\mathrm{NNN}} \bar{h}(x,y) - \bar{h}(x,y)\right], \quad (60)$$

where Σ_{NN} and Σ_{NNN} denote summation over the nearest neighbors and next-nearest neighbors correspondingly and $D = \text{const}$ is the surface relaxation rate. Despite its simplicity, simulation of the model reproduced the formation of ripples and consequently arrays of barchan (crescent-shaped) dunes; see Fig. 43. Nishimori and Ouchi (1993) have found that above a certain threshold, an almost linear relation holds between the selected wavelength of the dune pattern and the "wind strength" L.

In the long-wave limit, Eqs. (59)–(61) can be reduced to more traditional continuum models considered below: evolution of the sand surface profile h is governed by the mass conservation equation

$$\nu_s \partial_t h = -\nabla \mathbf{q}, \quad (61)$$

where ν_s is the density of sand and $\mathbf{q}$ is the sand flux. In order to close Eqs. (57) and (61), several authors proposed different phenomenological relations between shear stress at the bed surface τ and height h; see, for example, Nishimori and Ouchi (1993); Prigozhin (1999); Andreotti *et al.* (2002); Kroy *et al.* (2002a, 2002b); Schwämmle and Herrmann (2003); Hersen *et al.* (2004).

There are many theories generalizing the Nishimori and Ouchi (1993) approach; see, for example, Caps and Vandewalle (2001). Prigozhin (1999) has described the evolution of dunes by a system of two equations similar to the BCRE model discussed earlier in Sec. VI (Bouchaud *et al.*, 1994, 1995). One equation describes the evolution of the local height h while the other equation describes the density R of particles rolling above the stationary sand-bed profile (reptating particles),

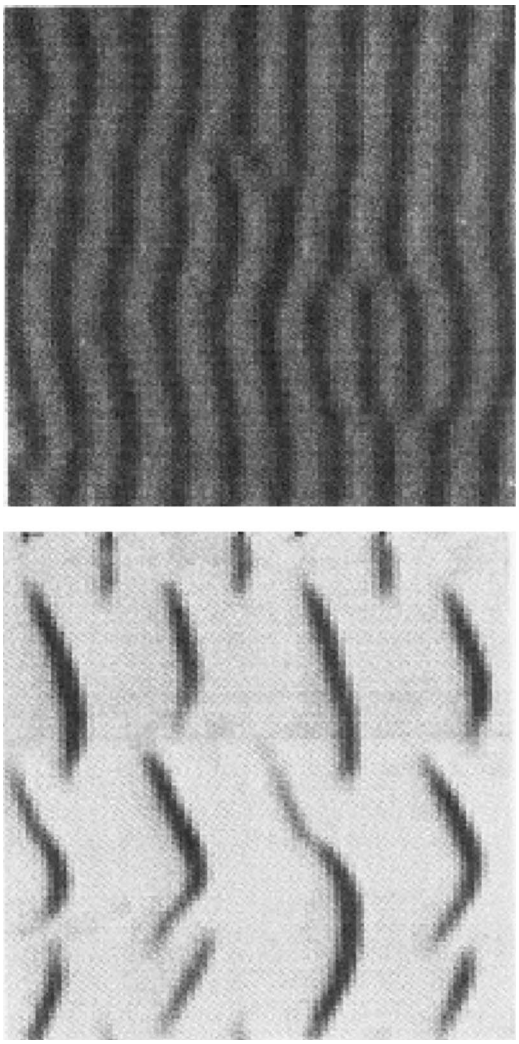

FIG. 43. Sand ripple pattern (top panel) and barchan dunes (lower panel) obtained from simulations of Eqs. (59)–(61). From Nishimori and Ouchi, 1993.

$$\partial_t h = \Gamma(h,R) - f, \quad (62)$$

$$\partial_t R = -\nabla \mathbf{J} + \mathbf{Q} - \Gamma(h,R), \quad (63)$$

where Γ is the rolling-to-steady sand transition rate, $\mathbf{J}$ is the horizontal projection of the flux of rolling particles, $\mathbf{Q}$ accounts for the influx of falling reptating grains, and f is the erosion rate. With an appropriate choice of rate functions Γ, f, Q and J, Eqs. (62) and (63) can reproduce many observed features of dune formation, such as the initial instability of the flat state, asymmetry of the dune profiles, coarsening and interaction of dunes, etc.; see Fig. 44.

Thus simplified models such as those of Nishimori and Ouchi (1993), Prigozhin (1999), Kroy *et al.* (2002a), and Schwämmle and Herrmann (2003) have been successful in explaining many features of individual dune growth and evolution; see, for example, Fig. 45 where the long-term evolution of two barchan dunes was studied nu-

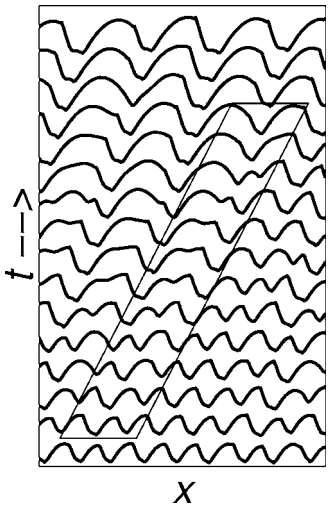

FIG. 44. Interaction and coarsening of a one-dimensional dune system. From Prigozhin, 1999.

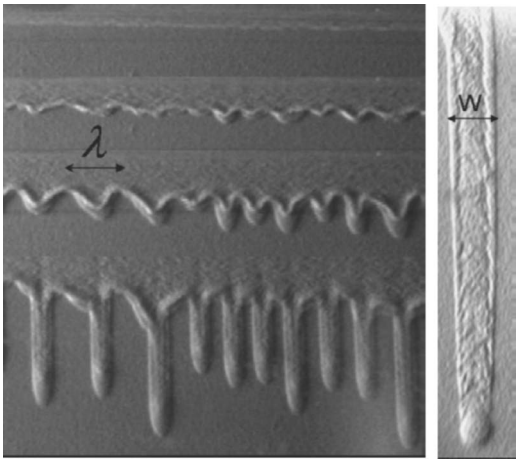

FIG. 46. Fingering instability of a planar avalanche in the underwater flow; the image on the right zooms on an individual finger. From Malloggi *et al.*, 2005.

merically. More recently, Schwämmle and Herrmann (2003) have demonstrated by means of a numerical solution of continuum equations similar to Eqs. (57) and (61) that the barchan dunes almost do not change their form due to collisions, consistent with experimental evidence. However, we should note that up to the present none of the dune models have been able to address satisfactorily the wavelength selection in large-scale dune fields (Andreotti *et al.*, 2002; Hersen *et al.*, 2004).

A phenomenon qualitatively similar to dune formation occurs in an oscillatory fluid flow above a granular layer: sufficiently strong flow oscillations produce vortex ripples on the surface of the underlying granular layer. Vortex ripple formation was first studied by Ayrton (1910) and Bagnold (1956), as well as by Scherer *et al.* (1999), Stegner and Wesfreid (1999), and others. It was found that ripples emerge via a hysteretic transition and are characterized by a near-triangular shape with slope angles close to the angle of repose. The characteristic size of the ripples λ is directly proportional to the displacement amplitude of the fluid flow a (with a proportionality constant ≈ 1.3) and is roughly independent of the frequency.

Andersen *et al.* (2001) have introduced order-parameter models for describing the dynamics of sand ripple patterns under an oscillatory flow based on the phenomenological mass transport law between adjacent ripples. The models predicted the existence of a stable band of wave numbers limited by secondary instabilities and coarsening of small ripples, in agreement with experiments.

Langlois and Valance (2005) have studied underwater ripple formation on a two-dimensional sand bed sheared by viscous fluid. The sand transport is described by a generalization of Eq. (57) taking into account both the local bed shear stress and local bed slope. A linear stability analysis revealed that ripple formation is attributed to a growing longitudinal mode. The weakly nonlinear analysis, taking into account the resonance interaction of only three unstable modes, revealed a variety of steady two-dimensional ripple patterns drifting along the flow at some speed.

Experiments in dune formation have been performed in water (Betat *et al.*, 1999). While water-driven and wind-driven dunes and ripples have a similar shape, the underlying physical processes are likely not the same due to a different balance between gravity and viscous drag in air and water.

Spectacular erosion patterns in sediment granular layers have been observed in experiments with underwater flows (Daerr *et al.*, 2003; Malloggi *et al.*, 2005). In particular, a fingering instability of flat avalanche fronts has been observed (see Fig. 46). These patterns are remarkably similar to those in thin films on inclined surfaces, with both clear and particle-laden fluids (Troian *et al.*, 1989; Zhou *et al.*, 2005). In the framework of the lubri-

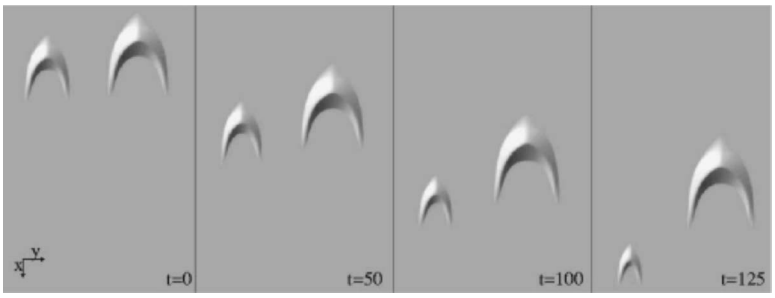

FIG. 45. Evolution of two barchan dunes described by Eqs. (57) and (61). The small dune is undersupplied and eventually shrinks. From Hersen *et al.*, 2004.

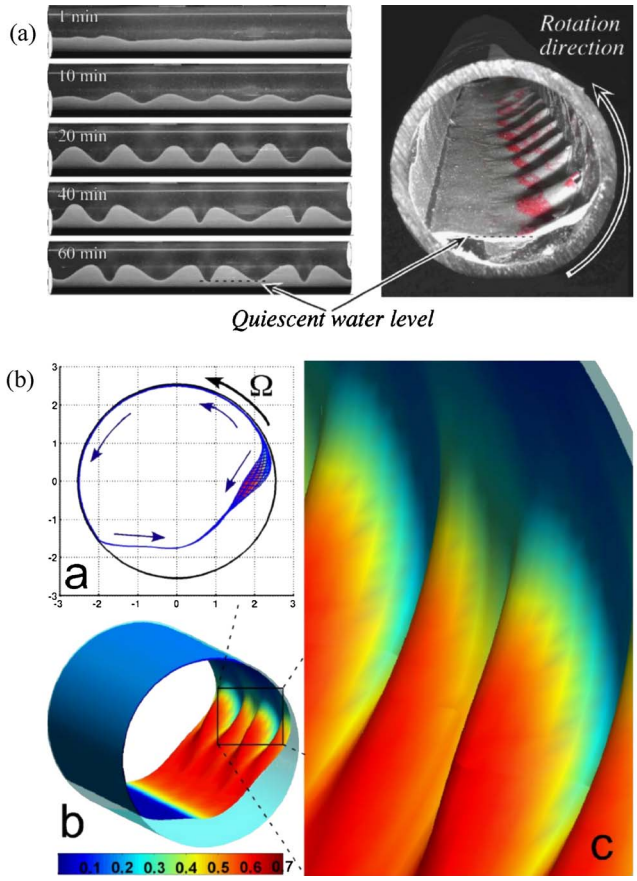

FIG. 47. (Color online) Knolls in a water and glass beads mixture. Upper panel: Self-supporting knolls formed in a water and glass beads suspension in a horizontally rotating cylinder (side and end views). Lower panel: Computational results. (a) Schematics of the flow; (b),(c) the height of the computed knoll structures. From Duong *et al.*, 2004.

cation approximation, the evolution of fluid film thickness h is described by the following dimensionless equation following from the mass conservation law:

$$\partial_t h + \nabla \cdot \{[h^3 \nabla \nabla^2 h] - \bar{D} h^3 \nabla h\} + \partial_x h^3 = 0, \tag{64}$$

where the dimensionless parameter $\bar{D}$ is inversely proportional to the water surface tension. The instability occurs for small $\bar{D}$ values, i.e., in the large surface-tension limit. However, despite the visual similarity the physical mechanism leading to this fingering instability is not obvious: in fluid films the instability is driven (and stabilized) by the surface tension, whereas in the underwater granular flow fluid surface tension plays no role.

Duong *et al.* (2004) have studied the formation of periodic arrays of knolls in a slowly rotating horizontal cylinder filled with a granular suspension (see Fig. 47). The solidified sediment knolls coexist with the freely circulating fluid. The authors have applied a variable fluid viscosity approximation, which formally allows a simultaneous treatment of the solid and liquid phase. In this model the effective flow viscosity μ_s diverges at the solid packing fraction ϕ_{rcp},

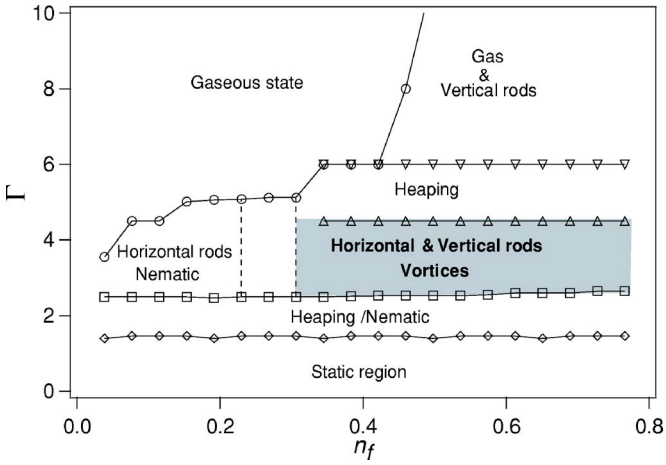

FIG. 48. (Color online) Phase diagram for the system of vertically vibrated rods; driving frequency 50 Hz. Vortices are observed for sufficiently high filling fraction n_f and above critical acceleration Γ. From Blair *et al.*, 2003.

$$\mu_s = \frac{\mu_0}{(1 - \phi/\phi_{\mathrm{rcp}})^b}, \tag{65}$$

where μ_0 is the clear fluid viscosity and b is an empirical coefficient. The model qualitatively reproduces the experiment (see Fig. 47). An interesting question in this context is whether there is a connection to the experiment by Shen (2002) in which somewhat similar structures were obtained for the flow of "dry" particles in a horizontally rotating cylinder.

As was mentioned in Sec. VII.C, Conway *et al.* (2004) have reported that an air-fluidized vertical column of bidisperse granular media sheared between counter-rotating cylinders exhibits the formation of a nontrivial vortex structure reminiscent of the Taylor vortices in a conventional fluid; see Andereck *et al.* (1986). The authors have argued that vortices in fluidized granular media, unlike Taylor vortices in a fluid, are accompanied by the novel segregation-mixing mechanism specific for granular systems (see Fig. 42). Interestingly, no vortices were observed in a similar experiment in Couette geometry with monodisperse glass beads (Losert *et al.*, 2000).

Ivanova *et al.* (1996) have studied patterns in a horizontal cylinder filled with a sand-liquid mixture and subjected to a horizontal vibration. For certain vibration parameters, standing-wave patterns were observed at the sand-liquid interface. The authors argued that these wave patterns were similar to the Faraday ripples found at a liquid-liquid interface under vertical vibrations.

B. Vortices in vibrated rods

In Sec. V we have reviewed instabilities and collective motion in mechanically vibrated layers. In most experiments the particle shape was not important. However, strong particle anisotropy may give rise to nontrivial effects. Villarruel *et al.* (2000) have observed the onset of nematic order in the packing of long rods in a narrow vertical tube subjected to vertical tapping. The rods ini-

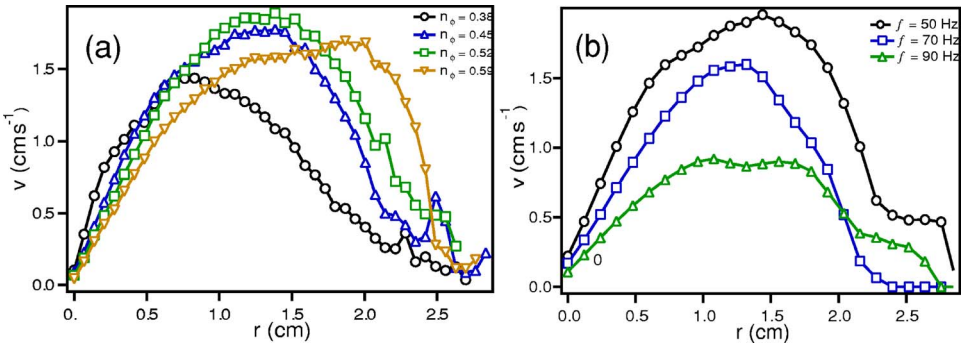

FIG. 49. (Color online) Azimuthal velocity of the vortex vs distance from the center for different parameter values. From Blair *et al.*, 2003.

tially compactify into a disordered state with predominantly horizontal orientation, but at later times (after thousands of taps) they align vertically, first along the walls and then throughout the volume of the pipe. The nematic ordering can be understood in terms of the excluded-volume argument put forward by Onsager (1949).

Blair *et al.* (2003) have studied the dynamics of vibrated rods in a shallow large aspect ratio system. Surprisingly, they found that the vertical alignment of rods at large enough filling fraction n_f and amplitude of vertical acceleration ($\Gamma > 2.2$) can occur in the bulk, and it does not require side walls. Eventually, most of the rods align themselves vertically in a monolayer synchronously jumping onto the plate and engage in a correlated horizontal motion in the form of propagating domains of tilted rods, multiple rotating vortices, etc. (see Figs. 12 and 48). The vortices exhibit an almost rigid-body rotation near the core, and then the azimuthal velocity falls off (see Fig. 49). The vortices merge in the course of their motion, and eventually a single vortex is formed in the cell.

Experiments have shown that the rod motion occurs when rods are tilted from the vertical, and it always occurs in the direction of tilt. In a subsequent work, Volfson, Kudrolli, *et al.* (2004) have experimentally demonstrated that the correlated transport of bouncing rods is also found in a quasi-one-dimensional geometry and explained this effect using molecular-dynamics simulations and a detailed description of inelastic frictional contacts between rods and the vibrated plate. Effectively, bouncing rods become self-propelled objects similar to other self-propelled systems, for which large-scale coherent motion is often observed [bird flocks, fish schools, chemotactic microorganism aggregation, etc.; see, for example, Toner and Tu (1995), Helbing *et al.* (2000), Helbing (2001), Grégoire and Chaté (2004), and Tu *et al.* (2005)].

Aranson and Tsimring (2003) have developed a phenomenological continuum theory describing coarsening and vortex formation in the ensemble of interacting rods. Assuming that the motion of rods is overdamped due to the bottom friction, the local horizontal velocity $\mathbf{v}=(v_x,v_y)$ of rods is of the form

$$\mathbf{v} = -[\boldsymbol{\nabla} p - \alpha \mathbf{n} f_0(n)\nu]/\zeta\nu, \tag{66}$$

where ν is the density, p is the hydrodynamic pressure, $\mathbf{n}=(n_x,n_y)$ the tilt vector is the projection of the rod director on the (x,y) plane normalized by the rod length, i.e., $n=|\mathbf{n}|$, and ζ is friction coefficient. According to Blair *et al.* (2003) and Volfson, Kudrolli, *et al.* (2004), the rod drift is determined by the average tilt of neighboring rods, thus the term $\alpha \mathbf{n} f_0(n)\nu$ accounts for the average driving force on the tilted rod from the vibrating bottom. Equation (66) combined with the mass conservation law yields

$$\partial_t \nu = -\operatorname{div}(\mathbf{v}\nu) = \zeta^{-1} \operatorname{div}[\nabla p - \alpha \mathbf{n} f_0(n)\nu]. \tag{67}$$

To account for the experimentally observed phase separation and coarsening, Aranson and Tsimring (2003) have employed the Cahn-Hilliard approach, which was developed earlier for the description of other phase-ordering systems [see Bray (1994) for a review], by assuming that pressure p can be obtained from the variation of a generic bistable "free-energy" functional F with respect to the density field ν, $p=\delta F/\delta\nu$.

To close the description, the equation for the evolution of tilt $\mathbf{n}$ is added onto generic symmetry arguments:

$$\partial_t \mathbf{n} = f_1(\nu)\mathbf{n} - |\mathbf{n}|^2\mathbf{n} + f_2(\nu)(\xi_1 \nabla^2 \mathbf{n} + \xi_2 \boldsymbol{\nabla} \operatorname{div} \mathbf{n}) + \beta \boldsymbol{\nabla} \nu. \tag{68}$$

Here $f_{1,2}$ are functions of ν and $\xi_{1,2}$ characterize diffusion coupling between the neighboring rods. Since the tilt field is not divergence-free, from general symmetry considerations $\xi_{1,2} \neq 0$.[6] Numerical and analytical studies of Eqs. (67) and (68) have revealed phase coexistence, nucleation, and coalescence of vortices in accord with experiment; see Fig. 50.

An interesting experiment with anisotropic chiral particles has been performed by Tsai *et al.* (2005). The role of particles was played by bent-wire objects, which rotated in a preferred direction under vertical vibration. The experiments have demonstrated that the individual angular rotation of particles was converted into the collective angular momentum of the granular gas of these chiral objects. The theoretical description of this system was formulated in the framework of two phenomenological equations for the density ν and center-of-mass momentum density $\nu\mathbf{v}$ and the spin angular momentum density $l=\mathcal{I}\Omega$ arising from the rotation of particles around their center of mass; Ω is the particle's rotation

[6]These constants are analogous to the first and second viscosity in ordinary fluids; see Landau and Lifshitz (1959).

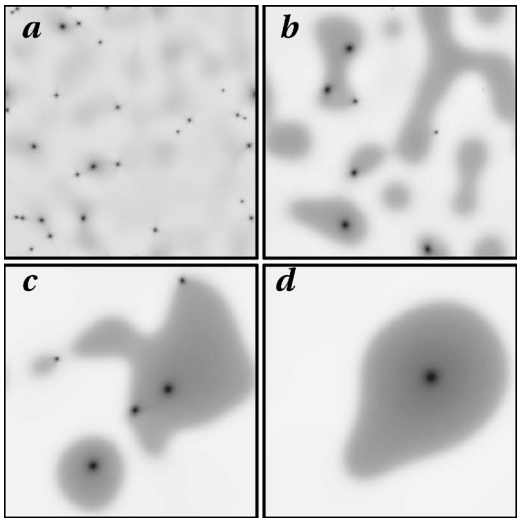

FIG. 50. Sequence of images illustrating coalescence of vortices in the model of vibrated rods; the field $|\mathbf{n}|$ is shown. Black dots corresponds to vortex cores where $|\mathbf{n}|=0$. From Aranson and Tsimring, 2003.

frequency. Whereas the equations for density and velocity are somewhat similar to those for the vibrated-rod system, the equation for the spin momentum clearly has no counterpart in the vibrated-rod system and was postulated in the following form:

$$\partial_t l + \nabla \mathbf{v} l = \tau - \Gamma^{\Omega}\Omega - \Gamma(\Omega - \omega) + D_{\Omega}\nabla^2\Omega, \tag{69}$$

where τ is the source of the angular rotation (due to chirality of the particles), ω is the coarse-grained or collective angular velocity, Γ^{Ω} and Γ are dissipative coefficients due to friction, and D_{Ω} is the angular momentum diffusion. Equation (69) predicts, in agreement with experiment, the onset of collective rotation of the gas of particles. Possibly it also exhibits nontrivial spatiotemporal dynamics similar to those in the system of vibrated rods. However, due to the small number of particles (about 350) in the experiment nontrivial collective regimes were not reported.

C. Electrostatically driven granular media

Large ensembles of small particles display fascinating collective behavior when they acquire an electric charge and respond to competing long-range electromagnetic and short-range contact forces. Many industrial technologies face the challenge of assembling and separating such single-component or multicomponent microsize and nanosize ensembles. Traditional methods, such as mechanical vibration and shear, are ineffective for fine powders due to agglomeration, charging, etc. Electrostatic effects often change the statistical properties of granular matter such as energy dissipation rate (Sheffler and Wolf, 2002), velocity distributions in granular gases (Aranson and Olafsen, 2002; Kohlstedt *et al.*, 2005), agglomeration rates in suspensions (Dammer and Wolf, 2004), etc.

Aranson *et al.* (2000), Aranson, Meerson, *et al.* (2002), Sapozhnikov, Aranson, *et al.* (2003, 2004), and Sapozhnikov, Tolmachev, *et al.* (2003) have studied electrostatically driven granular matter. This method relies on collective interactions between particles due to a competition between short-range collisions and long-range electromagnetic forces. Direct electrostatic excitation of small particles offers unique new opportunities compared to traditional techniques of mechanical excitation. It enables one to deal with extremely fine nonmagnetic and magnetic powders, which are not easily controlled by other means.

In most experimental realizations, several grams of monodispersed conducting microparticles were placed into a 1.5-mm gap between two horizontal 30×30-cm^2 glass plates covered by transparent conducting layers of indium tin dioxide. Typically 45-μm copper or 120-μm bronze spheres were used. Experiments were also performed with much smaller 1-μm particles (Sapozhnikov *et al.*, 2004). An electric field perpendicular to the plates was created by a high-voltage source (0–3 kV) connected to the inner surface of each plate. Experiments were performed in air, vacuum, or in a cell filled with a nonpolar weakly conducting liquid.

The basic principle of the electrostatic cell operation is as follows. A particle acquires an electric charge when it is in contact with the bottom conducting plate. It then experiences a force from the electric field between plates. If the upward force induced by the electric field exceeds gravity, the particle travels to the upper plate, reverses charge upon contact, and is repelled down to the bottom plate. This process repeats in a cyclical fashion. In an air-filled or evacuated cell, the particle remains immobile at the bottom plate if the electric field E is smaller than the first critical field E_1. For $E>E_1$, an isolated particle leaves the plate and starts to bounce. However, if several particles are in contact on the plate, screening of the electric field reduces the force on individual particles, and they remain immobile. A simple calculation shows that for the same value of the applied electric field the force acting on isolated particles exceeds by a factor of 2 the force acting on the particle inside the dense monolayer. If the field is larger than a second critical field value $E_2>E_1$, all particles leave the plate, and the system of particles transforms into a uniform gaslike phase. When the field is decreased below E_2 ($E_1<E<E_2$), localized clusters of immobile particles spontaneously nucleate to form static clusters (precipitate) on the bottom plate in air-filled or evacuated cells (Aranson *et al.*, 2000) The clusters exhibit Ostwald-type ripening (Bray, 1994; Meerson, 1996); see also Sec. IV.C.

1. Coarsening of clusters

Results for the electrostatically driven system yielded the following asymptotic scaling law (see Fig. 51):

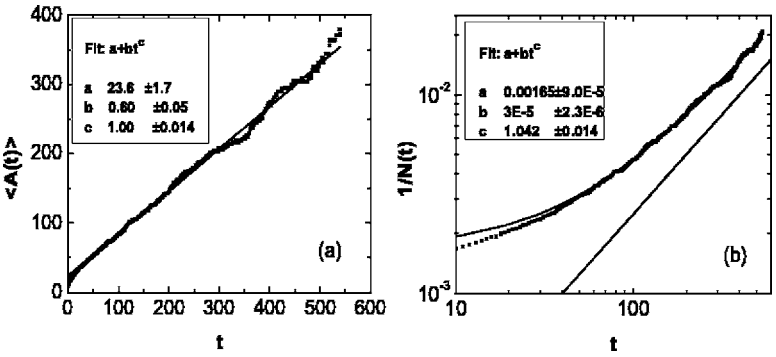

FIG. 51. Coarsening of clusters in an electrostatic cell. (a) Average cluster area $\langle A(t)\rangle$ and (b) inverse number of clusters $1/N(t)$ vs time in an air-filled cell. The straight line in (b) shows the theoretical prediction $1/N\sim t$. From Sapozhnikov *et al.*, 2005.

$$N\sim\frac{1}{t}, \tag{70}$$

where N is the number of clusters and t is time. Accordingly, the average cluster area $\langle A\rangle$ increases with time as $\langle A\rangle\sim t$. This behavior is consistent with interface-controlled Ostwald ripening (Meerson, 1996).

A theoretical description of coarsening in an electrostatically driven granular system was developed by Aranson, Meerson, *et al.* (2002) and Sapozhnikov *et al.* (2005). The theory was formulated in terms of a Ginzburg-Landau-type equation for the number density of immobile particles (precipitate or solid) n,

$$\partial_t n=\nabla^2 n+\phi(n,n_g), \tag{71}$$

where n_g is the number density of bouncing particles (gas) and $\phi(n,n_g)$ is a function characterizing a solid-gas conversion rate. The effectiveness of solid-gas transitions is controlled by the local gas concentration n_g. It was assumed that the gas concentration was almost constant because the particle's mean free pass in the gas state was very large. The gas concentration n_g is coupled to n due to the total mass conservation constraint

$$Sn_g+\int\int n(x,y)dxdy=M, \tag{72}$$

where S is the area of domain of integration and M is the total number of particles. The function $\phi(n,n_g)$ is chosen in such a way as to provide bistable local dynamics of concentration corresponding to the hysteresis of the gas-solid transition. The above description yields a similar evolution of clusters (see Fig. 52) and produces a correct scaling for the number of clusters given by Eq. (70).

In the sharp-interface limit, when the size of clusters is much larger than the width of interfaces between clusters and granular gas, Eq. (71) can be reduced to equations for the cluster radii R_i (assuming that clusters have circular form):

$$\frac{dR_i}{dt}=\kappa\left(\frac{1}{R_c(t)}-\frac{1}{R_i}\right), \tag{73}$$

where R_c is the critical cluster size and κ is the effective surface tension [experimental measurements of cluster surface tension have been conducted by Sapozhnikov, Aranson, *et al.* (2003)]. The critical radius R_c is a function of the granular gas concentration n_g that enters Eqs. (73) through the conservation law (72), which in two dimensions reads

$$n_g S+\pi\sum_{i=1}^{N}R_i^2=M. \tag{74}$$

The statistical properties of Ostwald ripening can be understood in terms of the probability distribution function $f(R,t)$ of cluster sizes. Following Lifsitz and Slyozov (1958, 1961) and Wagner (1961) and neglecting cluster merger, one obtains in the limit $N\to\infty$ that the probability distribution $f(R,t)$ satisfies the continuity equation

$$\partial_t f+\partial_R(\dot{R}f)=0. \tag{75}$$

From the mass conservation in the limit of small gas concentration Eq. (74), one obtains an additional constraint:

$$\pi\int_0^\infty R^2 f(R,t)dR=M. \tag{76}$$

Equations (75) and (76) have a self-similar solution in the form

$$f(R,t)=\frac{1}{t^{3/2}}F\left(\frac{R}{\sqrt{t}}\right). \tag{77}$$

For the total number of clusters $N=\int_0^\infty f dR$, the scaling Eq. (77) yields $N\sim 1/t$, which is in good agreement with

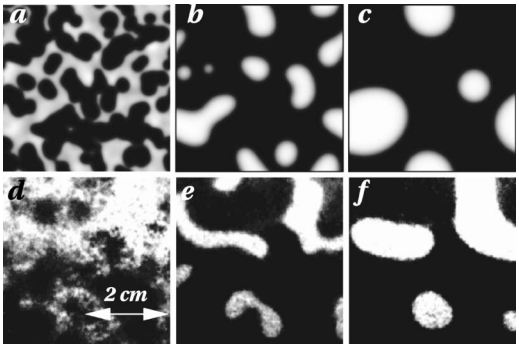

FIG. 52. Illustration of phase separation and coarsening dynamics. (a)–(c) Numerical solution of Eqs. (71) and (72); white corresponds to dense clusters, black to a dilute gas. (d)–(f) Experimental results. From Aranson, Meerson, *et al.*, 2002.

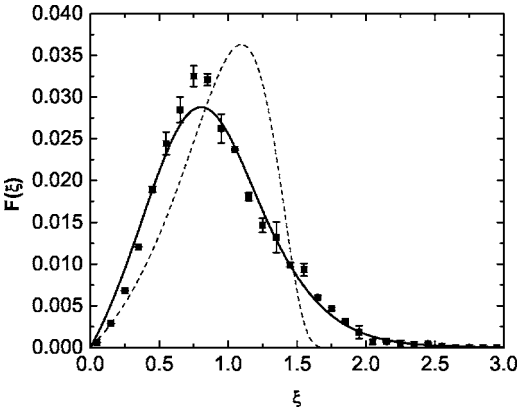

FIG. 53. Scaled cluster-size distribution function $F(\xi)$ with $\xi = R/\sqrt{t}$. The squares show experimental results, the dotted line shows analytic results from the Lifshitz-Slyozov-Wagner theory (Wagner, 1961), and the solid line shows F obtained from the theory accounting for binary coalescence. From Sapozhnikov *et al.*, 2005.

experiment (see Fig. 51). However, the cluster-size distribution function appears to be in strong disagreement (see Fig. 53). In particular, the Lifsitz and Slyozov (1958, 1961) and Wagner's (1961) theory predicts the distribution with a cutoff (dotted line), whereas experiment yields the function with an exponential tail. A much better agreement with experiment was obtained when a binary coalescence of clusters was incorporated in the Lifshitz-Slyozov-Wagner theory (Conti *et al.*, 2002; Sapozhnikov *et al.*, 2005). The coalescence events become important for a finite-area fraction of the clusters.

Ben-Naim and Krapivsky (2003) have applied an exchange-growth model to describe coarsening in granular media. In this theory, cluster growth rates are controlled only by the cluster area ignoring shape effects. Assuming that the number of particles in a cluster evolves via an uncorrelated exchange of single particles with another cluster, the following equation for the density of clusters containing k particles can be derived:

$$\frac{dA_k}{dt} = \sum_{i,j} A_i A_j K_{ij} (\delta_{k,i+1} + \delta_{k,i-1} - 2\delta_{k,i}), \tag{78}$$

where A_k is the probability of finding a cluster containing k particles, K_{ij} is the exchange kernel, and $\delta_{k,i}$ is the Kronecker symbol. For a homogeneous kernel $K_{ij} = (ij)^{\lambda}$ with $\lambda = 1$ this theory predicts correct scaling of the cluster size with time $R \sim \sqrt{t}$ and an exponential decay of the cluster-size distribution function, as in experiment. For $\lambda = 1$ this is equivalent to the assumption that the exchange rate is determined by the size of the cluster. In the theory of Sapozhnikov *et al.* (2005), cluster evolution is governed by the evaporation or deposition of particles at the interface of the cluster and controlled by the overall pressure of the granular gas. Thus both theories predict the same scaling behavior, however, the underlying assumptions are different. A possible explanation for this may be that while the exchange-growth model ignores the curvature of the cluster interface and the dependence of exchange rate on the pressure of the granular gas, the agreement is obtained by tuning the adjustable parameter λ.

2. Dynamics of patterns in a fluid-filled cell

Sapozhnikov, Aranson, *et al.* (2003) have performed experiments with electrostatically driven granular media immersed in a weakly conducting nonpolar fluid (toluene-ethanol mixture). Depending on the applied electric field and ethanol concentration (which controls the conductivity of the fluid), a plethora of static and dynamic patterns were discovered; see Fig. 15. For relatively low concentrations of ethanol (below 3%), the qualitative behavior of the liquid-filled cell is not different from that of the air-filled cell: clustering of immobile particles and coarsening were observed between two critical field values $E_{1,2}$, with the clusters being qualitatively similar to that of the air cell. However, when the ethanol concentration is increased, the phase diagram becomes asymmetric with respect to the direction of the electric field. Critical-field magnitudes $E_{1,2}$ are larger when the electric field is directed downward ("+" on the upper plate) and smaller when the field is directed upward ("−" on the upper plate). This difference increases with ethanol concentration. The observed asymmetry of the critical fields is apparently due to an excess negative charge in the bulk of the liquid.

The situation changes dramatically for higher ethanol concentrations. Increasing the applied voltage leads to the formation of two new immobile phases: honeycomb [Fig. 15(b)] for the downward direction of the applied electric field and two-dimensional crystal-type states for the upward direction.

A further increase of ethanol concentration leads to the appearance of a novel dynamic phase—a condensate [Figs. 15(c) and 15(d)], in which most particles are engaged in a circular vortex motion in the vertical plane resembling Rayleigh-Bénard convection, which occurs in a thin layer of ordinary fluid heated from below. The condensate coexists with the dilute granular gas. The direction of rotation is determined by the polarity of the applied voltage: particles stream towards the center of the condensate near the top plate for the upward field direction and vice versa. The evolution of the condensate depends on the electric-field direction. For the downward field, large structures become unstable due to the spontaneous formation of voids [Fig. 15(d)]. These voids exhibit complex intermittent dynamics. In contrast, for the upward field, large vortices merge into one, forming an asymmetric object which often performs a composite rotation in the horizontal plane. The pattern formation in this system is most likely caused by self-induced electrohydrodynamic microvortices created by particles in weakly conducting fluids. These microvortices create long-range hydrodynamic vortex flows, which often overwhelm electrostatic repulsion between like-charged particles and introduce attractive dipolelike hydrodynamic interactions. Somewhat similar microvorti-

ces are known in driven colloidal systems; see, for example, Yeh *et al.* (1997).

Aranson and Sapozhnikov (2004) have developed a phenomenological continuum theory of pattern formation for metallic microparticles in a weakly conducting liquid subject to an electric field. Based on an analogy with the previously developed theory of coarsening in an air-field cell (Aranson, Meerson, *et al.*, 2002), the model is formulated in terms of conservation laws for number densities of immobile particles (precipitate) n_p and bouncing particles (gas) n_g averaged over the thickness of the cell:

$$\partial_t n_p = \nabla \mathbf{J}_p + \phi, \quad \partial_t n_g = \nabla \mathbf{J}_g - \phi. \tag{79}$$

Here $J_{p,g}$ are mass fluxes of the precipitate and gas, respectively, and the function ϕ describes gas-precipitate conversion, which depends on $n_{p,g}$, electric field E, and local ionic concentration c. The fluxes are written as

$$\mathbf{J}_{p,g} = D_{p,g} \nabla n_{p,g} + \alpha_{p,g}(E) \mathbf{v}_\perp n_{p,g}[1 - \beta(E) n_{p,g}], \tag{80}$$

where $v_\perp$ is the horizontal hydrodynamic velocity and $D_{p,g}$ are precipitate-gas diffusivities. The last term, describing the advection of particles by the fluid, is reminiscent of the Richardson-Zaki relation for a drag force frequently used in the engineering literature (Richardson and Zaki, 1954). The factor $1-\beta(E)n_{p,g}$ describes the saturation of flux at large particle densities $n \sim 1/\beta$ due to the decrease of the void fraction. The terms $\sim \alpha_{p,g}$ describe the advection of particles by the fluid. Interestingly, in the limit of large gas diffusion $D_g \gg D_p$ and without advection terms ($\alpha_{p,g}=0$), the model reduces to Eqs. (71) and (72) applied to an air-filled cell (Aranson, Meerson, *et al.*, 2002).

Equation (79) is coupled to the cross-section averaged Navier-Stokes equation for vertical velocity v_z:

$$n_0(\partial_t v_z + \mathbf{v} \nabla v_z) = \mu \nabla^2 v_z - \partial_z p + E_z q, \tag{81}$$

where n_0 is the density of the liquid (we set $n_0=1$), μ is the viscosity, p is the pressure, and q is the charge density. The last term describes the electric force acting on a charged liquid. The horizontal velocity $v_\perp$ is obtained from v_z using the incompressibility condition $\partial_z v_z + \nabla_\perp v_\perp = 0$ in the approximation that vertical vorticity $\Omega_z = \partial_x v_y - \partial_y v_x$ is small compared to in-plane vorticity. This assumption allows one to find the horizontal velocity as a gradient of the quasipotential ϕ: $v_\perp = -\nabla_\perp \phi$.

For an appropriate choice of parameters, Eqs. (79) and (81) yield a qualitatively correct phase diagram and the patterns observed in experiment; see Figs. 15 and 54.

D. Magnetic particles

Electric and magnetic interactions allow the introduction of controlled long-range forces in granular systems. , Blair and Kudrolli (2003), Blair, *et al.* (2003), Stambaugh, Lanthrop, *et al.* (2004), and Stambaugh, Smith, *et al.* (2004) have performed experimental studies with vibrofluidized magnetic particles. Several interesting phase transitions have been reported, in particular, the formation of dense two-dimensional clusters and loose quasi-one-dimensional chains and rings. Blair *et al.* (2003) have considered pattern formation in a mixture of magnetic and nonmagnetic (glass) particles of equal mass. The glass particles played the role of "phonons." Their concentration allowed an adjustment of the typical fluctuation velocity of the magnetic subsystem. The phase diagram delineating various regimes in this system is shown in Fig. 55. While the phase diagram shows some similarity with equilibrium dipolar fluids (such as phase coexistence), most likely there are differences due to the nonequilibrium character of granular systems.

Stambaugh, Lanthrop, *et al.* (2004) have performed experiments with relatively large particles (about 1.7 cm) and near the close-packed density. It has been found that particles formed hexagonal close-packed clusters in which magnetic dipoles lay in the plane and assumed circulating vortical patterns. For lower density, ring patterns have been observed. Experiments with a mixture of particles with two different magnetic moments have revealed segregation effects (Stambaugh, Smith, *et al.*, 2004). The authors have argued that the static configurational magnetic energy is the primary factor in pattern selection.

Experiments by Blair and Kudrolli (2003), Stambaugh, Lanthrop, *et al.* (2004), and Stambaugh, Smith, *et al.* (2004) have been limited to a small number (about 10^3) of large particles due to the intrinsic limitation of the mechanical vibrofluidization technique. Snezhko *et al.* (2005) have performed experimental studies of 90-μm nickel microparticles subjected to electrostatic excitation; see also Sec. VIII.C. The electrostatic system has allowed researchers to perform experiments with a large number of particles (of the order of 10^6) and an experimental cell with a large aspect ratio. Thus the transition between small chains and large networks (Fig. 13) has been addressed in detail. An abrupt divergence of the chain length has been found when the frequency of field oscillations decreased, resulting in the formation of a giant interconnected network.

Studies of the collective dynamics and pattern formation of magnetic particles are still in the early phases. While it is natural to assume that the magnetic interaction plays a dominant role in pattern selection, further computational and theoretical studies of pattern formation in systems of driven dipolar particles are necessary. Besides being directly relevant to the physics of granular media, studies of magnetic granular media may provide additional insight into the behavior of dipolar hard-sphere fluids in which the nature of solid-liquid transitions is still debated (de Gennes and Pincus, 1970; Levin, 1999). Vibration or electrostatic fluidization of magnetic particles can also be viewed as a macroscopic model of a ferrofluid, where similar experiments are difficult to perform.

IX. OVERVIEW AND PERSPECTIVES

Studies of granular materials are intrinsically interdisciplinary and borrow ideas and methods from other

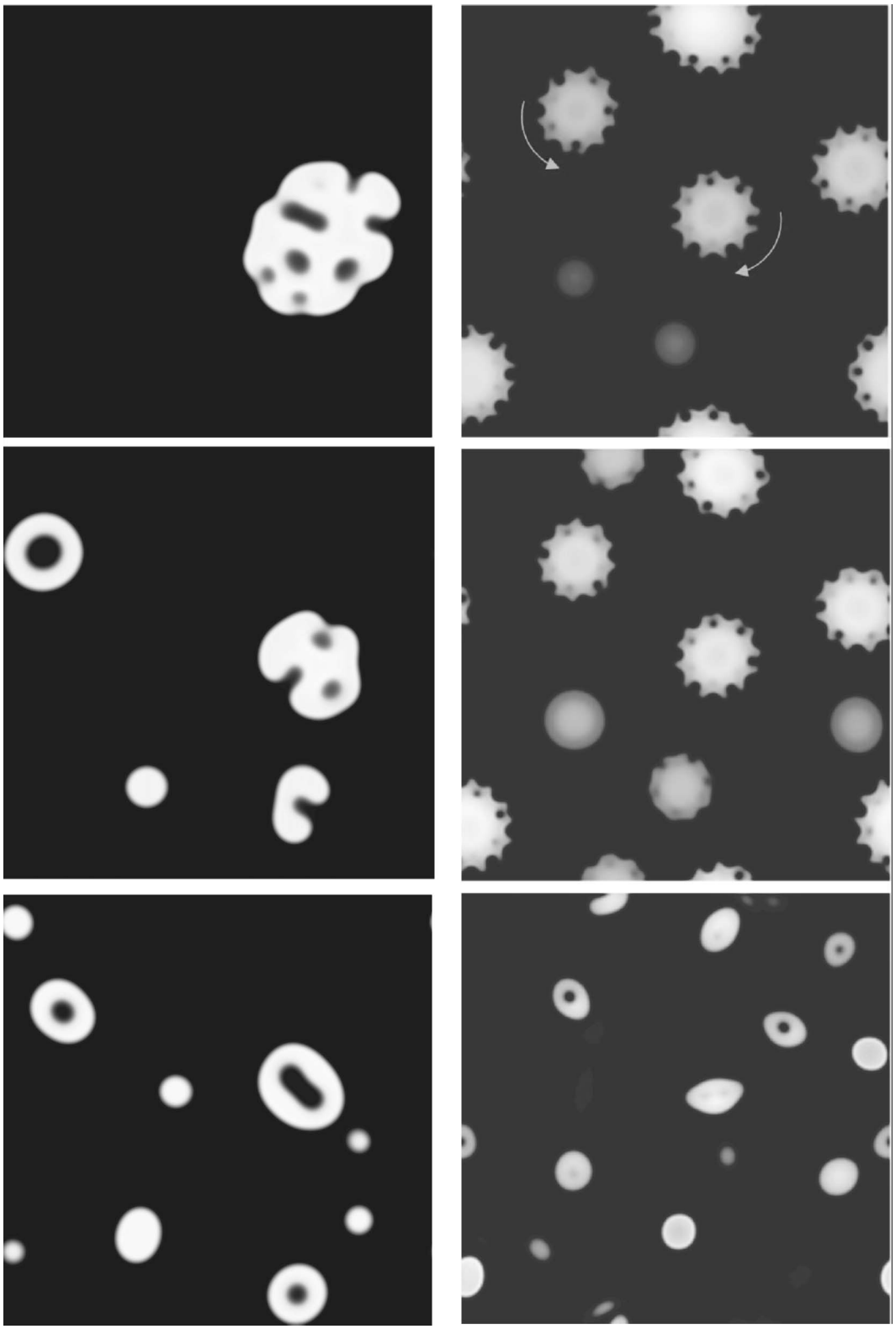

FIG. 54. Sequence of snapshots illustrating the evolution of pulsating rings (top row) and rotating vortices (bottom row) obtained from a numerical solution of Eqs. (79) and (81). From Aranson and Sapozhnikov, 2004.

fields of physics such as statistical physics, mechanics, fluid dynamics, and the theory of plasticity. On the flip side, progress in understanding granular matter can often be applied to seemingly unrelated physical and biological systems, such as foams, colloids, emulsions, suspensions, ultrathin liquid films, colonies of organisms, and other soft condensed-matter systems. The common feature shared by these systems is the discrete microstructure directly influencing macroscopic behavior.

Let us present here several examples. In the boundary

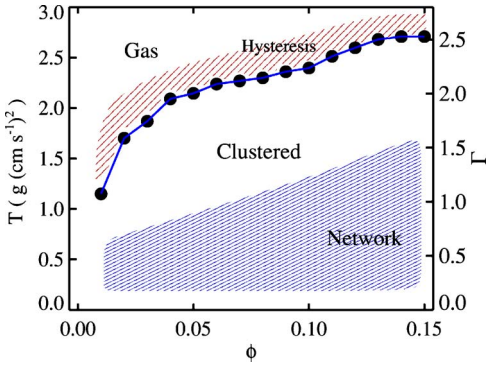

FIG. 55. (Color online) Phase diagram illustrating various regimes in magnetic granular media; T is the temperature determined from the width of the velocity distribution and Φ is the surface coverage fraction of glass particles. From Blair and Kudrolli, 2003.

FIG. 56. (Color online) Sequence of snapshots illustrating the evolution of a clay suspension drop poured over sandpaper. From Coussot, Nguyen, *et al.*, 2002.

lubrication problem, a sheared thin liquid film squeezed between two atomically flat surfaces often exhibits stick-slip behavior characteristic of dry friction, and the order-parameter description similar to that of Sec. VI.A.1 was developed for a description of this phenomenon; see Israelachvili *et al.* (1988), Carlson and Batista (1996), Aranson, Tsimring, *et al.* (2002), Urbach *et al.* (2004).

Lemaitre (2002) and Lemaitre and Carlson (2004) have applied the idea of a shear-transformation zone pioneered by Falk and Langer (1998) for amorphous solids, both to granular matter and to the boundary lubrication problem in a confined fluid. In this theory, the plastic deformation is represented by a population of mesoscopic regions which may undergo nonaffine deformations in response to stress. The concentration of shear-transformation zones in amorphous materials is somewhat similar to the order parameter (relative concentration of defects) introduced by Aranson, Tsimring, *et al.* (2002). A conceptually similar approach was proposed by Staron *et al.* (2002), who described the onset of fluidization as a percolation of the contact network with fully mobilized friction. Whereas derivation of the constitutive relations from first-principle rules is still a formidable challenge, these approaches are promising for the understanding of not only the boundary lubrication problem but also the onset of motion in dense granular matter.

Flowing liquid foams and emulsions share many similarities with granular matter. They have internal discrete structure (bubbles and drops play the role of grains), and two different mechanisms are responsible for the transmission of stresses: elastic deformation for small stress and viscoplastic deformation above a certain yield stress. However, there are additional complications: bubbles are highly deformable and, unlike granular matter, a number of particles may change due to the coalescence of bubbles.

Foams and granular materials often exhibit similar behavior, such as nontrivial stress relaxation and a power-law distribution of rearrangement events (Dennin and Knobler, 1997). Stick-slip behavior was reported for both sheared foams (Lauridsen *et al.*, 2002) and granular materials (Nasuno *et al.*, 1997). Remarkably, recent experiments with two-dimensional foams (Lauridsen *et al.*, 2004) and three-dimensional emulsions (Coussot, Nguyen, *et al.*, 2002; Coussot, Raynaud, *et al.*, 2002; DaCruz *et al.*, 2002) suggest the coexistence of flowing (liquid) and jammed (solid) states reminiscent of that in granular matter. Furthermore, avalanche behavior reminiscent of granular flows down an inclined plane (Daerr and Douady, 1999) was reported by Coussot, Nguyen, *et al.* (2002) for clay suspensions; see Fig. 56. There are many approaches treating foams, gels, and suspensions as complex fluids with a specific stress-strain constitutive relation. For example, Fuchs and Cates (2002) used the analogy between glasses and dense colloidal suspensions and applied the mode-coupling approach in order to understand the nonlinear rheology and yielding. Similar approaches can possibly be useful for granular materials (Schofield and Oppenheim, 1994).

Liu and Nagel (1998) suggested that a broad class of athermal soft-matter systems (glasses, suspensions, granular materials) showed universal critical behavior in the vicinity of the solid-fluid or jamming transition; see Fig. 57. Whether jammed systems have common features that can be described by a universal phase diagram is still an unresolved issue. An interesting question in this context is the possibility of a thermodynamic description of driven, macroscopic, athermal systems, like granular materials and foams, in terms of some kind of effective temperature. Studies of interacting particles under shear (Makse and Kurchan, 2002; Ono *et al.*, 2002; O'Hern *et al.*, 2004; Corvin *et al.*, 2005; Xu and O'Hern, 2005) have indicated that under certain conditions it is possible to define an effective temperature (for example, from the equivalent of the Einstein-Stokes relation) for a broad class of athermal systems from comparison of the mechanical linear response with the corresponding time-dependent fluctuation-dissipation relation. However, since different protocols lead to different values of granular temperature and the apparent absence of equipartition, it makes the possibility of developing nonequilibrium thermodynamics on the basis of the effective temperature problematic.

Granular flows exhibit many similarities to traffic flows and to the collective motion of self-propelled par-

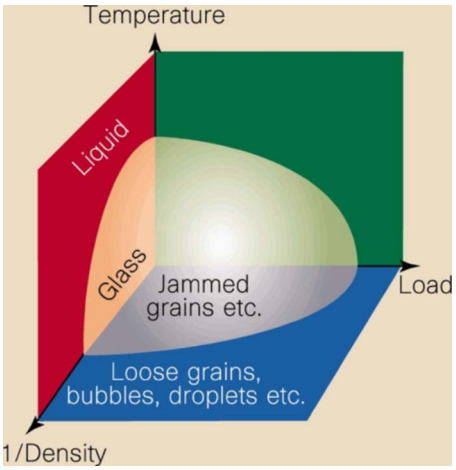

FIG. 57. (Color online) A possible phase diagram for jamming. The jammed region, near the origin, is enclosed by the depicted surface. The line in the temperature-load plane is speculative and indicates how the yield stress might vary for jammed systems in which there is thermal motion. From Liu and Nagel, 1998.

ticles such as swimming bacteria, fish schools, bird flocks, etc.; see, for a review, Helbing (2001). In particular, the jamming transitions in granular media and traffic jams show similar features, such as hysteresis and cluster formation. Continuum models of traffic flows are often cast in the form of a modified Navier-Stokes equation with density-dependent viscosity, similar to granular hydrodynamics.

In this paper, we have given a brief overview of recent theoretical developments in the rapidly developing field of granular physics. A number of subjects had to be left out as they are beyond the scope of this review, most importantly, the issues of granular statics and stress propagation (Goldenberg and Goldhirsch, 2002, 2005; Majmudar and Behringer, 2005), hopper flows (Samadani *et al.*, 1999), flows past obstacles and shock waves (Rericha *et al.*, 2002), crater formation in granular impacts (Uehara *et al.*, 2003; Walsh *et al.*, 2003; Lohse *et al.*, 2004; Ambroso *et al.*, 2005; Tsimring and Volfson, 2005), diffusion in granular systems (Dufty *et al.*, 2002), etc. We have focused our attention on the theoretical aspects of granular flows and pattern formation, i.e., the dynamic properties of driven granular systems. To conclude, we now discuss some open questions in the dynamics of granular matter.

(i) A unified description of granular patterns and flows. In this paper we have tried to give a broad overview of recent developments in the theoretical modeling of granular patterns. Unfortunately, despite much effort, no single unified theory able to describe the various experimental situations has so far emerged. Most theories have a distinctly phenomenological character, and as such they are tuned to a particular experiment or a class of experiments. Still, we hope that a unified theory will eventually emerge, at least for a class of well-defined granular media, such as that comprised of noncohesive round spheres in a vacuum. This future theory will likely be a crossover of granular hydrodynamics with a viscoplastic description of granular solids. Commonly accepted models of rapid granular flows (granular hydrodynamics) and quasistatic dense flows (elastic and viscoplastic models) are very different; see Goldenberg and Goldhirsch (2002, 2005) and Majmudar and Behringer (2005). However, near the fluidization transition, and in dense partially fluidized flows, differences between these two regimes become less obvious. The fluidization of sheared granular materials has many features of a first-order phase transition. The phenomenological partial fluidization theory, in principle, can be a bridge between the static and dynamic descriptions. The order parameter related to the local coordination number appears to be one of the hidden fields required for a consistent description of granular flows. One important question in this regard is the universality of the fluidization transition in different granular systems and geometries. On the opposite side of the fluidization transition, the static state of granular matter can be described by the order parameter related to the percentage of static contacts with fully activated dry friction (critical contacts) (Staron *et al.*, 2002). It was shown that once these contacts form a percolation cluster, the granular pack slips and fluidization occurs. It is of obvious interest to relate this "static" order parameter and the "dynamics" order parameter discussed above. We see one of the main future challenges as being the systematic derivation of a continuum theory that is valid for both flowing and static granular matter.

(ii) Statistical mechanics of dense granular systems. Clearly, discrete grain structure plays a major role in the dynamics and inherent stochasticity of granular response. The number of particles in a typical granular assembly is large (10^6 or more) but it is much smaller than the Avogadro number. Traditional tools of statistical physics do not apply to dense granular systems since grains do not exhibit thermal Brownian motion. One of the alternative ways of describing the statistics of granular media was suggested by Edwards and Grinev (1998), in which they proposed that volume rather than energy serve as the extensive variable in a static granular system, so that the role of temperature is played by the compactivity which is the derivative of the volume with respect to the usual entropy. Recent experiments (Makse and Kurchan, 2002; Schröter *et al.*, 2005) have aimed to test this theory experimentally. Connecting Edwards's theory with granular hydrodynamics will be an interesting challenge for future studies.

(iii) Realistic simulations of three-dimensional granu-

lar flows. Even the most advanced simulations of granular flows in three dimensions (Silbert *et al.*, 2003; Silbert, 2005) are limited to relatively small samples (e.g., $100\times40\times40$ particles/box) and are very time consuming. The granular problems are inherently very stiff: while the collisions between particles are very short [$O(10^{-4})$ sec], the collective processes of interest may take many seconds or minutes. As a result, due to time-step limitations, a simulation of realistic hard particles is not feasible. The "simulation" particles have elastic moduli several orders of magnitude smaller than sand or glass. The particle softness may introduce unphysical artifacts in the overall picture of the motion. Different approaches to handling this problem will be necessary to advance the state of the art in simulations. A new opportunity may be offered by the equation-free simulation method proposed by Kevrekidis *et al.* (2004). Another area of simulations which needs further refinement is an accurate account of dry friction. In the absence of a better solution, current methods [see, for a review, Luding (2004)] employ various approximate techniques to simulate dry friction, and the accuracy of these methods can be questionable.

(iv) Complex interactions. The understanding of the dynamics of granular systems with complex interactions is an intriguing and rapidly developing field. While the interaction of grains with an interstitial fluid is a traditional part of engineering research, the effects of particle anisotropy, long-range electromagnetic interactions mediating collisions, adhesion, agglomeration, and many other proccesses constitute a formidable challenge for theorists and a fertile field of future research.

(v) Granular physics on a nanoscale. There is a persistent trend in the industry, such as powder metallurgy and pharmaceutical and various chemical technologies, towards operating with smaller and smaller particles. Moreover, it has been recognized recently that microparticles and nanoparticles can be useful for the fabrication of desired ordered structures and templates for a broad range of nanotechnological applications through self-assembly processes. Self-assembly, the spontaneous organization of materials into complex architectures, constitutes one of the greatest hopes for realizing the challenge to create ever smaller nanostructures. It is an attractive alternative to traditional approaches such as lithography and electron-beam writing. Reduction of the particle size to microscales and nanoscales shifts the balance between forces controlling particle interaction, because the dominant interactions depend on the particle size. While for macroscopic grains the dynamics are governed mostly by gravity and collisional and frictional forces, for microparticles and nanoparticles the dominant interactions include long-range electromagnetic forces, short-range van der Waals interactions, etc. Nevertheless, some concepts and ideas developed in "traditional" granular physics have been successfully applied to understanding the dynamic self-assembly of microparticles (Sapozhnikov, Aranson, *et al.*, 2003, 2004) and even biological microtubules (Aranson and Tsimring, 2005). We expect to see more and more effort in this direction.

ACKNOWLEDGMENTS

The authors thank Guenter Ahlers, Bob Behringer, Eli Ben-Naim, Daniel Blair, Jean-Philippe Bouchaud, Paul Chaikin, Hugues Chaté, Philippe Claudin, Eric Clement, Sue Coppersmith, George Crabtree, Adrian Daerr, Pierre-Gilles de Gennes, James Dufty, Jacques Duran, Douglas Durian, Robert Ecke, Denis Ertas, Chay Goldenberg, Isaac Goldhirsch, Ray Goldstein, Jerry Gollub, Gary Grest, Thomas Halsey, Haye Hinrichsen, Jacob Israelachvili, Henrich Jaeger, James Jenkins, Leo Kadanoff, Devang Khakhar, Evelyne Kolb, Lorenz Kramer, Arshad Kudrolli, Wai Kwok, James Langer, Anaël Lemaître, Jie Li, Wolfgang Losert, Baruch Meerson, Francisco Melo, Sid Nagel, Jeff Olafsen, Julio Ottino, Len Pismen, Thorsten Pöschel, Olivier Pouliquen, Jacques Prost, Sriram Ramaswamy, Maksim Saposhnikov, Peter Schiffer, Leo Silbert, Alexey Snezhko, Harry Swinney, Julian Talbot, Paul Umbanhowar, Alexandre Valance, Martin van Hecke, Wim van Saarloos, Valerii Vinokur, Dmitrii Volfson, Thomas Witten, Dietrich Wolf, and many others for useful discussions and comments. This work was supported by the Office of the Basic Energy Sciences at the United States Department of Energy, Grants Nos. W-31-109-ENG-38 and DE-FG02-04ER46135. The review was partly written when one of the authors (I.S.A.) was attending Granular Session in Institute Henry Poincaré, Paris, and Granular Physics Program, Kavli Institute for Theoretical Physics in Santa Barbara.

REFERENCES

Aegerter, C. M., R. Günter, and R. J. Wijngaarden, 2003, Phys. Rev. E **67**, 051306.

Aegerter, C. M., K. A. Lorincz, M. S. Welling, and R. J. Wijngaarden, 2004, Phys. Rev. Lett. **92**, 058702.

Alexander, A., F. J. Muzzio, and T. Shinbrot, 2004, Granular Matter **5**, 171.

Ambroso, M. A., R. D. Kamien, and D. J. Durian, 2005, Phys. Rev. E **72**, 041305.

Andereck, D., S. S. Liu, and H. L. Swinney, 1986, J. Fluid Mech. **164**, 155.

Andersen, K. H., M. L. Chabanol, and M. van Hecke, 2001, Phys. Rev. E **63**, 066308.

Andreotti, B., P. Claudin, and S. Douady, 2002, Eur. Phys. J. B **28**, 341.

Aoki, K. M., T. Akiyama, Y. Maki, and T. Watanabe, 1996,

Phys. Rev. E **54**, 874.
Aradian, A., E. Raphaël, and P.-G. de Gennes, 2002, C. R. Acad. Sci., Ser IV: Phys., Astrophys. **3**, 187.
Aranson, I. S., D. Blair, V. A. Kalatsky, G. W. Crabtree, W.-K. Kwok, V. M. Vinokur, and U. Welp, 2000, Phys. Rev. Lett. **84**, 3306.
Aranson, I. S., D. Blair, W.-K. Kwok, G. Karapetrov, U. Welp, G. W. Crabtree, V. M. Vinokur, and L. S. Tsimring, 1999, Phys. Rev. Lett. **82**, 731.
Aranson, I. S., and L. Kramer, 2002, Rev. Mod. Phys. **74**, 99.
Aranson, I. S., B. Meerson, P. V. Sasorov, and V. M. Vinokur, 2002, Phys. Rev. Lett. **88**, 204301.
Aranson, I. S., and J. S. Olafsen, 2002, Phys. Rev. E **66**, 061302.
Aranson, I. S., and M. V. Sapozhnikov, 2004, Phys. Rev. Lett. **92**, 234301.
Aranson, I. S., and L. S. Tsimring, 1998, Physica A **249**, 103.
Aranson, I. S., and L. S. Tsimring, 1999, Phys. Rev. Lett. **82**, 4643.
Aranson, I. S., and L. S. Tsimring, 2001, Phys. Rev. E **64**, 020301(R).
Aranson, I. S., and L. S. Tsimring, 2002, Phys. Rev. E **65**, 061303.
Aranson, I. S., and L. S. Tsimring, 2003, Phys. Rev. E **67**, 021305.
Aranson, I. S., and L. S. Tsimring, 2005, Phys. Rev. E **71**, 050901(R).
Aranson, I. S., L. S. Tsimring, and V. M. Vinokur, 1999, Phys. Rev. E **59**, R1327.
Aranson, I. S., L. S. Tsimiring, and V. M. Vinokur, 1999b, Phys. Rev. E **60**, 1975.
Aranson, I. S., L. S. Tsimring, and V. M. Vinokur, 2002, Phys. Rev. B **65**, 125402.
Argentina, M., M. G. Clerc, and R. Soto, 2002, Phys. Rev. Lett. **89**, 044301.
Arndt, T., T. Siegmann-Hegerfeld, S. J. Fiedor, J. M. Ottino, and R. M. Lueptow, 2005, Phys. Rev. E **71**, 011306.
Asakura, S., and F. Oosawa, 1958, J. Polym. Sci. **33**, 183.
Aumaître, S., C. A. Kruelle, and I. Rehberg, 2001, Phys. Rev. E **64**, 041305.
Ayrton, H., 1910, Proc. R. Soc. London, Ser. A **84**, 285.
Babić, M., 1993, J. Fluid Mech. **254**, 127.
Bagnold, R. A., 1954, *The Physics of Blown Sand and Desert Dunes* (Methuen, London), p. 265.
Bagnold, R. A., 1956, Proc. R. Soc. London, Ser. A **187**, 1.
Bak, P., C. Tang, and K. Wiesenfeld, 1987, Phys. Rev. Lett. **59**, 381.
Barashenkov, I. V., N. V. Alexeeva, and E. V. Zemlyanaya, 2002, Phys. Rev. Lett. **89**, 104101.
Ben-Naim, E., and P. L. Krapivsky, 2003, Phys. Rev. E **68**, 031104.
Betat, A., V. Frette, and I. Rehberg, 1999, Phys. Rev. Lett. **83**, 88.
Bizon, C., M. D. Shattuck, J. R. de Bruyn, J. B. Swift, W. D. McCormick, and H. L. Swinney, 1998, J. Stat. Phys. **93**, 449.
Bizon, C., M. D. Shattuck, J. T. Newman, P. B. Umbanhowar, J. B. Swift, W. D. McCormick, and H. L. Swinney, 1997, Phys. Rev. Lett. **79**, 4713.
Bizon, C., M. D. Shattuck, J. B. Swift, W. D. McCormick, and H. L. Swinney, 1998, Phys. Rev. Lett. **80**, 57.
Blair, D., I. S. Aranson, G. W. Crabtree, V. Vinokur, L. S. Tsimring, and C. Josserand, 2000, Phys. Rev. E **61**, 5600.
Blair, D. L., and A. Kudrolli, 2003, Phys. Rev. E **67**, 021302.
Blair, D. L., T. Neicu, and A. Kudrolli, 2003, Phys. Rev. E **67**, 031303.
Börzsönyi, T., T. C. Halsey, and R. E. Ecke, 2005, Phys. Rev. Lett. **94**, 208001.
Bouchaud, J.-P., M. E. Cates, J. Ravi Prakash, and S. F. Edwards, 1994, J. Phys. I **4**, 1393.
Bouchaud, J.-P., M. E. Cates, J. R. Prakash, and S. F. Edwards, 1995, Phys. Rev. Lett. **74**, 1982.
Bougie, J., J. Kreft, J. B. Swift, and H. L. Swinney, 2005, Phys. Rev. E **71**, 021301.
Bougie, J., Sung Joon Moon, J. B. Swift, and H. L. Swinney, 2002, Phys. Rev. E **66**, 051301.
Boutreux, T., and P. G. de Gennes, 1996, J. Phys. I **6**, 1295.
Boutreux, T., E. Raphael, and P.-G. de Gennes, 1998, Phys. Rev. E **58**, 4692.
Bray, A. J., 1994, Adv. Phys. **43**, 357.
Brendel, L., T. Unger, and D. E. Wolf, 2004, in *The Physics of Granular Media*, edited by H. Hinrichsen and D. E. Wolf (Wiley-VCH, Weinheim), p. 325.
Brey, J. J., J. W. Dufty, C. S. Kim, and A. Santos, 1998, Phys. Rev. E **58**, 4638.
Brilliantov, N. V., and Th. Pöschel, 2004, *Kinetic Theory of Granular Gases* (Oxford University Press, Oxford), p. 329.
Brito, R., and M. H. Ernst, 1998, Int. J. Mod. Phys. C **8**, 1339.
Brown, R. L., 1939, J. Inst. Fuel **13**, 15.
Buehler, R. J., J. R. H. Wentorf, J. O. Hirschfelder, and C. F. Curtiss, 1951, J. Chem. Phys. **19**, 61.
Burtally, N., P. J. King, and M. R. Swift, 2002, Science **295**, 1877.
Cafiero, R., S. Luding, and H. J. Herrmann, 2000, Phys. Rev. Lett. **84**, 6014.
Caps, H., and N. Vandewalle, 2001, Phys. Rev. E **64**, 041302.
Carlson, J. M., and A. A. Batista, 1996, Phys. Rev. E **53**, 4153.
Carnahan, N. F., and K. E. Starling, 1969, J. Chem. Phys. **51**, 635.
Cattuto, C., and U. M. Marconi, 2004, Phys. Rev. Lett. **92**, 174502.
Cerda, E., F. Melo, and S. Rica, 1997, Phys. Rev. Lett. **79**, 4570.
Charles, C. R. J., Z. S. Khan, and S. W. Morris, 2005, Granular Matter **11**, 46.
Chicarro, R., R. Peralta-Fabi, and R. M. Velasco, 1997, in *Powders & Grains 97*, edited by R. P. Behringer and J. T. Jenkins (Balkema, Rotterdam), p. 479.
Chladni, E. F. F., 1787, *Entdeckungen ber die Theorie des Klanges* (Bey Weidmanns erben und Reich, Leipzig), p. 77.
Choo, K., M. W. Baker, T. C. A. Molteno, and S. W. Morris, 1998, Phys. Rev. E **58**, 6115.
Choo, K., T. C. A. Molteno, and S. W. Morris, 1997, Phys. Rev. Lett. **79**, 2975.
Ciamarra, M. P., A. Coniglio, and M. Nicodemi, 2005, Phys. Rev. Lett. **94**, 188001.
Clément, E., L. Vanel, J. Rajchenbach, and J. Duran, 1996, Phys. Rev. E **53**, 2972.
Conti, M., B. Meerson, A. Peleg, and P. V. Sasorov, 2002, Phys. Rev. E **65**, 046117.
Conway, S. L., D. J. Goldfarb, T. Shinbrot, and B. J. Glasser, 2003, Phys. Rev. Lett. **90**, 074301.
Conway, S. L., T. Shinbrot, and B. J. Glasser, 2004, Nature (London) **431**, 433.
Cooke, M. H., D. J. Stephens, and J. Bridgewater, 1976, Powder Technol. **15**, 1.
Corvin, E. I., H. M. Jaeger, and S. R. Nagel, 2005, Nature (London) **435**, 1075.
Costello, R. M., K. L. Cruz, C. Egnatuk, D. T. Jacobs, M. C.

Krivos, T. Sir Louis, R. J. Urban, and H. Wagner, 2003, Phys. Rev. E **67**, 041304.
Coullet, P., J. Lega, B. Houchmanzadeh, and J. Lajzerowicz, 1990, Phys. Rev. Lett. **65**, 1352.
Coussot, P., Q. D. Nguyen, H. T. Huynh, and D. Bonn, 2002, Phys. Rev. Lett. **88**, 175501.
Coussot, P., J. S. Raynaud, F. Bertrand, P. Moucheront, J. P. Guilbaud, H. T. Huynh, S. Jarny, and D. Lesueur, 2002, Phys. Rev. Lett. **88**, 218301.
Crawford, C., and H. Riecke, 1999, Physica D **129**, 83.
Cross, M. C., and P. C. Hohenberg, 1993, Rev. Mod. Phys. **65**, 851.
Cundall, P. A., and O. D. L. Strack, 1979, Geotechnique **29**, 47.
DaCruz, F., F. Chevoir, D. Bonn, and P. Coussot, 2002, Phys. Rev. E **66**, 051305.
Daerr, A., 2001a, Phys. Fluids **13**, 2115.
Daerr, A., 2001b, Ph.D. thesis, Univ. Paris VII, Paris, p. 181.
Daerr, A., and S. Douady, 1999, Nature (London) **399**, 241.
Daerr, A., P. Lee, J. Lanuza, and E. Clément, 2003, Phys. Rev. E **67**, 065201(R).
Dammer, S. M., and D. E. Wolf, 2004, Phys. Rev. Lett. **93**, 150602.
Das, S. K., and S. Puri, 2003, Europhys. Lett. **61**, 749.
Davies, R. H., 1990, J. Hydrol. **29**, 18.
de Bruyn, J. R., C. Bizon, M. D. Shattuck, D. Goldman, J. B. Swift, and H. L. Swinney, 1998, Phys. Rev. Lett. **81**, 1421.
de Gennes, P.-G., 1999, Rev. Mod. Phys. **71**, S374.
de Gennes, P.-G., and P. Pincus, 1970, Phys. Kondens. Mater. **11**, 189.
Dennin, M., and C. M. Knobler, 1997, Phys. Rev. Lett. **78**, 2485.
Dinkelacker, F., A. Hübler, and E. Lüscher, 1987, Biol. Cybern. **56**, 51.
Dolgunin, V. N., A. N. Kudy, and A. A. Ukolov, 1998, Powder Technol. **96**, 211.
Douady, S., B. Andreotti, and A. Daerr, 1999, Eur. Phys. J. B **11**, 131.
Douady, S., B., Andreotti, A. Daerr, and P. Clade, 2002, C. R. Acad. Sci., Ser IV: Phys., Astrophys. **3**, 177.
Douady, S., S. Fauve, and C. Laroche, 1989, Europhys. Lett. **8**, 621.
Dufty, J. W., J. J. Brey, and J. Lutsko, 2002, Phys. Rev. E **65**, 051303.
Duong, Nhat-Hang P., A. E. Hosoi, and T. Shinbrot, 2004, Phys. Rev. Lett. **92**, 224502.
Duran, J., 1999, *Sands, Powders and Grains: Introduction to the Physics of Granular Materials* (Springer-Verlag, New York), p. 214.
Duran, J., 2000, Phys. Rev. Lett. **84**, 5126.
Duran, J., 2001, Phys. Rev. Lett. **87**, 254301.
Duru, P., M. Nicolas, E. J. Hinch, and C. Guazelli, 2002, J. Fluid Mech. **452**, 371.
Edwards, S. F., and D. V. Grinev, 1998, Phys. Rev. E **58**, 4758.
Efrati, E., E. Livne, and B. Meerson, 2005, Phys. Rev. Lett. **94**, 088001.
Eggers, J., and H. Riecke, 1999, Phys. Rev. E **59**, 4476.
Ehrhardt, G. C. M. A., A. Stephenson, and P. M. Reis, 2005, Phys. Rev. E **71**, 041301.
Elperin, T., and A. Vikhansky, 1998, Europhys. Lett. **42**, 619.
Eshuis, P., K. van deer Weele, D. van deer Meer, and D. Lohse, 2005, Phys. Rev. Lett. **95**, 258001.
Evesque, P., 1990, J. Phys. II **311**, 393.
Evesque, P., and J. Rajchenbach, 1989, Phys. Rev. Lett. **62**, 44.
Falcon, E., K. Kumar, K. M. S. Bajaj, and J. K. Bhattacharjee, 1999, Phys. Rev. E **59**, 5716.
Falcon, É., R. Wunenburger, P. Évesque, S. Fauve, C. Chabot, Y. Garrabos, and D. Beysens, 1999, Phys. Rev. Lett. **83**, 440.
Falk, M. L., and J. S. Langer, 1998, Phys. Rev. E **57**, 7192.
Faraday, M., 1831, Philos. Trans. R. Soc. London **52**, 299.
Fauve, S., S. Douady, and C. Laroche, 1989, J. Phys.: Condens. Matter **50**, 187.
Ferguson, A., B. Fisher, and B. Chakraborty, 2004, Europhys. Lett. **66**, 277.
Fiedor, S. J., and J. M. Ottino, 2003, Phys. Rev. Lett. **91**, 244301.
Forterre, Y., and O. Pouliquen, 2001, Phys. Rev. Lett. **86**, 5886.
Forterre, Y., and O. Pouliquen, 2002, J. Fluid Mech. **467**, 361.
Forterre, Y., and O. Pouliquen, 2003, J. Fluid Mech. **486**, 21.
Fraerman, A. A., A. S. Melnikov, I. M. Nefedov, I. A. Shereshevskii, and A. V. Shpiro, 1997, Phys. Rev. B **55**, 6316.
Frette, V., and J. Stavans, 1997, Phys. Rev. E **56**, 6981.
Fried, E., A. Q. Shen, and S. T. Thoroddsen, 1998, Phys. Fluids **10**, 10.
Fuchs, M., and M. E. Cates, 2002, Phys. Rev. Lett. **89**, 248304.
Gallas, J. A. C., H. J. Herrmann, and S. Sokołowski, 1992a, Phys. Rev. Lett. **69**, 1371.
Gallas, J. A. C., H. J. Herrmann, and S. Sokołowski, 1992b, J. Phys. II **2**, 1389.
Gallas, J. A. C., H. J. Herrmann, and S. Sokołowski, 1992c, Physica A **189**, 437.
Gallas, J. A. C., and S. Sokołowski, 1992, Int. J. Mod. Phys. B **7**, 2037.
Gao, D., S. Subramaniam, R. O. Fox, and D. K. Hoffman, 2005, Phys. Rev. E **71**, 021302.
Garcimartín, A., D. Maza, J. L. Ilquimiche, and I. Zuriguel, 2002, Phys. Rev. E **65**, 031303.
Garzó, V., and J. W. Dufty, 1999, Phys. Rev. E **59**, 5895.
G. D. R. MiDi (collective work), 2004, Eur. Phys. J. E **14**, 341.
Gidaspow, D., 1994, *Multiphase Flows and Fluidization* (Academic, Boston), p. 467.
Goldenberg, C., and I. Goldhirsch, 2002, Phys. Rev. Lett. **89**, 084302.
Goldenberg, C., and I. Goldhirsch, 2005, Nature (London) **435**, 188.
Goldfarbs, D., B. Glasser, and T. Shinbrot, 2002, Nature (London) **415**, 302.
Goldhirsch, I., 2003, Annu. Rev. Fluid Mech. **35**, 267.
Goldhirsch, I., and G. Zanetti, 1993, Phys. Rev. Lett. **70**, 1619.
Goldman, D. I., J. B. Swift, and H. L. Swinney, 2004, Phys. Rev. Lett. **92**, 174302.
Goldsmith, W., 1964, *Impact: The Theory and Physical Behaviour of Colliding Solids* (Edward Arnold, London), p. 379.
Goldstein, A., and M. Shapiro, 1995, J. Fluid Mech. **282**, 75.
Gollub, J. P., and J. S. Langer, 1999, Rev. Mod. Phys. **71**, S396.
Gray, J. M. N. T., and K. Hutter, 1997, Continuum Mech. Thermodyn. **9**(1), 341.
Gray, J. N. M. T., and A. R. Thornton, 2005, Proc. R. Soc. London, Ser. A **461**, 1447.
Grégoire, G., and H. Chaté, 2004, Phys. Rev. Lett. **92**, 025702.
Grossman, E. L., T. Zhou, and E. Ben-Naim, 1997, Phys. Rev. E **55**, 4200.
Gurbatov, S. N., A. I. Saichev, and S. F. Shandarin, 1985, Sov. Phys. Dokl. **30**, 921.
Haff, P. K., 1983, J. Fluid Mech. **134**, 401.
He, H., B. Meerson, and G. Doolen, 2002, Phys. Rev. E **65**, 030301(R).

Helbing, D., 2001, Rev. Mod. Phys. **73**, 1067.
Helbing, D., I. J. Farkas, and T. Vicsek, 2000, Phys. Rev. Lett. **84**, 1240.
Hersen, P., K. H. Andersen, H. Elbelrhiti, B. Andreotti, P. Claudin, and S. Douady, 2004, Phys. Rev. E **69**, 011304.
Hill, J. M., 1997, in *IUTAM Symposium on Mechanics of Granular and Porous Materials*, edited by N. A. Fleck and A. C. E. Cocks (Kluwer, Dordrecht), pp. 251–262.
Hill, K. M., and J. Kakalios, 1994, Phys. Rev. E **49**, R3610.
Hill, K. M., and J. Kakalios, 1995, Phys. Rev. E **52**, 4393.
Hill, S. A., and G. F. Mazenko, 2003, Phys. Rev. E **67**, 061302.
Israelachvili, J. N., P. M. McGuiggan, and A. M. Homola, 1988, Science **240**, 189.
Ivanova, A., V. Kozlov, and P. Evasque, 1996, Europhys. Lett. **35**, 159.
Iverson, R. M., 1997, Rev. Geophys. **35**, 245.
Jackson, R., 2000, *The Dynamics of Fluidized Particles* (Cambridge University Press, Cambridge, England), p. 368.
Jaeger, H. M., C. H. Liu, and S. R. Nagel, 1989, Phys. Rev. Lett. **62**, 40.
Jaeger, H. M., S. R. Nagel, and R. P. Behringer, 1996, Rev. Mod. Phys. **68**, 1259.
Jenkins, J. T., and M. W. Richman, 1985, Phys. Fluids **28**, 3485.
Jenkins, J. T., and D. K. Yoon, 2002, Phys. Rev. Lett. **88**, 194301.
Jenkins, J. T., and C. Zhang, 2002, Phys. Fluids **14**, 1228.
Jenny, H., 1964, *Wave Phenomena, Vibrational Effects, Harmonic Oscillations, with their Structure, Kinetics, and Dynamics*, Cymatics Vol. 2 (Basilius, Basel), p. 368.
Jia, L. C., P.-Y. Lai, and C. K. Chan, 1999, Phys. Rev. Lett. **83**, 3832.
Kadanoff, L. P., 1999, Rev. Mod. Phys. **71**, 435.
Kevrekidis, I., C. W. Gear, and G. Hummer, 2004, AIChE J. **50**, 1346.
Khain, E., and B. Meerson, 2002a, Phys. Rev. E **66**, 021306.
Khain, E., and B. Meerson, 2002b, Phys. Rev. E **67**, 021306.
Khain, E., and B. Meerson, 2004, Europhys. Lett. **65**, 193.
Khain, E., B. Meerson, and P. V. Sasorov, 2004, Phys. Rev. E **70**, 051310.
Khakhar, D. V., J. J. McCarthy, and J. M. Ottino, 1997, Phys. Fluids **9**, 3600.
Khakhar, D. V., J. J. McCarthy, and J. M. Ottino, 1999, Chaos **9**, 594.
Khakhar, D. V., A. V. Opre, P. Andersén, and J. M. Ottino, 2001, J. Fluid Mech. **441**, 255.
Khan, Z. S., and S. W. Morris, 2005, Phys. Rev. Lett. **94**, 048002.
Khan, Z. S., W. A. Tokaruk, and S. W. Morris, 2004, Europhys. Lett. **66**, 212.
Kiyashko, S. V., L. N. Korzinov, M. I. Rabinovich, and L. S. Tsimring, 1996, Phys. Rev. E **54**, 5037.
Knight, J. B., H. M. Jaeger, and S. R. Nagel, 1993, Phys. Rev. Lett. **70**, 3728.
Koeppe, J. P., M. Enz, and J. Kakalios, 1998, Phys. Rev. E **58**, R4104.
Kohlstedt, K., A. Snezhko, M. V. Sapozhnikov, I. S. Aranson, J. S. Olafsen, and E. Ben-Naim, 2005, Phys. Rev. Lett. **95**, 068001.
Kroy, K., G. Sauermann, and H. J. Herrmann, 2002a, Phys. Rev. Lett. **88**, 054301.
Kroy, K., G. Sauermann, and H. J. Herrmann, 2002b, Phys. Rev. E **66**, 031302.
Kudrolli, A., 2004, Rep. Prog. Phys. **67**, 209.
Kudrolli, A., M. Wolpert, and J. P. Gollub, 1997, Phys. Rev. Lett. **78**, 1383.
Kunii, D., and O. Levenspiel, 1991, *Fluidization Engineering* (Butterworth, Boston), p. 491.
Lajeunesse, E., A. Mangeney-Castelnau, and J.-P. Vilotte, 2004, Phys. Fluids **14**, 7.
Landau, L. D., and E. M. Lifshitz, 1959, *Fluid Mechanics* (Pergamon, London), p. 536.
Landry, J. W., G. S. Grest, L. E. Silbert, and S. J. Plimpton, 2003, Phys. Rev. E **67**, 041303.
Langlois, V., and A. Valance, 2005, Phys. Rev. Lett. **94**, 248001.
Laroche, C., S. Douady, and S. Fauve, 1989, J. Phys. (France) **50**, 699.
Lauridsen, J., G. Chanan, and M. Dennin, 2004, Phys. Rev. Lett. **93**, 018303.
Lauridsen, J., M. Twardos, and M. Dennin, 2002, Phys. Rev. Lett. **89**, 098303.
Lemaître, A., 2002, Phys. Rev. Lett. **89**, 195503.
Lemaître, A., and J. Carlson, 2004, Phys. Rev. E **69**, 061611.
Lemieux, P.-A., and D. J. Durian, 2000, Phys. Rev. Lett. **85**, 4273.
Levin, Y., 1999, Phys. Rev. Lett. **83**, 1159.
Levine, D., 1999, Chaos **9**, 573.
Levitan, B., 1998, Phys. Rev. E **58**, 2061.
Li, H., and J. J. McCarthy, 2005, Phys. Rev. E **71**, 021305.
Li, J., I. S. Aranson, W.-K. Kwok, and L. S. Tsimring, 2003, Phys. Rev. Lett. **90**, 134301.
Liffman, K., G. Metcalfe, and P. Cleary, 1997 Phys. Rev. Lett. **79**, 4574.
Lifshitz, I. M., and V. V. Slyozov, 1958, Zh. Eksp. Teor. Fiz. **35**, 479 [Sov. Phys. JETP **8**, 331 (1959)].
Lifshitz, I. M., and V. V. Slyozov, 1961, J. Phys. Chem. Solids **19**, 35.
Linz, S. J., and P. Hänggi, 1995, Phys. Rev. E **51**, 2538.
Lioubashevski, O., Y. Hamiel, A. Agnon, Z. Reches, and J. Fineberg, 1999, Phys. Rev. Lett. **83**, 3190.
Liu, A., and S. R. Nagel, 1998, Nature (London) **396**, 21.
Livne, E., B. Meerson, and P. V. Sasorov, 2002a, Phys. Rev. E **65**, 021302.
Livne, E., B. Meerson, and P. V. Sasorov, 2002b, Phys. Rev. E **66**, 050301(R).
Lohse, D., R. Bergmann, R. M. Rauhe, and D. van der Meer, 2004, Nature (London) **432**, 689.
Lois, G., A. Lemaître, and J. M. Carlson, 2005, Phys. Rev. E **72**, 051303.
Losert, W., L. Bocquet, T. C. Lubensky, and J. P. Gollub, 2000, Phys. Rev. Lett. **85**, 1428.
Losert, W., D. G. W. Cooper, and J. P. Gollub, 1999, Phys. Rev. E **59**, 5855.
Luding, S., 2001, Phys. Rev. E **63**, 042201.
Luding, S., 2004, in *The Physics of Granular Media*, edited by H. Hinrichsen and D. E. Wolf (Wiley-VCH, Weinheim), p. 299.
Luding, S., E. Clément, A. Blumen, J. Rajchenbach, and J. Duran, 1994, Phys. Rev. E **50**, R1762.
Luding, S., E. Clément, J. Rajchenbach, and J. Duran, 1996, Europhys. Lett. **36**, 247.
Majmudar, T. S., and R. P. Behringer, 2005, Nature (London) **435**, 1079.
Makse, H. A., 1999, Phys. Rev. Lett. **83**, 3186.
Makse, H. A., P. Cizeau, and H. E. Stanley, 1997, Phys. Rev. Lett. **78**, 3298.
Makse, H. A., S. Havlin, P. R. King, and H. E. Stanley, 1997,

Nature (London) **386**, 379.
Makse, H. A., and J. Kurchan, 2002, Nature (London) **415**, 614.
Malloggi, F., J. Lanuza, B. Andreotti, and E. Clement, 2005, in *Powders and Grains 2005*, edited by R. Garcia-Rojo, H. J. Herrmann, and S. McNamara (Rotterdam, Balkema), p. 997.
McNamara, S., R. García-Rojo, and H. Herrmann, 2005, Phys. Rev. E **72**, 021304.
McNamara, S., and W. R. Young, 1996, Phys. Rev. E **53**, 5089.
Meerson, B., 1996, Rev. Mod. Phys. **68**, 215.
Meerson, B., Th. Pöschel, and Y. Bromberg, 2003, Phys. Rev. Lett. **91**, 024301.
Meerson, B., Th. Pöschel, P. V. Sasorov, and T. Schwager, 2004, Phys. Rev. E **69**, 021302.
Meerson, B., and A. Puglisi, 2005, Europhys. Lett. **70**, 478.
Mehta, A., 1994, in *Granular Matter. An Interdisciplinary Approach*, edited by A. Mehta (Springer-Verlag, New York), p. 306.
Mehta, A., and J. M. Luck, 1990, Phys. Rev. Lett. **65**, 393.
Melo, F., P. Umbanhowar, and H. L. Swinney, 1994, Phys. Rev. Lett. **72**, 172.
Melo, F., P. B. Umbanhowar, and H. L. Swinney, 1995, Phys. Rev. Lett. **75**, 3838.
Metcalfe, G., and M. Shattuck, 1998, Physica A **233**, 709.
Metcalfe, G., T. Shinbrot, J. J. McCarthy, and J. M. Ottino, 1995, Nature (London) **374**, 39.
Möbius, M., B. E. Lauderdale, S. R. Nagel, and H. M. Jaeger, 2001, Nature (London) **414**, 270.
Moon, S. J., D. I. Goldman, J. B. Swift, and H. L. Swinney, 2003, Phys. Rev. Lett. **91**, 134301.
Moon, S. J., M. D. Shattuck, C. Bizon, D. I. Goldman, J. B. Swift, and H. L. Swinney, 2002, Phys. Rev. E **65**, 011301.
Moreau, J. J., 1994, Eur. J. Mech. A/Solids **13**, 93.
Mujica, N., and F. Melo, 1998, Phys. Rev. Lett. **80**, 5121.
Mullin, T., 2000, Phys. Rev. Lett. **84**, 4741.
Mullin, T., 2002, Science **2002**, 1851.
Nasuno, S., A. Kudrolli, and J. P. Gollub, 1997, Phys. Rev. Lett. **79**, 949.
Nedderman, R. M., 1992, *Statics and Kinematics of Granular Materials* (Cambridge University Press, Cambridge, England), p. 368.
Newey, M., J. Ozik, S. M. van der Meer, E. Ott, and W. Losert, 2004, Europhys. Lett. **66**, 205.
Nie, X., E. Ben-Naim, and S. Y. Chen, 2000, Europhys. Lett. **51**, 679.
Nie, X., E. Ben-Naim, and S. Y. Chen, 2002, Phys. Rev. Lett. **89**, 204301.
Nishimori, H., and N. Ouchi, 1993, Phys. Rev. Lett. **71**, 197.
Oh, J., and G. Ahlers, 2003, Phys. Rev. Lett. **91**, 094501.
O'Hern, C. S., A. J. Liu, and S. R. Nagel, 2004, Phys. Rev. Lett. **93**, 165702.
Olafsen, J. S., and J. S. Urbach, 1998, Phys. Rev. Lett. **81**, 4369.
Ono, I. K., C. S. O'Hern, D. J. Durian, S. A. Langer, A. J. Liu, and S. R. Nagel, 2002, Phys. Rev. Lett. **89**, 095703.
Onsager, L., 1949, Ann. N.Y. Acad. Sci. **51**, 627.
Orpe, A., and D. Khakhar, 2006, unpublished.
Orpe, A. V., and D. V. Khakhar, 2001, Phys. Rev. E **64**, 031302.
Ottino, J. M., and D. V. Khakhar, 2000, Annu. Rev. Fluid Mech. **32**, 55.
Ottino, J. M., and D. V. Khakhar, 2002, Chaos **12**, 400.
Oyama, Y., 1939, Chaos **5**, 600.
Paczuski, M., and S. Boettcher, 1996, Phys. Rev. Lett. **77**, 111.
Pak, H. K., and R. P. Behringer, 1993, Phys. Rev. Lett. **71**, 1832.
Pak, H. K., E. Van Doorn, and R. P. Behringer, 1995, Phys. Rev. Lett. **74**, 4643.
Paolotti, D., A. Barrat, Umberto Marini Bettolo Marconi, and A. Puglisi, 2004, Phys. Rev. E **69**, 061304.
Park, H.-K., and H.-T. Moon, 2002, Phys. Rev. E **65**, 051310.
Pooley, C. M., and J. M. Yeomans, 2004, Phys. Rev. Lett. **93**, 118001.
Pöschel, Th., and Th. Schwager, 2005, *Computational Granular Dynamics* (Springer, Berlin), p. 322.
Pouliquen, O., 1999, J. Fluid Mech. **11**, 542.
Pouliquen, O., C. Cassar, Y. Forterre, P. Jop, and M. Nicolas, 2005, in *Powders & Grains 2005*, edited by R. García-Rojo, H. J. Herrmann, and S. McNamara (Balkema, Rotterdam), pp. 859–865.
Pouliquen, O., J. Delour, and S. B. Savage, 1997, Nature (London) **386**, 816.
Prevost, A., P. Melby, D. A. Egolf, and J. S. Urbach, 2004, Phys. Rev. E **70**, 050301(R).
Prigozhin, L., 1999, Phys. Rev. E **60**, 729.
Pye, K., and H. Tsoar, 1991, *Aeolian Sand and Sand Dunes* (Unwin Hyman, London), p. 396.
Radjai, F., D. E. Wolf, M. Jean, and J. J. Moreau, 1998, Phys. Rev. Lett. **80**, 61.
Rajchenbach, J., 1990, Phys. Rev. Lett. **65**, 2221.
Rajchenbach, J., 2000, Adv. Phys. **49**, 229.
Rajchenbach, J., 2002a, Phys. Rev. Lett. **88**, 014301.
Rajchenbach, J., 2002b, Phys. Rev. Lett. **89**, 074301.
Rajchenbach, J., 2003, Phys. Rev. Lett. **90**, 144302.
Ramirez, R., T. Pöschel, N. V. Brilliantov, and T. Schwager, 1999, Phys. Rev. E **60**, 4465.
Rapaport, D. C., 2002, Phys. Rev. E **65**, 061306.
Rapaport, D. C., 2004, *The Art of Molecular Dynamics Simulations*, 2nd ed. (Cambridge University Press, Cambridge, England), p. 549.
Reis, P. M., and T. Mullin, 2002, Phys. Rev. Lett. **89**, 244301.
Rericha, E. C., C. Bizon, M. D. Shattuck, and H. L. Swinney, 2002, Phys. Rev. Lett. **88**, 014302.
Richardson, J. F., and W. N. Zaki, 1954, Trans. Inst. Chem. Eng. **32**, 35.
Risso, D., R. Soto, S. Godoy, and P. Cordero, 2005, Phys. Rev. E **72**, 011305.
Ristow, G. H., 2000, *Pattern Formation in Granular Materials* (Springer, New York), p. 161.
Ristow, G. H., G. Strassburger, and I. Rehberg, 1997, Phys. Rev. Lett. **79**, 833.
Rosato, A., K. J. Strandburg, F. Prinz, and R. H. Swendsen, 1987, Phys. Rev. Lett. **58**, 1038.
Samadani, A., and A. Kudrolli, 2000, Phys. Rev. Lett. **85**, 5102.
Samadani, A., and A. Kudrolli, 2001, Phys. Rev. E **64**, 051301.
Samadani, A., A. Pradhan, and A. Kudrolli, 1999, Phys. Rev. E **60**, 7203.
Sapozhnikov, M. V., I. S. Aranson, W. K. Kwok, and Y. V. Tolmachev, 2004, Phys. Rev. Lett. **93**, 084502.
Sapozhnikov, M. V., I. S. Aranson, and J. S. Olafsen, 2003, Phys. Rev. E **67**, 010302(R).
Sapozhnikov, M. V., A. Peleg, B. Meerson, I. S. Aranson, and K. L. Kohlstedt, 2005, Phys. Rev. E **71**, 011307.
Sapozhnikov, M. V., Y. V. Tolmachev, I. S. Aranson, and W. K. Kwok, 2003, Phys. Rev. Lett. **90**, 114301.
Savage, S., 1979, J. Fluid Mech. **92**, 53.
Savage, S., and K. Hutter, 1989, J. Fluid Mech. **199**, 177.
Savage, S. B., 1988, J. Fluid Mech. **194**, 457.
Savage, S. B., 1993, in *Disorder and Granular Media*, edited by D. Bideau (North-Holland, Amsterdam), p. 264.

Schäffer, J., S. Dippel, and D. E. Wolf, 1996, J. Phys. I **6**, 5.
Scherer, M. A., F. Melo, and M. Marder, 1999, Phys. Fluids **11**, 58.
Schofield, J., and I. Oppenheim, 1994, Physica A **204**, 555.
Schröter, M., D. I. Goldman, and H. L. Swinney, 2005, Phys. Rev. E **71**, 030301(R).
Schwämmle, V., and H. J. Herrmann, 2003, Nature (London) **426**, 619.
Sela, N., and I. Goldhirsch, 1998, J. Fluid Mech. **361**, 44.
Shandarin, S. F., and Ya. B. Zeldovich, 1989, Rev. Mod. Phys. **61**, 185.
Sheffler, T., and D. E. Wolf, 2002, Granular Matter **4**, 103.
Shen, A. Q., 2002, Phys. Fluids **14**, 462.
Shinbrot, T., 1997, Nature (London) **389**, 574.
Shinbrot, T., 2004, Nature (London) **429**, 352.
Shoichi, S., 1998, Mod. Phys. Lett. B **12**, 115.
Silbert, L. E., 2005, Phys. Rev. Lett. **94**, 098002.
Silbert, L. E., D. Ertas, G. S. Grest, T. C. Halsey, and D. Levine, 2002a, Phys. Rev. E **65**, 031304.
Silbert, L. E., D. Ertas, G. S. Grest, T. C. Halsey, and D. Levine, 2002b, Phys. Rev. E **65**, 051307.
Silbert, L. E., G. S. Grest, and J. W. Landry, 2002, Phys. Rev. E **66**, 061303.
Silbert, L. E., J. W. Landry, and G. S. Grest, 2003, Phys. Fluids **15**, 1.
Snezhko, A., I. S. Aranson, and W. K. Kwok, 2005, Phys. Rev. Lett. **94**, 108002.
Song, Y., E. A. Mason, and R. M. Stratt, 1989, J. Phys. Chem. **93**, 6916.
Stambaugh, J., D. P. Lanthrop, E. Ott, and W. Losert, 2004, Phys. Rev. E **68**, 026207.
Stambaugh, J., Z. Smith, E. Ott, and W. Losert, 2004, Phys. Rev. E **70**, 031304.
Staron, L., J.-P. Vilotte, and F. Radjai, 2002, Phys. Rev. Lett. **89**, 204302.
Stegner, A., and J. E. Wesfreid, 1999, Phys. Rev. E **60**, R3487.
Sunthar, P., and V. Kumaran, 2001, Phys. Rev. E **64**, 041303.
Swift, J. B., and P. C. Hohenberg, 1977, Phys. Rev. A **15**, 319.
Taberlet, N., W. Losert, and P. Richard, 2004, Europhys. Lett. **68**, 522.
Taguchi, Y.-H., 1992, J. Phys. II **69**, 1367.
Talbot, J., and P. Viot, 2002, Phys. Rev. Lett. **89**, 064301.
Tan, M.-L., and I. Goldhirsch, 1998, Phys. Rev. Lett. **81**, 3022.
Tegzes, P., T. Vicsek, and P. Schiffer, 2002, Phys. Rev. Lett. **89**, 094301.
Tegzes, P., T. Vicsek, and P. Schiffer, 2003, Phys. Rev. E **67**, 051303.
Tennakoon, S. G. K., L. Kondic, and R. P. Behringer, 1998, Europhys. Lett. **99**, 1.
Thomas, C. C., and J. P. Gollub, 2004, Phys. Rev. E **70**, 061305.
Toner, J., and Y. Tu, 1995, Phys. Rev. Lett. **75**, 4326.
Troian, S. M., E. Herbolzheimer, S. A. Safran, and J. F. Joanny, 1989, Europhys. Lett. **10**, 25.
Tsai, J.-C., F. Ye, J. Rodriguez, J. P. Gollub, and T. C. Lubensky, 2005, Phys. Rev. Lett. **94**, 214301.
Tsimring, L. S., and I. S. Aranson, 1997, Phys. Rev. Lett. **79**, 213.
Tsimring, L. S., and D. Volfson, 2005, in *Powders & Grains 2005*, edited by H. H. R. Garcia-Rojo, and S. McNamara (Balkema, Rotterdam), Vol. 2, p. 1215.
Tu, Y., J. Toner, and S. Ramaswamy, 2005, Ann. Phys. (N.Y.) **318**, 170.
Uehara, J., M. Ambroso, R. Ojha, and D. Durian, 2003, Phys. Rev. Lett. **90**, 194301.
Umbanhowar, P. B., F. Melo, and H. L. Swinney, 1996, Nature (London) **382**, 793.
Umbanhowar, P. B., and H. L. Swinney, 2000, Physica A **288**, 344.
Unger, T., J. Kertész, and D. E. Wolf, 2005, Phys. Rev. Lett. **94**, 178001.
Urbach, M., J. Klafter, D. Gourdon, and J. Israelachvili, 2004, Nature (London) **699**, 255.
van Noije, T. P. C., and M. H. Ernst, 2000, Phys. Rev. E **61**, 1765.
Venkataramani, S. C., and E. Ott, 1998, Phys. Rev. Lett. **80**, 3495.
Venkataramani, S. C., and E. Ott, 2001, Phys. Rev. E **63**, 046202.
Villarruel, F. X., B. E. Lauderdale, D. M. Mueth, and H. M. Jaeger, 2000, Phys. Rev. E **61**, 6914.
Volfson, D., A. Kudrolli, and L. S. Tsimring, 2004, Phys. Rev. E **70**, 051312.
Volfson, D., L. S. Tsimring, and I. S. Aranson, 2003a, Phys. Rev. Lett. **90**, 254301.
Volfson, D., L. S. Tsimring, and I. S. Aranson, 2003b, Phys. Rev. E **68**, 021301.
Volfson, D., L. S. Tsimring, and I. S. Aranson, 2004, Phys. Rev. E **69**, 031302.
Voth, G. A., B. Bigger, M. R. Buckley, W. Losert, M. P. Brenner, H. A. Stone, and J. P. Gollub, 2002, Phys. Rev. Lett. **88**, 234301.
Wagner, C., 1961, Z. Elektrochem. **65**, 681.
Walker, J., 1982, Sci. Am. **247** (2), 166.
Walsh, A., K. Holloway, P. Habdas, and J. de Bruyn, 2003, Phys. Rev. Lett. **91**, 104301.
Walton, O. R., 1993, Mech. Mater. **16**, 259.
Wildman, R. D., J. M. Huntley, and D. J. Parker, 2001, Phys. Rev. Lett. **86**, 3304.
Wildman, R. D., T. W. Martin, P. Krouskop, J. Talbot, J. M. Huntley, and D. J. Parker, 2005, Phys. Rev. E **71**, 061301.
Williams, J. C., 1976, Powder Technol. **15**, 245.
Xu, N., and C. S. O'Hern, 2005, Phys. Rev. Lett. **94**, 055701.
Yanagita, T., 1999, Phys. Rev. Lett. **82**, 3488.
Yeh, S.-R., M. Seul, and B. I. Shraiman, 1997, Nature (London) **386**, 57.
Zhang, W., and J. Viñals, 1997, J. Fluid Mech. **336**, 301.
Zhou, J., B. Dupuy, A. L. Bertozzi, and A. E. Hosoi, 2005, Phys. Rev. Lett. **94**, 117803.
Zik, O., D. Levine, S. G. Lipson, S. Shtrikman, and J. Stavans, 1994, Phys. Rev. Lett. **73**, 644.